Study of Static and Dynamic Properties of Cracked Functionally Graded Materials Using Special
Finite Elements

by

Mohamad Molavi Nojumi

A thesis submitted in partial fulfillment of the requirements for the degree of

Doctor of Philosophy

Department of Mechanical Engineering
University of Alberta

Abstract

Functionally graded materials (FGMs), the new generation of materials in which composition and material properties vary continuously with the change of the coordinate position, provide a good opportunity for combining desired properties of different materials for engineering applications such as: wear resistance or thermal barrier coatings avoiding problems like weak bonding strength or high thermal stresses. One of the main types of FGMs is ceramic/metals. Ceramics are brittle; therefore, there is a high possibility of crack existence during the fabrication process or under in-service loading conditions. Analytical solutions available for crack problems in FGMs are restricted to simple geometries and loading conditions due to the mathematical complexity of the governing equations. Therefore, advanced numerical methods should be applied for general analysis of the crack problems in FGMs. In the scope of this research, the static and dynamic properties of FGMs will be investigated using special finite elements with a focus on fracture mechanics. At first, a general finite element procedure is evaluated for investigating the general elasticity problems for linear elastic isotropic FGMs. An accurate 9-node quadrilateral graded element is investigated in which the influence of the variation of material properties is considered at the element level. The implementation of graded elements prevents potential problems in sudden jumps of material properties in traditional finite elements for modelling FGMs. By employing a finite element-finite difference procedure, the performance of the multiple isoparametric graded elements can be studied in dynamic problems. The main contribution of this research is to develop a new graded singular element with built-in higher order terms based on an asymptotic analysis coupled with the Westergaard stress function approach. Using this novel element at the crack tip surrounded with introduced regular graded elements provides an accurate and efficient model for discussing the role of the material gradient

over the crack tip stress field in FGMs. This element is also extended to cover dynamic crack problems by constructing the consistence mass matrix considering the kinetic energy of the singular elements. It eliminates the need to use very fine mesh of regular elements near the crack tip. As a result the efficiency is considerably increased and less computational effort is required at each time step. Furthermore, this element does not require any post processing technique to obtain the stress intensity factors which makes it convenient for studying the influence of the gradient of elastic properties, mass density and loading type on the fracture parameters.

Preface

This thesis is an original work by Mohamad Molavi Nojumi. Chapter 5 of this thesis has been published as Mohamad Molavi Nojumi, Xiaodong Wang, "A new graded singular finite element for crack problems in functionally graded materials," *International Journal of Fracture*, vol. 205, 203-220, 2017. Also, Chapter 6 of this thesis is published as Mohamad Molavi Nojumi, Xiaodong Wang, "Dynamic analysis of crack problems in functionally graded materials using a new graded singular finite element," *Theoretical and Applied Fracture Mechanics*, vol. 93, 183-194, 2018. I was responsible for the data collection and analysis as well as the manuscript composition. Professor X.D. Wang was the supervisory author and was involved with concept formation and manuscript editing.

Acknowledgments

I would like to express my deep thanks to Professor Xiaodong Wang for his expert advice, technical guidance and financial assistance. This research was also financially supported by Natural Sciences and Engineering Research Council of Canada (NSERC). I wish to thank all the members of the Advanced Materials and Structures Laboratory for their friendship and help during undertaking this study. Finally, I wish to thank my parents for their understanding and encouragement.

Table of Contents

List of Tables

List of Figures

Chapter 1

Introduction

1.1 Motivation

Functionally graded materials (FGMs) known as the new generation of materials are an important part of advanced materials in which composition and material properties change gradually and continuously with the coordinate position. The main motivation of the use of such materials is to combine desired properties of different materials to obtain an ideal system of materials for multi-functional engineering applications under severe working conditions such as high temperature gradient, wear, corrosion, etc (Suresh and Mortensen 1998; Hirano, Teraki, and Yamada 1990b; Miyamoto et al. 1999). Thermal barrier coatings, wear resistance linings, and medical implants are some examples of the application of FGMs. This type of advanced material has attracted high interests among researchers so that the number of publication in this area shows an exponential increase in the past 20 years (Naebe and Shirvanimoghaddam 2016).

Metal/ceramic FGMs are an important class of FGMs in which the composition gradually changes from the metal phase and approaches the ceramic phase. Desired properties of ceramics

like the high resistance against heat, wear and corrosion coupled with advantageous properties of metals such as high strength, toughness, and bonding provide an excellent system of materials for working in severe conditions. Unlike bi-material interfaces such FGMs do not suffer disadvantages like high thermal and residual stresses and poor interfacial bonding strength. Ceramic materials are brittle and the existence of cracks during the fabrication process of FGMs or under in-service loading conditions is an important issue. Therefore, fracture mechanics is a main perspective for designing and analyzing FGMs in such advanced structures.

A fundamental question in the modeling of FGMs is how to deal with the spatial variation of elastic parameters, which creates the major difference from the traditional solution techniques for homogeneous elastic media. Analytical solutions for crack problems in a FGM medium are available for simple geometries and loading conditions. However, due to the mathematical complexity of the governing partial differential equations with variable coefficients, advanced numerical techniques should be applied for general analysis of the fracture behaviour of FGMs. Furthermore, the optimum design of material properties for reaching the most efficient fracture behaviour is not a deduced knowledge yet. As a result, the numerical computation of fracture parameters in FGMs is demanding.

The finite element method (FEM) as an efficient numerical tool widely used for simulating structural behaviour of homogeneous materials can be extended to study the static and dynamic properties of FGMs. Although previous works established a good background for understanding graded elements (Y. D. Lee and Erdogan 1994; Giannakopoulos and Suresh 1997; M. H. Santare and Lambros 2000; Kim and Paulino 2002a), there is still no detailed discussion on potential issues when conventional homogeneous elements are applied for studying structural properties of FGMs. Indeed, natural disparity in local field behaviour of homogeneous and graded materials

cause the difference in solutions achieved with conventional homogeneous and graded elements. This issue can be shown in specific examples and will be discussed in subsequent sections of this work.

Considerable effort has been devoted to study the fracture behaviour of FGMs by using the FEM. A variety of methods like the *J*-integral, the modified crack closure method and the displacement correlation technique have been implemented in the FEM for investigating the mixed mode stress intensity factor (SIF) in FGMs (Kim and Paulino 2002b). Alternatively, mixed mode SIFs are investigated based on the interaction integral method coupled with the extended finite element method (XFEM) (Dolbow and Gosz 2002). Because of the unique property of the crack tip field, the most robust description of the crack problem in FGMs can be achieved with considering the higher order terms in asymptotic analysis. A hybrid crack element for homogeneous materials is suggested for fracture problems in plane elasticity (Tong, Pian, and Lasry 1973), and investigated later for determining the coefficients of elastic crack-tip asymptotic field (Karihaloo and Xiao 2001). The crack-tip stress field has been scrutinized in FGMs by an asymptotic analysis jointed with the Westergaard stress function approach (Jain, Rousseau, and Shukla 2004). However, the asymptotic field of cracked FGMs has not been used in finite element analysis. It is essential to set up a singular graded element for more accurate analysis of crack problems in FGMs. In subsequent sections of this research, the procedure of developing such a new singular element is explained and accompanied with numerical results and discussions for static and dynamic crack problems.

1.2 Objectives of the study

This research is conducted to reach the following objectives:

i)   Evaluate the performance of graded elements against conventional homogeneous elements in general linear elastic isotropic static and dynamic problems for FGMs,

ii) Investigate the crack tip fields, and fracture parameters in FGM layers with sharp gradient of material properties under thermo-mechanical loading using a regular graded element,

iii) Develop and implement a new graded singular element for accurate description of the crack tip stress field in FGMs for static problems,

iv) Develop an efficient and reliable procedure for analyzing dynamic crack parameters such as mode-I and mode-II of SIFs, and stress field in FGMs using the developed graded singular element.

1.3 Layout of thesis

This thesis includes seven chapters. *Chapter one* provides an introduction to the current research including the necessity of the undertaking works and objectives. *Chapter two* is devoted to the literature review. In this chapter, topics related to the static and dynamic fracture mechanics of FGMs using various analytical and numerical approaches are thoroughly reviewed. *Chapter three* discuss about the application of regular graded elements for modelling FGMs in static and dynamic problems. The performance of graded elements is investigated and compared with conventional homogeneous elements. *Chapter four* represents a comprehensive study on the application of regular graded finite elements to the analysis of linear elastic isotropic nonhomogeneous plates containing crack under thermomechanical loading. In *Chapter five* the procedure of developing a new graded singular finite element for analyzing crack problems in

FGMs is explained. A set of simulations are performed using this element to investigate the fracture behaviour of cracked FGM plates under quasi-static loading condition. ***Chapter six*** explains the extension of the recently developed graded singular element for studying dynamic crack problems in FGMs. The influence of the mass density, elastic constants, and loading parameters on SIFs is scrutinized. ***Chapter seven*** represents the conclusion of the thesis, summarizes the findings and contribution of the current research.

Chapter 2

Literature Review

This chapter represents the review of the research works presented in literature for studying static and dynamic properties of FGMs. At the beginning a brief introduction to the FGMs and their application in engineering is provided. Special attention has been paid in the investigation of fracture mechanics of FGMs. Both analytical and numerical approaches are scrutinized. Among the numerical methods considered, FEM as one of the most popular methods has been focused and its progresses for analyzing FGMs is reviewed.

2.1 An introduction to FGMs and their applications

FGMs are the advanced generation of materials in which the composition and material properties vary continuously based on the coordinate position. A main issue in advanced technologies such as power generation, transportation, aerospace, micro-electronics, and biomechanics is to develop materials which are consistent with these environments. Materials operating in these environments require special properties such as high temperature resistance, wear resistance and high toughness. Bonding dissimilar materials to achieve their desired properties usually leads to

the difficulties such as weak bonding strength and/or high residual stresses. To overcome these difficulties the concept of FGMs was introduced in 1984 during an aerospace project in Japan. Thereafter, FGMs as a unified system of materials containing at least two different phases have been extensively studied for tailoring material properties in specific application. Comprehensive introductions about FGMs are represented in literature (Hirano, Teraki, and Yamada 1990; Suresh and Mortensen 1998; Miyamoto et al. 1999; Sobczak and Drenchev 2013; Udupa, Rao, and Gangadharan 2014; Naebe and Shirvanimoghaddam 2016). Table 2.1 shows a list of FGMs with required material properties designed for specific applications (Richter 1995).

Table 2.1 A list of FGM types with requirements and applications (Richter 1995)

FGM type	Requirements	Application
SiC-SiC	Corrosion resistance and hardness	Combustion chambers
Al-SiC	Hardness and toughness	Combustion chambers
SiCw/Al-alloy	Thermal resistance and chemical resistance	CNG storage cylinders, Diesel engine pistons
E-glass/epoxy	Hardness and damping properties	Brake rotors, Leaf springs
Al-C		Drive shafts, Hublle space telescope metering truss assembly, Turbine rotor, Turbine wheels
Al-SiC		Flywheels, Racing car brakes
SiCp/Al-alloy	High melting point, low plasticity and high hardness	Motorcycle drive sprocket, Pulleys, Torque converter reactor, Shock absorber
Carbon and glass fibers		Propulsion shaft
Glass/Epoxy		Cylindrical pressure hull, sonar domes
TiAl-SiC fibers		Composite piping system, scuba diving cylinders
Be-Al		Floats, boat hulls, wing tunnel blades, spacecraft truss structure, reflectors, solar panels, camera housing
Al_2O_3/Al-alloy	Good thermal and corrosive resistance	Rocket nozzle, wings, rotary launchers, engine casing
Carbon/Bismale imide		Drive shaft, propeller blades, landing gear doors, thrust reverser, heat exchanger panels, engine parts
Carbon/Epoxy	Lightweight and good damping properties	Helicopter components viz. rotor driving shaft, mast mount, main rotor blades
SiCw/6061	Hard and toughness	Racing bicycle frame, racing vehicle frame
Al-alloy/CNT	Light weight and high stiffness	Artificial ligaments, MRI scanner cryogenic tubes, wheelchairs, hip joint implants, eyeglass frames, camera tripods, musical instruments

2.2 Fabrication process of FGMs

FGMs are often fabricated by a controlled distribution of the constituent phases such as metals, ceramics and polymers under continuous and delicate change of the composition make up. There are different approaches to fabricate FGMs. These approaches include gas based, liquid phase and solid phase methods which can be used to physically or chemically get the desired gradient of material properties (Makoto Sasaki 1991). Chemical vapour deposition (CVD), ion plating, plasma spraying and ion mixing are some examples of gas based methods (Makoto Sasaki 1991; Malik and Kadoli 2016). In vapour phase process such as CVD and physical vapour deposition (PVD), deposited products can achieve different gradient composition depending on phases reaction's ratio in the mixture and production controlling system. For liquid phase processes such as plasma spray, flexibility for production and high deposition rate as well as complex geometry of coating make them extremely popular for coating applications. In electrodeposition methods, composition gradient closely depends on electrochemical factors and proper selection of electrolytic solution (Ding et al. 1993; Cherradi, Kawasaki, and Gasik 1994; Allahyarzadeh et al. 2016). Table 2.2 shows a list of FGMs with their fabrication techniques. More detailed information about the fabrication process can be found in (Gupta and Talha 2015; Naebe and Shirvanimoghaddam 2016).

Table 2.2 Fabrication process of different FGM systems (Naebe and Shirvanimoghaddam 2016)

FGM system	Fabrication process
ZrB_2-SiC/ZrO_2	Spark plasma sintering (SPS)
Al_2O_3-Ti_3SiC_2	SPS
TiB-Ti	SPS
HAp-Al_2O_3-YSZ	SPS
W-Cu	SPS
SiC-Al_3BC_3	SPS
WC-TiC-Cr_3C_2	SPS
NiCrAl/$MgZrO_3$	Plasma spray
ZrO_2- Al_2O_3	Plasma spray

FGM system	Fabrication process
WC-NiCrBSi	Plasma spray and post treatment: Hot isostatic, Vacuum heating
NiCrAl/MgZrO$_3$	Plasma spray
TiO$_2$-HAp	Plasma spray
Mullite/Mo	Powder metallurgy
Al(A356)-SiC	Centrifugal casting
Al(2124)-SiC	Centrifugal casting
WC-Co	Electrophoretic deposition
Ce-TZP/Al$_2$O$_3$	Electrophoretic deposition
Al$_2$O$_3$/ZrO$_2$	Gel-casting with dip coating
TiC-Ni	Combustion
TiC-Inconel 690	Laser deposition
AlBrnz-420 SS	Laser direct metal deposition
Al/SiC$_p$	Remelting and sedimentation

2.3 General static and dynamic mechanical and thermal properties of FGMs

The opportunity of designing materials to reach their optimum mechanical and thermal behaviour has provided a nourishing background for research in this area. FGMs as an effective idea for tailoring material properties have been the target of many research works to obtain the desired behaviour of materials for specific purposes. At first, FGMs were used as thermal barrier coatings. From a thermomechanical view point, FGMs considerably improve the life and reliability of thermal barrier coatings. Thermal barrier coatings used in aircraft engines typically consists of a 125-250 µm thermally insulating ceramic layer and a 50-125 µm metallic bond coat layer between the ceramic layer and the metal component surface. Y$_2$O$_3$-stabilized ZrO$_2$ (YSZ) is usually used as the ceramic layer owing to its low thermal conductivity. Metallic bond coat protects the substrate from high temperature oxidation because the transport of the oxygen through the YSZ layer, via ionic diffusion and/or through microcracks or connected porosity, is relatively fast at typical turbine temperatures (Lee et al. 1996). Fig. 2.1 shows a continuous graded microstructure with metal/ceramic constituents. Fig. 2.2 schematically illustrates the

stress concentration which occurs in conventional thermal protection panels at the tile/superstructure interface.
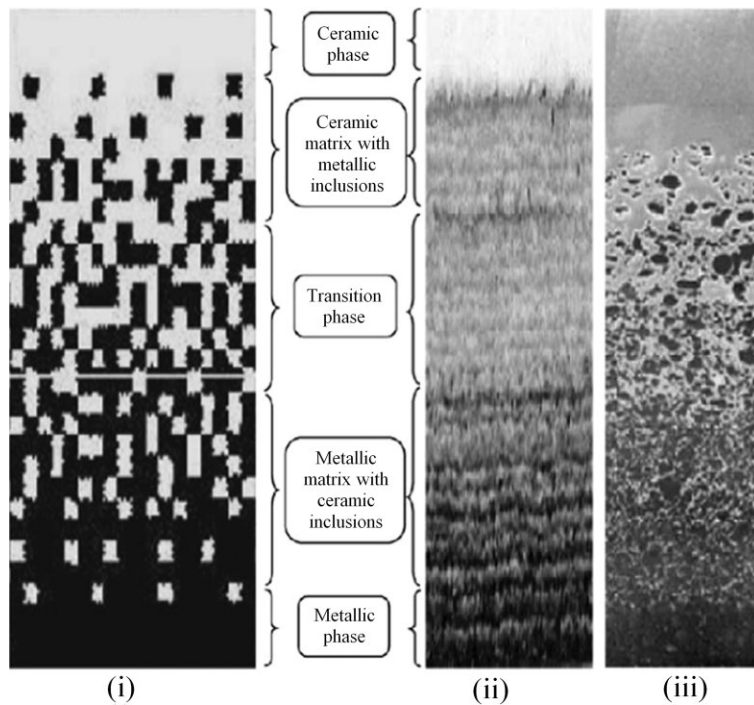
Fig. 2.1. Gradation of microstructure with metal–ceramic constituents (i) smoothly graded microstructure (ii) enlarged view and (iii) ceramic–metal FGM (Jha, Kant, and Singh 2013)
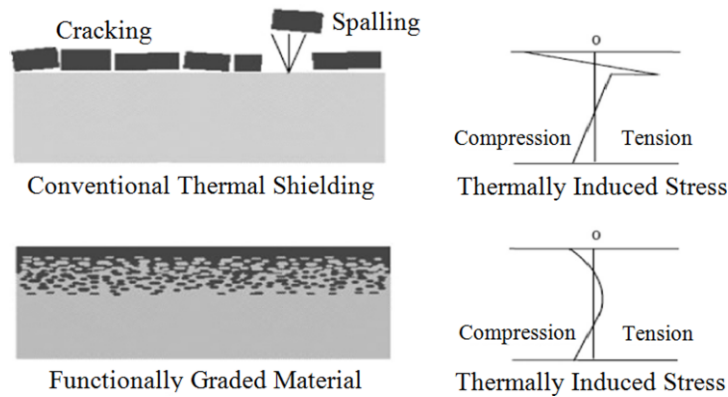
Fig. 2.2. Thermal protection of conventional materials and FGM (http://asm.matweb.com/search/SpecificMaterial.asp?bass num¼MTA641)

Extensive researches are performed in the field of thermoelastic static analysis of FGM. The thermoelastic behaviour of FGM rectangular ceramic-metal plates was studied by considering the Von Karman nonlinear effects and employing four-noded isoparametric plate FE (Praveen and Reddy 1998). A large group of exact solutions of the three dimensional elasticity problems for FGMs were established. It was shown that the exact solution for a thick plate can be achieved by using solutions of the two dimensional classical equations for stretching and bending of an equivalent plate (Main and Spencer 1998). A laminated composite plate made of numerous layers with homogeneous and different isotropic material properties was analyzed as a step-formed FGM plate for which a genetic algorithm was applied to optimize the material composition (Ootao, Tanigawa, and Ishimaru 2000). The three dimensional thermoelastic behaviour of simply supported FGM rectangular plates under thermal and mechanical loads on its top and/or bottom surfaces was studied by using an asymptotic expansion approach for the heat conduction problem (Reddy and Cheng 2001). The transient thermoelastic problem of a FGM rectangular plate with nonuniform heat supply was treated using the methods of Laplace and finite cosine transformations (Ootao and Tanigawa 2005). Then, researches on FGM plates have been continuing by focusing on different features such as nonlinearity, anisotropy, large deformation, etc (A M Zenkour 2005; Ashraf M Zenkour 2006; Ramirez, Heyliger, and Pan 2006; Ghannadpour and Alinia 2006; Ferreira et al. 2007; Abrate 2008; Hassaine et al. 2013). A recently developed sampling surface method and its implementation for three dimensional stress analysis of FGM plates is discussed (Kulikov and Plotnikova 2015). The solution is further extended to three dimensional vibration analysis of layered and FGM plates (Kulikov et al. 2016). Based on homogenization methods, effective properties of FGM panels are evaluated (C. Lee and Kim 2015). Piecewise homogeneous layered model of FGMs and sandwiched FGMs are

studied using different methodologies such as meshless method and FEM (Bernardo et al. 2016). The solution for the static bending and free vibration problems of thermally loaded FGM circular micro-plates is presented based on the couple stress theory (Eshraghi, Dag, and Soltani 2016). Thermoelasticity solution of a sandwiched circular plate with FGM core is investigated using generalized differential quadrature method (Alibeigloo 2016). Thermal analysis of FGM plates including review of various modelling techniques and solution methods is presented (Swaminathan and Sangeetha 2017). A comprehensive review of researches on FGM cylindrical structures with an emphasis on coupled mechanics, including thermo-elastic coupling, multi-physic fields coupling, structure–foundation coupling and fluid–solid coupling is presented (Dai, Rao, and Dai 2016).

In many real and potential applications, FGMs are imposed to dynamic mechanical loadings. So the effect of inertia forces should be considered. The dynamic analysis of FGMs has also contributed in developing new achievements in general field of FGMs. Elastic waves in FGM plates excited by plane pressure waves were investigated by using quadratic layer elements and the response of the plate to an incident pressure wave was obtained by the Fourier transform technique (Han, Liu, and Lam 2000). Also the effects of shear (SH) waves in FGM plate was analyzed (Han and Liu 2002). The propagation of one dimensional stress waves in a FGM plate excited by a harmonic force is studied by assuming the FGM as a multilayer structure with linear material property at each layer (Moghaddam and Ahmadian 2013). Rayleigh waves in a functionally graded piezoelectric material layer bonded to a semi-infinite homogenous solid are assessed by an exact solution (Ben Salah, Njeh, and Ben Ghozlen 2012). The propagation of the Lamb wave in a FGM plate is studied by power series technique (Cao, Jin, and Jeon 2011). The wave propagation in a three-layer structure have been analyzed in numerical examples in order to

show the effect of a functionally graded (FG) soft middle layer on Love waves propagating in layered piezoelectric systems (Ben et al. 2015). The propagation of anti-plane waves close to the interface of two half-spaces of piezoelectric ceramics is accomplished (N. Liu et al. 2010). The propagation of the lowest-order symmetric (S0) and antisymmetric (A0) Lamb wave modes in a functionally graded piezoelectric material (FGPM) plate is scrutinized by means of the Peano-series expansion (Ben Amor and Ben Ghozlen 2015). In another study, the Love wave propagation is investigated in a structure consisting two homogeneous layers and a functionally graded piezoelectric material (FGPM) buffer layer between them (Cao et al. 2009). The wave propagation and dynamic response of the rectangular FGM plates with clamped supports under impulse loads have also been evaluated (Sun and Luo 2011b). The transient response of an FGM annular sector plate with arbitrary circular boundary conditions is solved by a semi-analytical methodology (Liang et al. 2015). The two dimensional investigation of a guided wave propagation in a FGM ring with rectangular cross section is proposed with using a double orthogonal polynomial series method (J. G. Yu et al. 2015).

As mentioned above, the assessment of guided waves in FGMs is an interesting topic which has attracted significant research interests in this area (J. Yu and Zhang 2014; J. Yu and Wu 2009; Jiangong, Bin, and Cunfu 2007; J. G. Yu, Ratolojanahary, and Lefebvre 2011; Shuvalov, Le Clezio, and Feuillard 2008; J. Yu, Wu, and He 2010). The exact solution for the wave propagation and transient response of an infinite functionally graded circular plate under a point impact load is presented (Sun and Luo 2011a). An accurate numerical solution is performed to study the wave propagation in inhomogeneous materials by considering impact loading (Idesman 2014). In-plane wave propagation in layered phononic crystals composed of functionally graded interlayers is investigated, and wave transmission and band-gaps due to the material gradation

and incident wave-field are studied (Fomenko et al. 2014). The scattering of elastic waves and dynamic stress concentrations in infinite exponential graded materials with two holes are handled by means of employing complex functions and conformal mapping methods (Zhou et al. 2014). The wave propagation behavior of an exponentially graded transversely isotropic half-space is analyzed based on a new set of potential functions (Eskandari-Ghadi and Amiri-Hezaveh 2014). The wave propagation through a FG layer is studied by expanding displacement components in power series in the thickness direction which results in recursion relations among the displacement expansion functions (Golub, Boström, and Folkow 2013). Wave propagation has been analytically studied in gradient solids and structures like an infinite space, a simple axial bar, a Bernoulli–Euler flexural beam and a Kirchhoff flexural plate, and the influence of the micro-elastic and micro-inertia characteristics on dispersion curves has also been probed (Papargyri-Beskou, Polyzos, and Beskos 2009). A functionally graded piezoelectric slab is discussed to explore its transient response by using Laplace transform technique (Lin, Ing, and Ma 2015). An analytical model for small-scaled FG beams was presented to analyze the flexural wave propagation based on the nonlocal strain gradient theory (L. Li, Hu, and Ling 2015). In a recent research, nanotubes conveying fluid are subjected to wave propagation, in which, tubes are modeled as FG beams whose material properties varies through the thickness direction (Filiz and Aydogdu 2015).

2.4 Gradient of material properties in FGMs

A key point in modelling FGMs is how to model their property gradient. In literature different methods have been used to model the variation of material property in FGMs. Most common methods employed by researchers are exponential functions, power-law functions and sigmoid

functions. The reason for using these specific functions is to simplify the governing equations. The exponential law is generally applied for studying fracture mechanics of FGMs (Delale and Erdogan 1983; Suresh and Mortensen 1998; Chalivendra, Shukla, and Parameswaran 2003). The power-law function is also applied in many researches (Bao and Wang 1995b; Sun and Luo 2011b; F. Jin and Guo 2013) in which the material properties depend on the volume fraction of FGMs. In cases of exponential and power law functions, it has been observed that the stress concentration occurs in one of the interfaces in which the material is continuous but experience a sharp gradient. To resolve this issue, another law called sigmoid law was suggested which is the combination of two power-law functions (Chung and Chi 2006).

Modelling the behaviour of FGMs analytically is limited to the use of specific functions mentioned above. To represent the solution for general material gradient in FGM structures with complex geometries and boundary conditions, numerical methods are necessary. FEM known as one of the most popular numerical methods for engineering problems can be used to study static and dynamic properties of FGMs. In some efforts, FGMs were modelled by using conventional homogeneous elements (Anlas, Santare, and Lambros 2000; Marur and Tippur 2000). Considering the elastic property as a function of the position at the element level, the idea of graded element in the finite element formulation was suggested (Lee and Erdogan 1994). A multiple isoparametric element was investigated to calculate stress intensity factor in a cracked FGM plate, and it was concluded that graded elements are much more efficient than conventional homogeneous elements (Zou, Wu, and Li 2000). The performance of graded elements was compared to conventional elements in some boundary value problems and the result showed that quadratic graded elements are superior to conventional homogeneous elements with the same shape functions (Kim and Paulino 2002a). The consistency and stability

conditions for solutions obtained with graded elements are also investigated (Paulino and Kim 2007). Graded elements have been used to study fracture mechanics of FGMs as will be discussed in following parts. However, the potential difficulties which may occur in using conventional homogeneous elements, instead of graded elements, in fracture problems have still not been fully discussed.

2.5 Fracture mechanics of FGMs

As mentioned in previous parts, there is a wide range of applications for FGMs in engineering problems. Ceramic-metal FGMs are a main category of these materials. Since ceramic materials are brittle, studying the fracture mechanics of FGMs is demanding and will help in better understanding the FGMs bahaviour. In the following discussion, the most important researches performed about fracture of FGMs are reviewed. These works are categorized based on static or dynamic loading conditions, also based on analytical or numerical methods of solutions. In numerical methods, the main attention has been paid to the FEM.

2.5.1 Analytical approaches in static problems

The influence of spatial variation of elastic parameters on the fracture behaviour of FGMs has stimulated significant interests among researchers. The behaviour of crack tip fields in general nonhomogeneous materials has been extensively studied. It has been shown that the square root singularity of the stress field at the crack tip prevails for nonhomogeneous materials (Delale and Erdogan 1983). The basic idea of fracture mechanics of FGMs has been studied based on the extension of the traditional fracture mechanics concepts (Erdogan 1995). It was shown that when the crack grows from the ceramic-rich region to metal-rich region in alumina-nickel FGM, the

fracture toughness increases (Z. H. Jin and Batra 1996). The stress field at the crack tip of stationary crack aligned along the exponential gradient direction was determined by using an asymptotic analysis coupled with the Westergaard stress function. The first six terms of the stress field were determined for both opening and shear modes, and the influence of the material gradient on the stress field was discussed (Parameswaran and Shukla 2002). A similar approach was employed to study the crack inclined to the material gradient direction. Exponential form of the material gradient was considered and the first four terms in the expansion of the stress field were determined by superimposing the opening and shear modes. The influence of the inclination direction on the stress field was evaluated (V. B. Chalivendra, Shukla, and Parameswaran 2003). The solution was further extended to model linear material gradient using the same approach. The material gradient was considered along and inclined to the crack alignment and the influence of material gradient on the stress field was investigated (Jain, Rousseau, and Shukla 2004). Fracture of FGM strips with embedded or surface cracks was considered by modelling the FGM strips as piecewise homogeneous layers and solving the governing integral equations numerically (Wang, Mai, and Noda 2006). The effect of FGM coating on apparent fracture toughness of a thick-walled cylinder was studied for the case where two diametrically-opposed edge cracks emanate from the inner surface of the cylinder (Afsar and Song 2010). The thermo-mechanical fracture behaviour of interface cracks in a FGM/homogeneous bimaterial has been studied (Petrova and Schmauder 2014). Recently a theoretical approach was proposed for extending the double cantilever beam model to FGMs based on two-dimensional theory of elasticity (Chu et al. 2015). An analytical model was developed for investigating collinear cracks in FGMs (Pan, Song, and Wang 2015).

2.5.2 Numerical approaches in static problems with focus on FEM

Although, analytical solutions provide good background for better understanding of FGMs behaviour, due to the complexity of governing equations, they are limited to simple boundary conditions. Therefore, more attention has been paid to establishing effective numerical solutions for analyzing fracture behaviour of FGMs. Systematic finite element calculations were conducted to examine the multi-crack fracture of ceramic/metal coatings under mechanical and thermal loading (Bao and Wang 1995a). The application of the finite element method (FEM) for analyzing cracked and uncracked FGM plates was probed by using homogeneous elements with different elastic properties (Anlas, Santare, and Lambros 2000). Characteristics of the singular crack tip field in a FGM with linear material variation is inspected using FEM with very fine rectangular elements around the crack tip (Marur and Tippur 2000).

Other numerical techniques have been used or integrated to FEM for investigating stress fields near the crack tips. For instance, the strain smoothing technique used in the meshless nodal integration method has been adapted to the standard FEM to introduce the smoothed finite element method (SFEM) (G. R. Liu, Dai, and Nguyen 2007). SFEM provides more flexible treatment of element shapes and easier evaluation of shape functions, among other advantages (G. R. Liu, Nguyen-thoi, and Lam 2009; G. R. Liu, Nourbakhshnia, and Zhang 2011; Chen et al. 2011). Extended finite element method (XFEM) has also been extensively used in analyzing crack growth by adding discontinuity to the FEM (Belytschko and Black 1999; Moes, Dolbow, and Belytschko 1999). The main advantages of the XFEM are allowing the application of regular mesh for crack problems without remeshing around the crack tip as the crack advance (Dolbow and Gosz 2002; Singh, Mishra, and Bhattacharya 2011; Bayesteh and Mohammadi 2013; S. S. Hosseini, Bayesteh, and Mohammadi 2013; Goli and Kazemi 2014; Shojaee and Daneshmand

2015). The boundary element method (BEM) or boundary integral equation method (BIEM) has been employed for describing the crack problems in FGMs (Galvis and Sollero 2014; C. Zhang, Sladek, and Sladek 2003; Ch Zhang et al. 2003; Ch Zhang, Sladek, and Sladek 2005; Gao et al. 2008). Scaled boundary finite element method (SBFEM) which is a semi-analytical approach has been proposed for analyzing crack problems (C. Song and Wolf 1998), which is advantageous in relaxing mesh refinement and using asymptotic enrichment functions to deal with the singularity around the crack tip (C. Song, Tin-loi, and Gao 2010) together with the flexible element shapes (Ean Tat Ooi et al. 2012; E T Ooi et al. 2013). Recently, a new SBFEM procedure was proposed to investigate the fracture behaviour of FGMs in which the cracked polygon shape functions reproduce the singularity at the crack tip (T. Lee, Leok, and McClamroch 2011; Tat, Sundararajan, and Tin-loi 2015). Besides the discussed methods, the singular quarter point elements are also popular in modeling the FGM crack problems since they remove the need for very fine mesh at the crack tip. Graded finite elements have been used for evaluating mode-I and mixed mode two-dimensional crack problems and compared with different approaches (Kim & Paulino 2002b), in which the singularity is treated by moving the middle node of the element to the quarter point.

2.5.3 Analytical approaches in dynamic problems

Crack problems for FGMs have been extensively studied. The crack problem in a FGM under torsional impact loading was studied by using Laplace transform and Hankel Transform and solving the Fredholm integral equation (C. Y. Li, Zou, and Duan 1999). Dividing the elastic region in a FGM into layers with different material properties, Laplace transform and Fourier transform techniques were used, and the singular integral equations of the entire elastic region

were solved by considering the boundary conditions between layers under transient anti-plane loading (Wang, Han, and Du 2000). Laplace and Fourier transform methods were further employed to investigate dynamic crack problems in FGMs with more general loadings and boundary conditions (C Li et al. 2001; Chunyu Li and Weng 2001; Itou 2001; Guo et al. 2004; Choi 2004). The orientation of the crack with respect to the material gradient direction was considered, and a finite crack arbitrarily oriented with respect to the material gradient direction in a FGM subjected to incident elastic time harmonic waves was investigated by using Fourier transform (Ma et al. 2005; Ma et al. 2007). The asymptotic analysis of the crack tip fields with higher order terms originated from the material gradient was represented to study a transient crack propagating inclined to the property gradient direction in FGMs (V. Chalivendra and Shukla 2005). Crack problems in orthotropic FGMs were also analyzed. A closed form solution of DSIFs was suggested using Laplace and Fourier transform methods for a semi-infinite crack in an orthotropic FGM under in-plane impact loading (Hongmin et al. 2008). Further, a model was established including two different FGM media with collinear cracks located at each of these FGM media. Using Fourier transform method the anti-plane transient fracture problem was solved and the influence of the mismatch of material properties on DSIFs was investigated (Y. D. Li, Lee, and Dai 2008). The fracture behaviour of a FGM coating with multiple defects under time harmonic excitation was studied by employing distributed dislocation technique and Fourier transform (Bagheri, Ayatollahi, and Asadi 2013). Although, the above mentioned works provide analytical solutions for dynamic fracture of FGMs, but, due to the complexity of governing equations, they are limited to simple geometries and boundary conditions.

2.5.4 Numerical approaches in dynamic problems with focus on FEM

Different numerical methods such as FEM, BEM, Mesh free method, SBFEM, and XFEM have been used in literature to study dynamic fracture mechanics. The BEM significantly reduce the computational burden since only the boundary of the model should be discretized (Dominguez and Gallego 1992). Meshless methods are able to provide the solution without need to a mesh (Belytschko et al. 1995). This method is more suitable for growing cracks in dynamic problems. The SBFEM developed from the governing equations of elastodynamics, has been introduced as a semi-analytical numerical technique for modelling engineering problems. This method is based on finite elements but require a discretization only on the boundary. So, it combines the advantages of the FEM and BEM (C. Song and Wolf 1997). The above mentioned methods have been extended to study dynamic fracture of FGMs. The *J*-integral has been coupled with the FEM and element free Galerkin method to describe dynamic fracture problems in FGMs (Chang-Chun, Peixiang, and Ziran 2002). Using the BEM a hyper-singular time-domain traction BIEM was proposed for investigation of the transient dynamic crack properties in FGMs. Employing this method, a finite crack in an infinite linear elastic FGM under anti-plane crack-face impact loading was studied (Ch Zhang et al. 2003). DSIFs in FGMs under a transient dynamic loading were evaluated by using meshless method (Sladek et al. 2006). Determination of the DSIFs in cracked FGMs was studied by extending the interaction integral method (conservation integral) to the dynamic condition for non-homogeneous materials, and implemented in FEM (S. H. Song and Paulino 2006). Also, XFEM has been used to study moving cracks in FGMs, since it resolves the issues for remeshing the model as the crack grows. In addition, enriched shape functions are employed to represent the displacement discontinuity along the crack faces and singularity of stress at crack tips. The dynamic behaviour of a fixed crack in an orthotropic

media was simulated by means of an XFEM procedure (Motamedi and Mohammadi 2010). Further, transient dynamic behaviour of a stationary crack in a FGPM under impact loading was studied by using XFEM (P. Liu et al. 2013). The scaled boundary polygons formulation, in which the domain is discretized using polygons with arbitrary number of sides, was extended to elastodynamic problems for computing the SIF in FGMs. For uncracked polygons shape functions were considered to be linearly complete. In a cracked polygon, singularity was modelled analytically (Chiong et al. 2014a; Chiong et al. 2014b).

Numerical methods also play a significant role in the analysis of the dynamic behaviour of uncracked FGMs. A drawback of FEM is that a large number of finite elements are required to reach the accurate solution at high frequencies. To remove this drawback, spectral finite element, which uses the exact solution of the governing differential equation in the frequency domain as the interpolating function for element formulation, was suggested (Doyle 1988). Regular graded finite elements have been suggested to simulate elastic wave propagation in functionally graded materials under low frequency dynamic loading (Santare, Thamburaj, and Gazonas 2003). The spectral method has been used to study the wave propagation in FGMs. A Spectral Layer Element has been employed to study the wave propagation in anisotropic inhomogeneous layered media under high frequency impact loading (Chakraborty and Gopalakrishnan 2004). Also, wave propagation in FGMs and layered media was analyzed by using the space-time discontinuous Galerkin method (Aksoy and Şenocak 2009). In addition, piecewise homogeneous models have been used, in which the FGM was divided into homogeneous subdomains. Then, existing techniques available for homogeneous materials were used to solve the problem. A layer-wise finite element formulation was introduced for scrutinizing the behavior of a dynamically loaded FGM cylindrical shell (Yas et al. 2011). In order to obtain an efficient finite

element mesh, a topology-based data structure and a parallel framework for unstructured mesh were integrated, and wave propagation in three dimensional FGM was studied (Park and Paulino 2011). A generalized finite difference method which does not need to generate any mesh for solving the equation of motion was also employed to compute wave velocity in a thick hollow FGM cylinder under shock loading (S. M. Hosseini 2012a; S. M. Hosseini 2012b). Numerical modelling of the Lamb wave propagation in FGMs was conducted by using a two-dimensional time-domain spectral finite element method under high frequency loading (Hedayatrasa et al. 2014).

Although different numerical methods have been used to investigate fracture of FGMs, still there is no detailed discussion about the role of material gradient in describing the stress field at the crack tip in the FEM format. In this research, a special finite element procedure will be suggested to determine static and dynamic fracture parameters in FGMs with involving the influence of the material gradient at the crack tip. Based on this method, SIFs and higher order terms originated from the material gradient can be obtained explicitly, which result in an accurate solution.

Chapter 3

Graded regular finite elements in static and dynamic problems

In this chapter regular graded finite elements (FEs) will be discussed and their applications for modelling the static and dynamic behaviour of linearly elastic isotropic FGMs in two dimensional problems will be investigated. Comparison with conventional homogeneous FEs will be conducted and the performance of graded FEs in terms of accuracy and reliability of the solution will be evaluated.

3.1 Graded regular FEs for modelling static problems

The procedure of analyzing the static behaviour of FGMs using FEM begins with considering the equilibrium equation in Cartesian coordinate system as presented in Eq. (3.1).

$$\sigma_{ij,j} + b_i = 0, \quad (i,j = 1,2) \tag{3.1}$$

where, σ_{ij} and b_i are the components of the Cauchy stress tensor and the components of the body force vector respectively, and the comma denotes differentiation with respect to the coordinate. The stress-strain and the strain-displacement relations are

$$\sigma_{ij} = \lambda \delta_{ij} \varepsilon_{kk} + 2\mu \varepsilon_{ij}, \qquad (i, j = 1,2) \tag{3.2}$$

$$\varepsilon_{ij} = (1/2)(u_{j,i} + u_{i,j}). \qquad (i, j = 1,2) \tag{3.3}$$

In the above relations, δ_{ij} is the Kronecker delta defined as,

$$\delta_{ij} = \begin{cases} 0 & \text{if i} \neq \text{j,} \\ 1 & \text{if i} = \text{j.} \end{cases} \tag{3.4}$$

ε_{ij} represent the components of Eulerian small strain tensor. λ and μ are Lame constants defined as,

$$\lambda = \frac{E\nu}{(1 + \nu)(1 - 2\nu)}, \quad \mu = \frac{E}{2(1 + \nu)}, \tag{3.5}$$

where E and ν are the Young's modulus and the Poisson's ratio, respectively.

Substituting Eqs. (3.2) and (3.3) into the equilibrium equation, the governing equations will be obtained, and are known as the Navier-Cauchy equations,

$$\mu u_{i,jj} + (\lambda + \mu)u_{j,ji} + b_i = 0. \tag{3.6}$$

In FE analysis, the displacement field in a typical n-node isoparametric FE can be interpolated from the nodal values (u_i) using shape functions denoted by N_i,

$$\boldsymbol{u} = \sum_{i=1}^{n} N_i \, u_i. \tag{3.7}$$

For a 9-node quadrilateral Lagrangian element shown in Fig. 3.1, the shape functions can be represented in the following form,
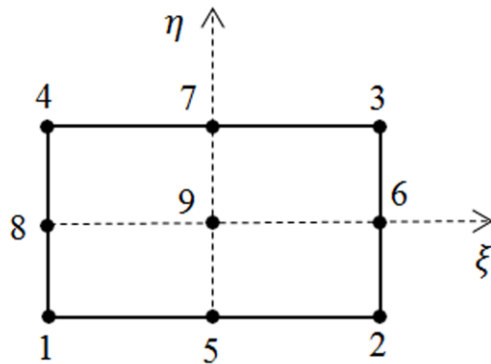
Fig. 3.1. Illustration of a 9-node quadrilateral Lagrangian element

$$N_1 = \frac{1}{4}(\xi^2 - \xi)(\eta^2 - \eta), N_2 = \frac{1}{4}(\xi^2 + \xi)(\eta^2 - \eta), \; N_3 = \frac{1}{4}(\xi^2 + \xi)(\eta^2 + \eta)$$

$$N_4 = \frac{1}{4}(\xi^2 - \xi)(\eta^2 + \eta), N_5 = \frac{1}{2}(1 - \xi^2)(\eta^2 - \eta), N_6 = \frac{1}{2}(\xi^2 + \xi)(1 - \eta^2) \tag{3.8}$$

$$N_7 = \frac{1}{2}(1 - \xi^2)(\eta^2 + \eta), N_8 = \frac{1}{2}(\xi^2 - \xi)(1 - \eta^2), N_9 = (1 - \xi^2)(1 - \eta^2),$$

where, ξ and η are natural coordinates used for describing the geometry and local field variables at the element level. The relation between (ξ, η) and (x, y) is

$$x = \sum_{i=1}^{9} N_i(\xi, \eta) x_i, \tag{3.9}$$

$$y = \sum_{i=1}^{9} N_i(\xi, \eta) y_i,$$ (3.10)

in which, x_i and y_i are nodal coordinate positions in the global coordinates.

Correspondingly, the elastic strain in the element can be determined as,

$$\{\boldsymbol{\varepsilon}\} = \begin{bmatrix} \dfrac{\partial N_1}{\partial x} & 0 & \dfrac{\partial N_i}{\partial x} & 0 & \dfrac{\partial N_n}{\partial x} & 0 \\[2mm] 0 & \dfrac{\partial N_1}{\partial y} & \cdots & 0 & \dfrac{\partial N_i}{\partial y} & \cdots & 0 & \dfrac{\partial N_n}{\partial y} \\[2mm] \dfrac{\partial N_1}{\partial y} & \dfrac{\partial N_1}{\partial x} & \dfrac{\partial N_i}{\partial y} & \dfrac{\partial N_i}{\partial x} & \dfrac{\partial N_n}{\partial y} & \dfrac{\partial N_n}{\partial x} \end{bmatrix} \begin{Bmatrix} u_{x_1} \\ u_{y_1} \\ \vdots \\ u_{x_i} \\ u_{y_i} \\ \vdots \\ u_{x_n} \\ u_{y_n} \end{Bmatrix} = [B]\{\boldsymbol{u}\},$$ (3.11)

in which, $[B]$ represents the derivative of the shape functions with respect to the global coordinates. Since shape functions in Eq. (3.8) are implied in terms of local coordinates, the partial differentials with respect to x and y in Eq. (3.11) should be converted to partial differentials with respect to ξ and η by using the chain rule as,

$$\begin{Bmatrix} \dfrac{\partial N_i}{\partial \xi} \\[2mm] \dfrac{\partial N_i}{\partial \eta} \end{Bmatrix} = \begin{bmatrix} \dfrac{\partial x}{\partial \xi} & \dfrac{\partial y}{\partial \xi} \\[2mm] \dfrac{\partial x}{\partial \eta} & \dfrac{\partial y}{\partial \eta} \end{bmatrix} \begin{Bmatrix} \dfrac{\partial N_i}{\partial x} \\[2mm] \dfrac{\partial N_i}{\partial y} \end{Bmatrix} = [J] \begin{Bmatrix} \dfrac{\partial N_i}{\partial x} \\[2mm] \dfrac{\partial N_i}{\partial y} \end{Bmatrix},$$ (3.12)

$$\begin{Bmatrix} \dfrac{\partial N_i}{\partial x} \\[2mm] \dfrac{\partial N_i}{\partial y} \end{Bmatrix} = [J]^{-1} \begin{Bmatrix} \dfrac{\partial N_i}{\partial \xi} \\[2mm] \dfrac{\partial N_i}{\partial \eta} \end{Bmatrix},$$ (3.13)

where $[J]$ is the Jacobian matrix relating the local coordinate derivatives to the global coordinate derivatives.

The stress inside the element can then be calculated using the Hooke's law,

$$\{\boldsymbol{\sigma}\} = [D(x,y)]\{\boldsymbol{\varepsilon}\}, \tag{3.14}$$

where $[D]$ is the elastic matrix, for the plane stress condition,

$$[D(x,y)] = \frac{E(x,y)}{1-v^2(x,y)}\begin{bmatrix} 1 & v(x,y) & 0 \\ v(x,y) & 1 & 0 \\ 0 & 0 & \dfrac{1-v(x,y)}{2} \end{bmatrix}, \tag{3.15}$$

and for plane strain condition,

$$[D(x,y)] = \frac{E(x,y)}{(1+v(x,y)).(1-2v(x,y))}\begin{bmatrix} 1-v(x,y) & v(x,y) & 0 \\ v(x,y) & 1-v(x,y) & 0 \\ 0 & 0 & \dfrac{1-2v(x,y)}{2} \end{bmatrix}, \tag{3.16}$$

with $E(x,y)$ and $v(x,y)$ being the Young's modulus and the Poisson's ratio which vary with position. Since mechanical properties of FGMs vary continuously with the coordinate position, it is essential to consider this variation of material properties through the element level in order to have an accurate estimation for the elastic problems. An efficient way for achieving this goal is to interpolate material properties through the element based on its nodal values using the same shape functions used for description of displacements and field variables.

In general, the variation of material property P in such an element can be expressed as,

$$P = \sum_{i=1}^{n} N_i P_i, \tag{3.17}$$

where P_i represent the values of P at nodes of the element and N_i are the shape functions. Fig. 3.2 illustrates a graded element with distributed material properties in contrast with a conventional homogeneous element which has a uniform property over the element.
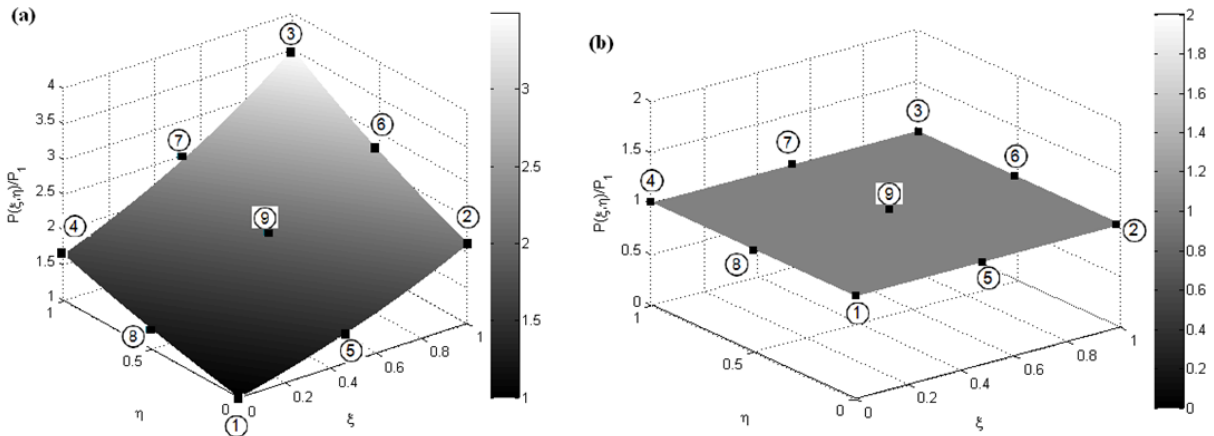
Fig. 3.2. Schematic illustration of the distribution of material properties in a 9-node quadrilateral (a) graded element and (b) conventional homogeneous element

The elastic matrix $[D(x, y)]$, for the plane strain condition, can then be represented in the following form,

$$[D] = \frac{\sum_i N_i E_i}{(1 + \sum_i N_i \nu_i)(1 - 2\sum_i N_i \nu_i)} \begin{bmatrix} 1 - \sum_i N_i \nu_i & \sum_i N_i \nu_i & 0 \\ \sum_i N_i \nu_i & 1 - \sum_i N_i \nu_i & 0 \\ 0 & 0 & \frac{1 - 2\sum_i N_i \nu_i}{2} \end{bmatrix}. \tag{3.18}$$

where E_i and ν_i are values of the Young's modulus and the Poisson's ratio at nodal positions and the summation is over all nodes of the element.

The total potential energy for the element can be obtained as,

$$\Pi = \frac{1}{2}\int_{A_e} \{\varepsilon\}^T\{\sigma\}dA_e - \{u\}^T\{f\} = \frac{1}{2}\{u\}^T \int_{A_e} [B]^T[D][B]dA_e \{u\} - \{u\}^T\{f\}, \tag{3.19}$$

where A_e is the area of the element, and $\{f\}$ is a load vector given by

$$\{f\} = \int_{A_e} [N]^T [F] dA,$$ (3.20)

where body forces are neglected and $[F]$ is the vector of surface force. Superscript T represents the transpose of the matrix.

Differentiating the total potential energy with respect to the nodal displacements and equating it to zero lead to the minimum potential energy which corresponds to the equilibrium condition. Therefore, the equilibrium equation in the FEM format appears as,

$$\int_{A_e} [B]^T [D][B] dA_e \{u\} = \{f\},$$ (3.21)

which is usually written in the following form.

$$[K]\{u\} = \{f\}.$$ (3.22)

$[K]$ is the element stiffness matrix represented as,

$$[K] = \int_{A_e} [B]^T [D][B] dA_e,$$ (3.23)

Material properties contribute to the build up of the stiffness matrix $[K]$. Hence, the importance of proper modelling of the variation of material properties in the FEM format is quite clear.

By solving the system of algebraic equations mentioned in Eq. (3.22) the displacement field can be achieved. Stresses must be calculated from the attained solution for strains. For FGMs when traditional elements are used the stress-strain relation is approximated inside the elements. Thus, in the FE analysis of FGMs using regular elements, higher price should be paid by making the

element size very small. While, it is possible to reach the desired accuracy level with less effort by implementing graded elements which satisfies the stress-strain relation.

3.2 Investigation of the performance of regular graded elements in static problems

In this section, three specific examples will be studied using the introduced finite element procedure for modelling FGMs by using 9-node quadrilateral graded elements. In these examples the attempt is made to compare the performance of graded elements with conventional homogeneous elements to explain the advantages of graded elements from a new perspective less discussed in the literature.

3.2.1 The Saint-Venant principle in a FGM beam under simple tension

In the first example, the Saint-Venant principle in a FGM beam under simple tension will be investigated. Consider the plane-stress problem of an isotropic elastic two dimensional FGM beam under uniform tension applied to its free end as shown in Fig. 3.3 (L. Zhao, Chen, and Lü 2012). Dimensions and loading conditions of the problem are the same as those considered in the reference work and shown in Fig. 3.3 (i.e. $2h = 1$ m, $l/2h = 5$, $\tilde{\sigma} = 1$ N/m). It is assumed that the variation of the Young's modulus in the FGM beam is exponential in both axial and transverse directions, i.e.

$$E(x, y) = E_0 \, e^{\alpha x + \beta y}, \tag{3.24}$$

where α and β are gradient indices, and E_0 is the value of the Young's modulus at the coordinate reference point. It is supposed that $\alpha h = 0.01$, $\beta h = 1$, and $E_0 = 200$ GPa. Also, it is assumed that the Poisson's ratio has the constant value of $\nu = 0.29$ through the beam.
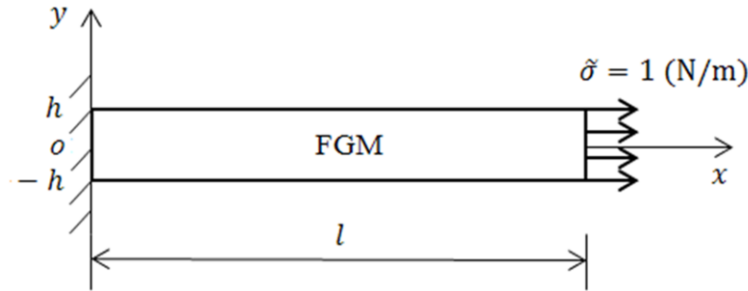
Fig. 3.3. A two dimensional FGM cantilever beam under uniform tension at its free side

3.2.1.1 Comparison of the graded element solution with the analytical solution

Figs. 3.4 and 3.5 represent the distribution of the axial stress along the contours defined in the vertical direction at the clamped end $(x = 0)$ and its vicinity $(x = 0.5h)$, respectively. In these figures the local behavior of the axial stress predicted by the Saint-Venant principle is well depicted. It should be mentioned that the analytical solution involves numerical calculations with truncating a specific series (with infinite terms) at a certain number and forming a finite expansion, which in turn may affect the solution accuracy. However, good agreement between the results obtained by using the graded elements and the analytical technique demonstrates the validity of the solution from graded elements.

Table 3.1 introduces the meshing information used for modelling the problem by graded elements. Since the major variation of the Young's modulus occurs in the transverse direction, it is tried to observe the convergence of the results by increasing the number of graded elements in the transverse direction. In Fig. 3.4 the stress converges reasonably with about 500 graded

elements, whereas, the similar convergence happens with about 250 grade elements at a little farther distance from the clamped end as shown in Fig. 3.5. This issue can be explained by the Saint-Venant principle. Since the stress distribution becomes smoother at farther distances from the clamped end, therefore, relatively less number of elements is required to reach a similar accuracy at those locations.

Table 3.1. Meshing information used for modelling the problem with 9-node graded elements

Total number of FG elements	250	500	750	1000
Number of elements in each column	5	10	15	20
Number of elements in each row	50	50	50	50
Total number of nodes	1111	2121	3131	4141
Total number of DOFs	2222	4242	6262	8282
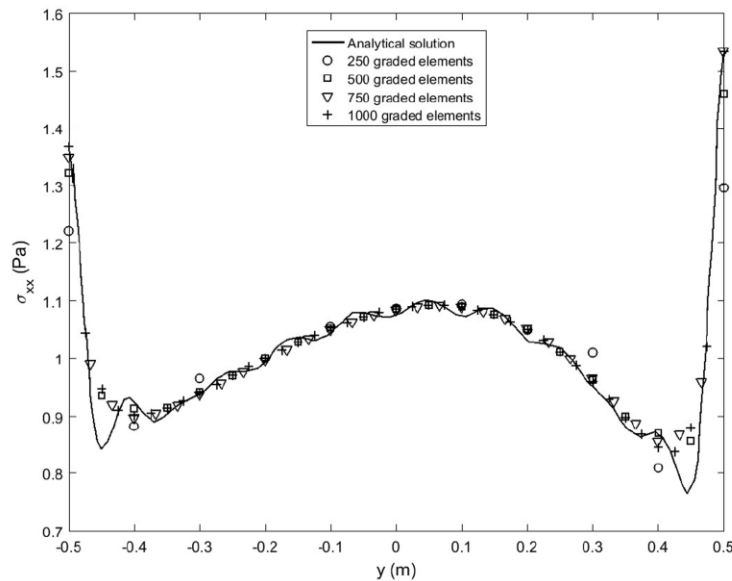
Fig. 3.4. The comparison of the axial stress along the beam thickness at $x = 0$ between the obtained solution by using graded elements and the analytical solution (L. Zhao, Chen, and Lü 2012)
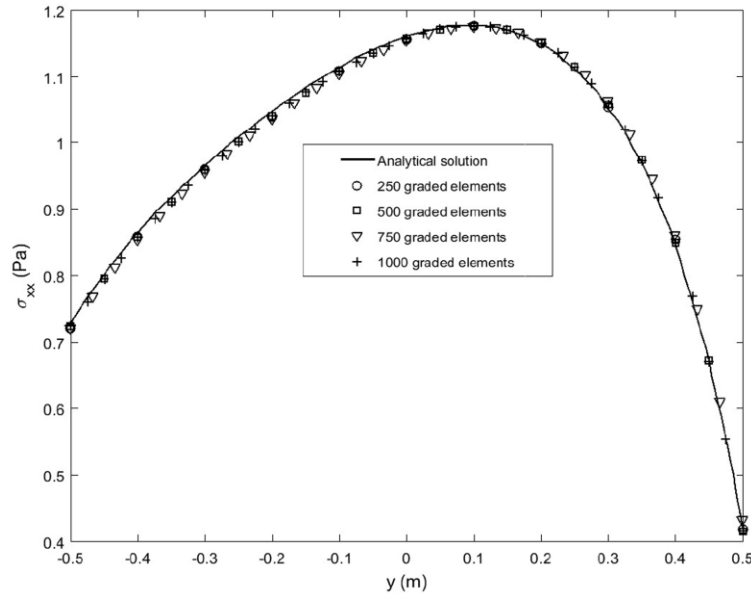
Fig. 3.5. The comparison of the axial stress along the beam thickness at $x = 0.5h$ between the obtained solution by using graded elements and the analytical solution (L. Zhao, Chen, and Lü 2012)

3.2.1.2 Comparing the performance of graded elements and conventional homogeneous elements

In this part, the problem is modelled first using graded elements and then using conventional homogeneous elements. For convenience it is assumed that the Young's modulus varies only in the vertical direction. When the homogeneous elements are employed, the problem is treated as a piecewise homogeneous layered structure whose material properties experience a sudden change at the interface of layers, whereas, the average value for material properties at each layer has been considered. This average value is equal to the actual value of the material properties at the middle of each layer.

To provide a background for the comparison between the performance of graded and homogeneous elements, first, the behaviour of the FGM beam is compared to the homogeneous beam. The normal stress distribution on the contour along the thickness direction at $x = 0$ and $x = 0.5h$ is drawn in Figs. 3.6 and 3.7 for different gradient indexes, using the graded elements. The response of the homogeneous beam is obtained when the gradient index βh equals to zero.

The difference in the behaviour of the homogeneous and FGM beams is clearly displayed. This difference is an important aspect in the investigation of the performance of homogeneous and graded elements. As mentioned, use of homogeneous elements for modelling FGMs leads to a piecewise homogeneous model in which each homogeneous layer follows the solution achieved for $\beta h = 0$. Therefore, the natural distinction in the behaviour of the homogeneous and FGM structures can be regarded as a source of dissimilarity in the performance of the two element types. This reasoning can well explain how homogeneous elements are not reliable for modelling FGMs. It can also predict the cases for which homogenous elements provide good estimation.

Fig. 3.6. The stress contour along the beam thickness at $x = 0$ for different indexes of material gradient βh
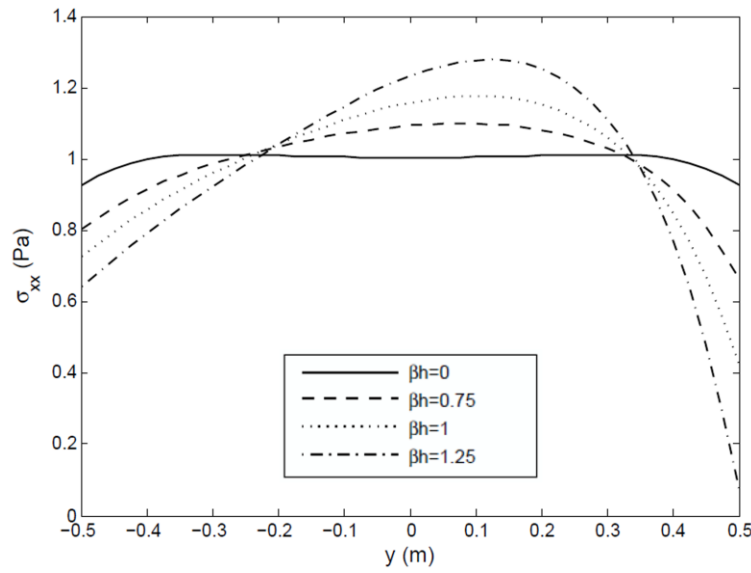
Fig. 3.7. The stress contour along the beam thickness at $x = 0.5h$ for different indexes of material gradient βh

Figs. 3.8 and 3.9 display the axial stress distribution on the contour along the beam thickness at $x = 0$ and $0.5h$ for a gradient index of $\beta h = 0.75$ achieved by graded elements against homogeneous elements. These figures show that results converge faster when graded element are employed. Therefore, much less effort is required to reach the reliable solution by graded elements. For instance, it can be seen from Fig. 3.8 that there is a good estimation at the middle of the beam thickness by employing 250 graded elements, while, for reaching the same level of accuracy by using homogeneous elements, more than 1000 elements are needed. There will usually be about 20% error for the estimation using homogeneous elements with the same number of graded elements. In Fig. 3.9 there is a similar comparison between the results reached by graded elements and homogeneous elements at $x = 0.5h$. It can be observed that by refining the mesh in the case of homogeneous elements, the results approach to the solution obtained from graded elements.

Fig. 3.8. The comparison of the axial stress along the beam thickness at $x = 0$ for $\beta h = 0.75$ between the obtained solutions by using graded elements and homogeneous elements

Fig. 3.9. The comparison of the axial stress along the beam thickness at $x = 0.5h$ for $\beta h = 0.75$ between the obtained solutions by using graded elements and homogeneous elements

Besides, it is found that the use of homogeneous elements for analyzing FGMs may result in a wrong trend of stress distribution inside homogeneous elements. This problem is indicated in the following comparisons between conventional and graded element solutions. For example, the accurate axial stresses obtained by graded element solution in Fig. 3.9 within the interval of $y = [-0.5,0]$ exhibits an ascending trend, while in contrast, the axial stresses through each homogeneous layer, i.e. using homogeneous elements, represent a descending trend. This weakness is originated from the contribution of axial and lateral strains for computing the axial stress based on the Eq. (3.14) in which the material gradient is neglected. This drawback can be eliminated by using the real stress-strain relations as pointed in Eq. (3.14). Although the axial strain decreases within the vertical direction at $y = [-0.5,0]$ in the graded element model, however, the elastic constants simultaneously grow in that direction so that the overall contribution of strains and elastic constants leads to a continuous ascending pattern of axial stress. This interpretation can also be repeated in other examples.

Figs. 3.10 and 3.11 indicate the graded and homogeneous element solution for axial stresses with a higher material gradient index $\beta h = 1.25$. As expected, with sharper change of material properties, the difference between the stress profiles for homogeneous and FGM beam at the considered path increases, which in turn leads to a higher dissimilarity between the homogeneous and graded element solutions. Table 3.2 summarizes these differences at selected locations, and implies that the percentage error for homogeneous element outputs rises with sharper gradient of material properties.

Fig. 3.10. The comparison of the axial stress along the beam thickness at $x = 0$ for $\beta h = 1.25$ between the

obtained solutions by using graded elements and homogeneous elements

Fig. 3.11. The comparison of the axial stress along the beam thickness at $x = 0.5h$ for $\beta h = 1.25$ between the

obtained solutions by using graded elements and homogeneous elements

Table 3.2. The percentage of error for the axial stresses through the beam thickness at $x = 0$ and $x = 0.5h$ obtained by using various numbers of homogeneous elements

		$\beta h = 0.75, x = 0$					
	Hom. elements	$y = -0.5$	$y = -0.3$	$y = -0.1$	$y = 0.1$	$y = 0.3$	$y = 0.5$
	250	1.46	21.47	16.97	15.74	18.67	21.28
	500	4.29	9.14	8.26	7.54	8.51	9.21
	1000	4.87	4.48	4.17	3.80	4.64	2.71
		$\beta h = 0.75, x = 0.5h$					
		$y = -0.5$	$y = -0.3$	$y = -0.1$	$y = 0.1$	$y = 0.3$	$y = 0.5$
	250	13.46	15.71	14.67	15.35	16.90	11.48
	500	7.26	7.51	7.39	7.51	7.70	8.28
	1000	3.80	3.82	3.81	3.71	3.83	5.26
Error %		$\beta h = 1.25, x = 0$					
		$y = -0.5$	$y = -0.3$	$y = -0.1$	$y = 0.1$	$y = 0.3$	$y = 0.5$
	250	10.69	34.83	29.53	26.90	26.48	29.52
	500	9.31	15.42	14.18	13.09	14.37	13.80
	1000	7.62	7.33	6.96	6.63	7.68	5.07
		$\beta h = 1.25, x = 0.5h$					
		$y = -0.5$	$y = -0.3$	$y = -0.1$	$y = 0.1$	$y = 0.3$	$y = 0.5$
	250	24.32	24.79	24.53	25.81	26.96	38.12
	500	12.37	12.54	12.39	12.75	12.20	0
	1000	6.14	6.37	6.25	6.40	6.75	0.48

The strain profiles at the same paths are plotted for the homogeneous and FGM beams in Figs. 3.12 and 3.13. It is worthy to mention that the slope of the strain curves is almost constant through the beam thickness except for the lower and upper boundaries of both homogeneous and FGM beams. The discrepancy in strains obtained using homogeneous and graded elements can be justified by considering Eqs. (3.22) and (3.23). In other words, the stiffness matrix is dominant in determining strains. The agreement between the strains reached by homogeneous and graded elements in Figs. 3.14 and 3.15 shows that the varying elastic matrix $[D]$ does not cause the stiffness matrix to change significantly. However, at the lower boundary of the beam where a sharper change happens in strains, some differences occur as displayed in Fig. 3.14. It means that the solution is more sensitive to the material gradient at the lower boundary of the beam. Since, such a sharp change of strains does not exist in Fig. 3.13, strains achieved by the two element types are very close to each other at $x = 0.5h$.
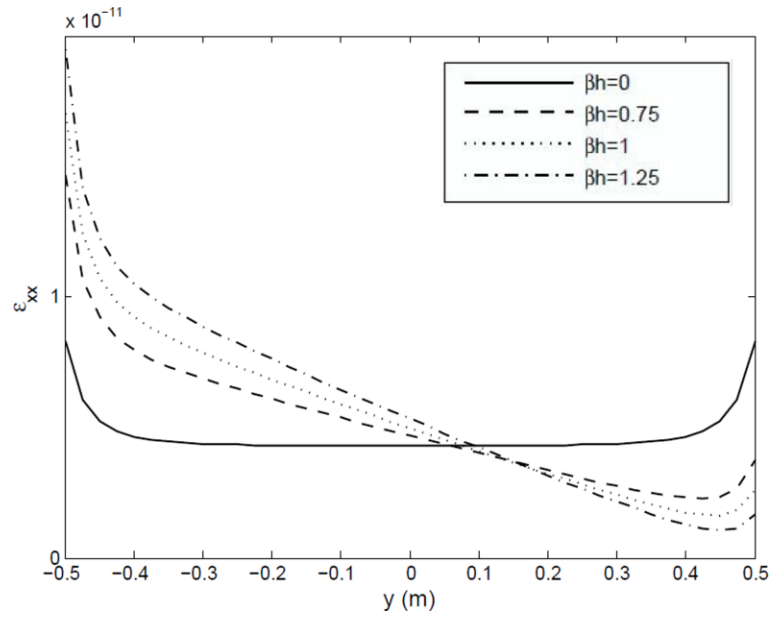
Fig. 3.12. The strain contour along the beam thickness at $x = 0$ for different indexes of material gradient βh
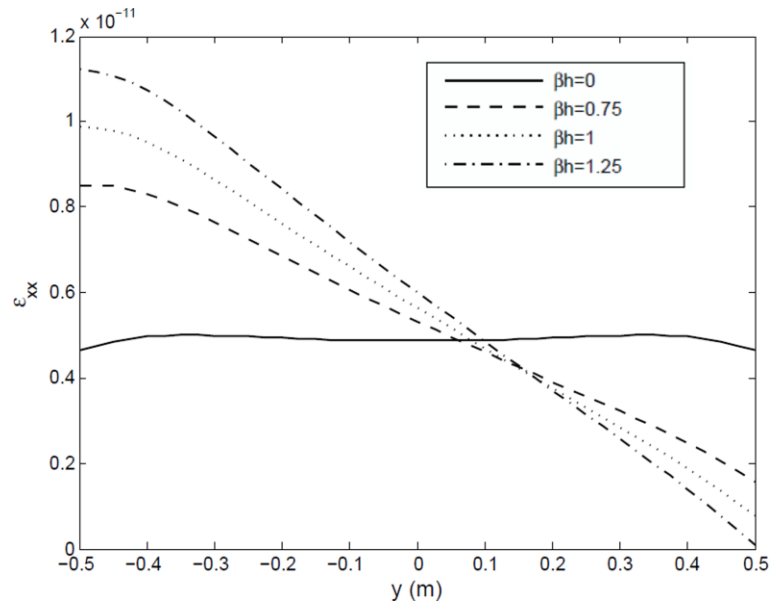
Fig. 3.13. The strain contour along the beam thickness at $x = 0.5h$ for different indexes of material gradient βh
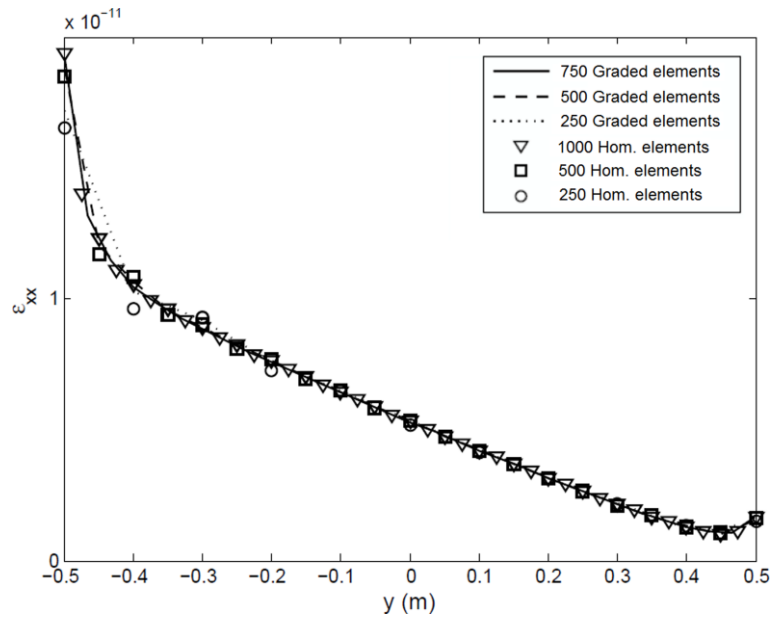
Fig. 3.14. The comparison of the axial strain along the beam thickness at $x = 0$ for $\beta h = 1.25$ between the

obtained solutions by using graded elements and homogeneous elements
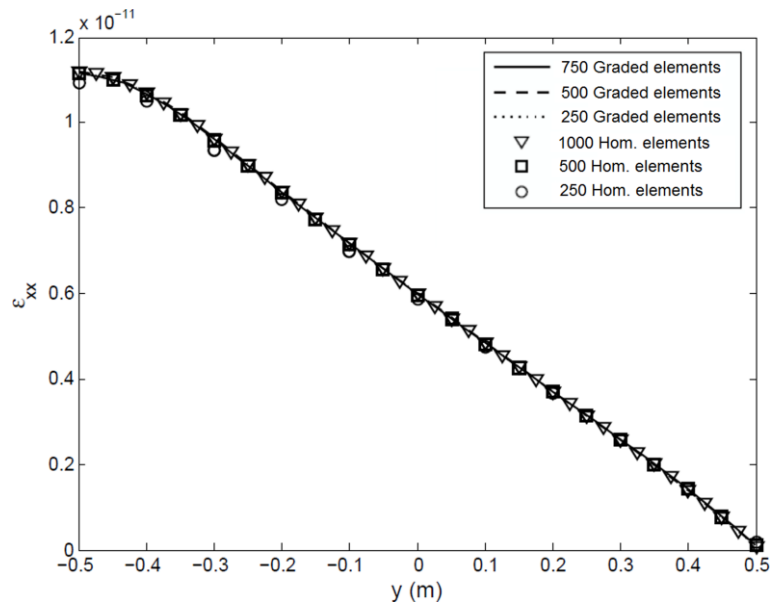
Fig. 3.15. The comparison of the axial strain along the beam thickness at $x = 0.5h$ for $\beta h = 1.25$ between the

obtained solutions by using graded elements and homogeneous elements

3.2.2 FGM beam under uniform bending moment

In the second example, the same FGM beam considered in the previous part is investigated under a uniform bending loading as shown in Fig. 3.16. The profiles of the axial stress at the same paths mentioned before are drawn in Figs. 3.17 and 3.18. Dissimilar profiles of the stress along the beam thickness for FGM and homogeneous material point to the natural difference in solutions achieved by using graded and homogeneous elements. Here, because of the slight changes in stress profiles at the clamped end and its neighborhood, it is sufficient to probe the solutions at $x = 0.5h$ for the case that $\beta h = 1.25$.
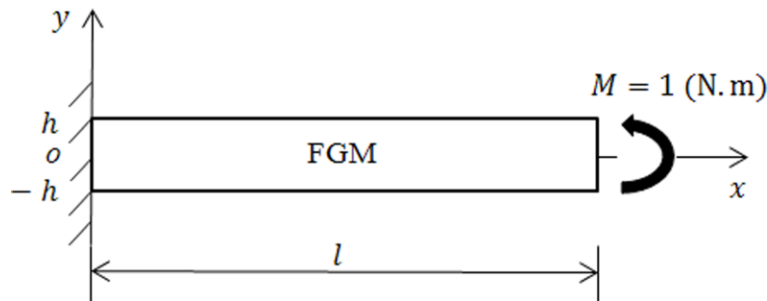
Fig. 3.16. A two dimensional FGM cantilever beam under uniform bending
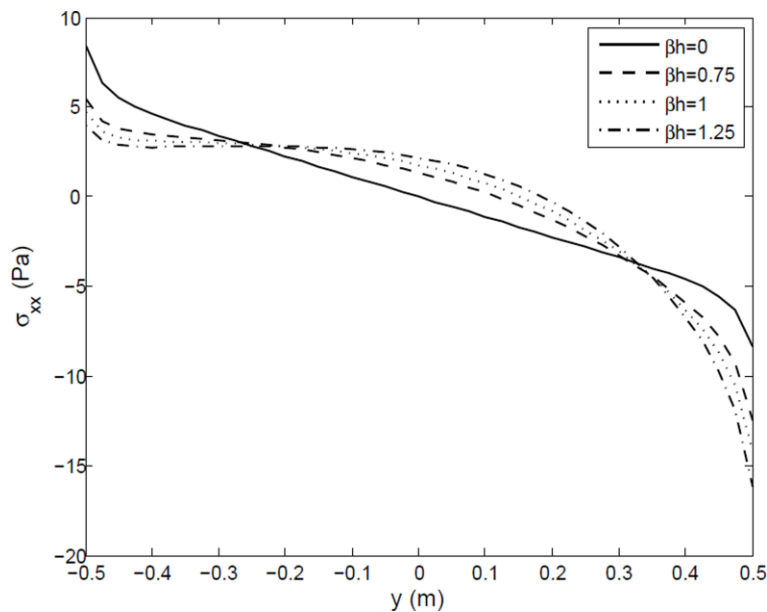
Fig. 3.17. The stress contour along the beam thickness at $x = 0$ for different indexes of material gradient $\boldsymbol{\beta h}$
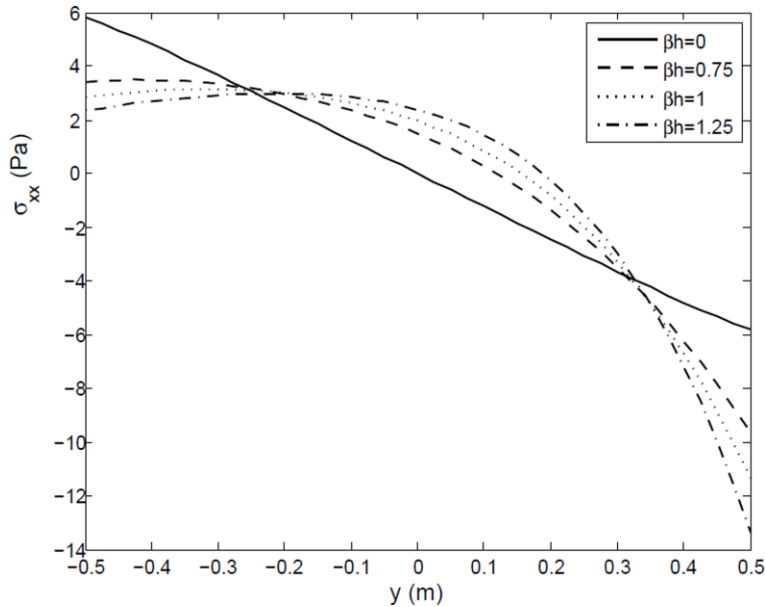
Fig. 3.18. The stress contour along the beam thickness at $x = 0.5h$ for different indexes of material gradient βh

The comparison between solutions reached by using graded and homogeneous elements in Figs. 3.19 and 3.20 shows that greater number of conventional homogeneous elements are required in order to achieve the same accuracy obtained by employing graded elements. In these plots it is indicated that the solution has converged using only 250 graded elements. In contrast, when homogeneous elements are employed, considerable error is observed even after using 1000 elements which implies the necessity of refining the mesh further. In table 3.3 the error in axial stresses caused by modelling the problem with homogeneous elements is calculated. It is found that using 250 homogeneous elements results in about 25% error, while it reduces to about 12% and 6% by utilizing 500 and 1000 elements, respectively.
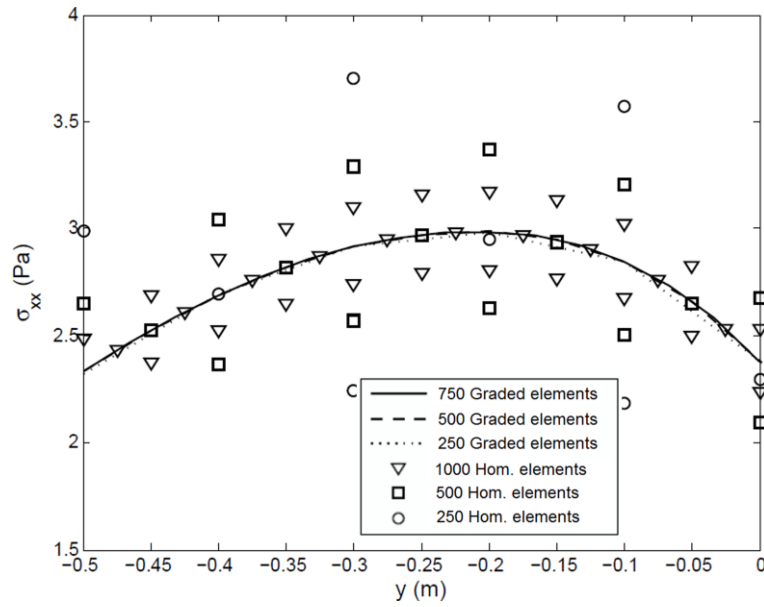
Fig. 3.19. The comparison of the axial stress along the beam thickness from $y = -0.5$ to 0 at $x = 0.5h$ for $\beta h = 1.25$ between the obtained solutions by using graded elements and homogeneous elements
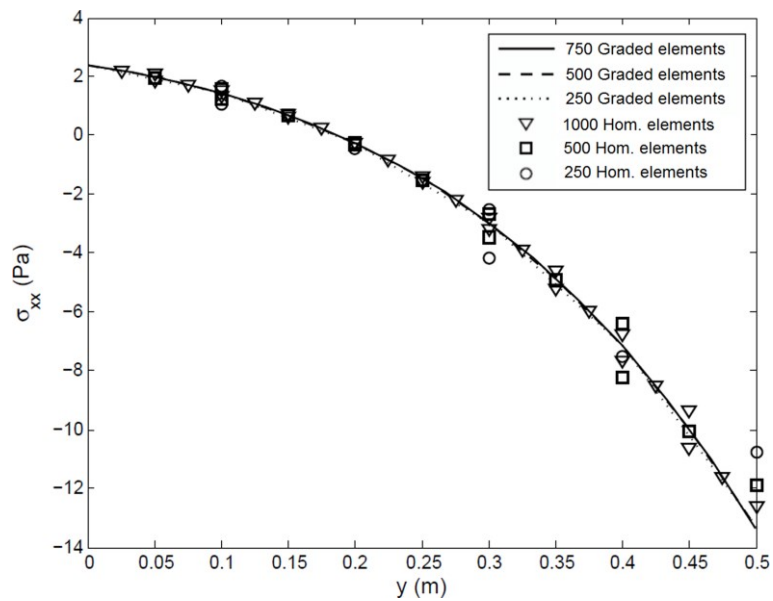
Fig. 3.20. The comparison of the axial stress along the beam thickness from $y = 0$ to 0.5 at $x = 0.5h$ for $\beta h = 1.25$ between the obtained solutions by using graded elements and homogeneous elements

Table 3.3. The percentage of error for the axial stresses through the beam thickness at $x = 0.5h$ obtained by using various numbers of homogeneous elements

	$\beta h = 1.25, x = 0.5h$						
	Homogeneous elements	$y = -0.5$	$y = -0.3$	$y = -0.1$	$y = 0.1$	$y = 0.3$	$y = 0.5$
	250	28.08	26.86	25.51	27.25	39.10	19.38
Error %	500	13.50	12.87	12.55	13.06	15.67	10.93
	1000	6.67	6.29	6.20	6.30	6.97	5.77

The axial strains along the considered contours are displayed in Figs. 3.21 and 3.22. The similarity between the shape of profiles of strains obtained for homogeneous and FGM beam implies that good estimation can be achieved for axial strains even by modelling the problem with homogeneous elements. That is proved by computing strains with different element numbers for both element types as shown in Fig. 3.23.
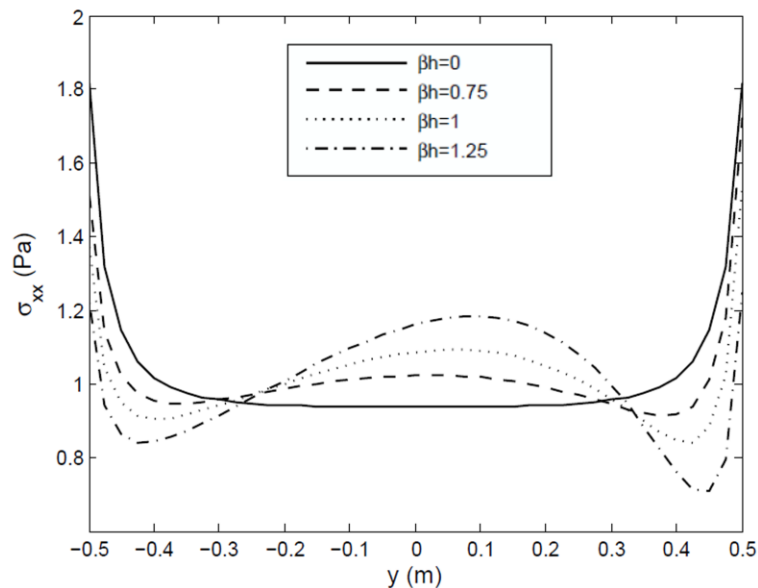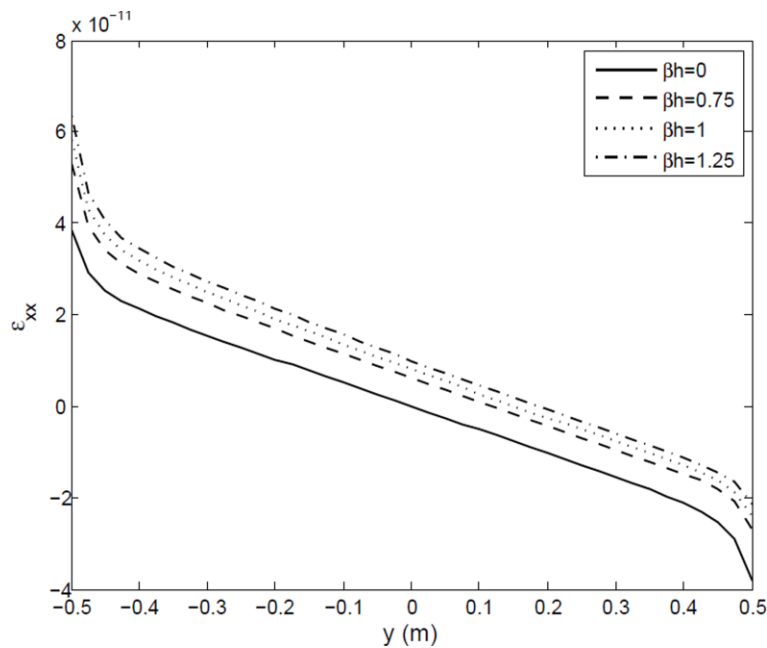

Fig. 3.21. The strain contour along the beam thickness at $x = 0$ for different indexes of material gradient βh
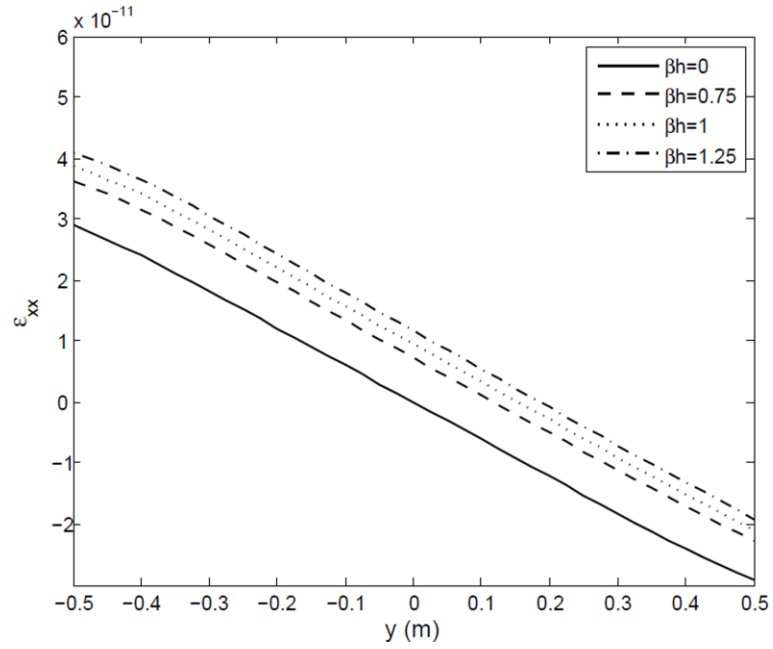
Fig. 3.22. The strain contour along the beam thickness at $x = 0.5h$ for different indexes of material gradient $\boldsymbol{\beta h}$
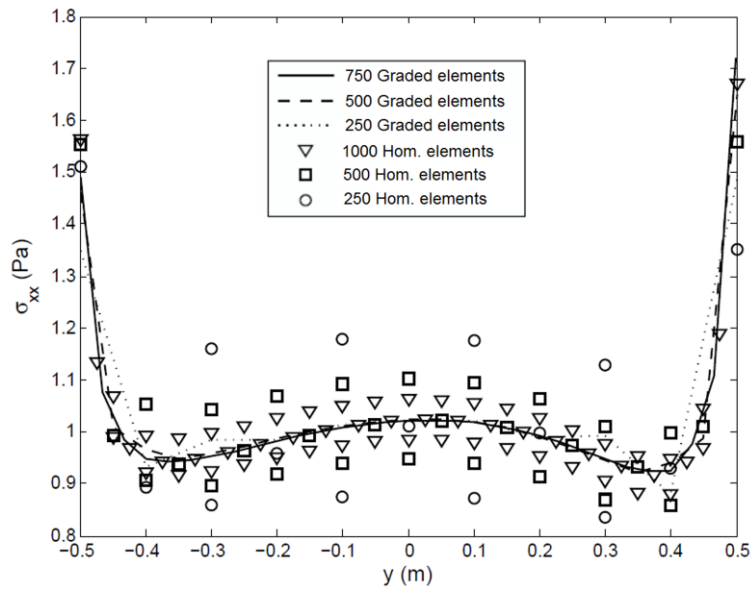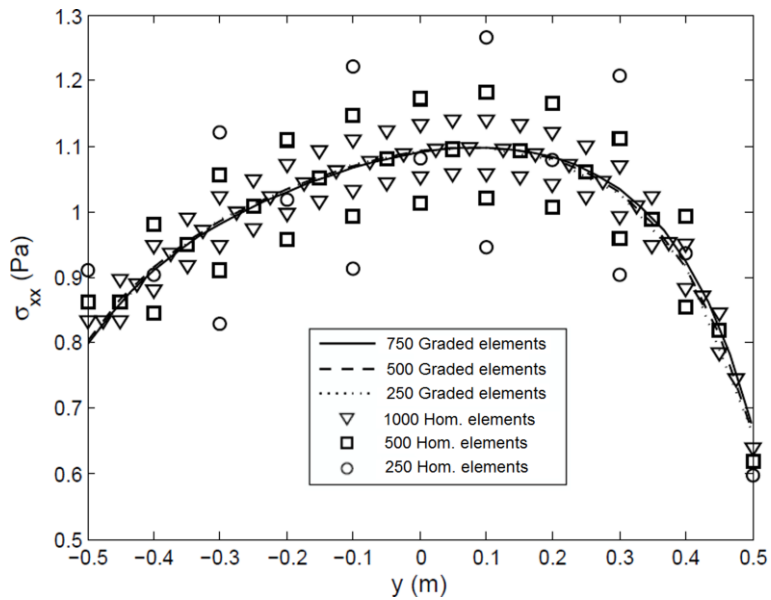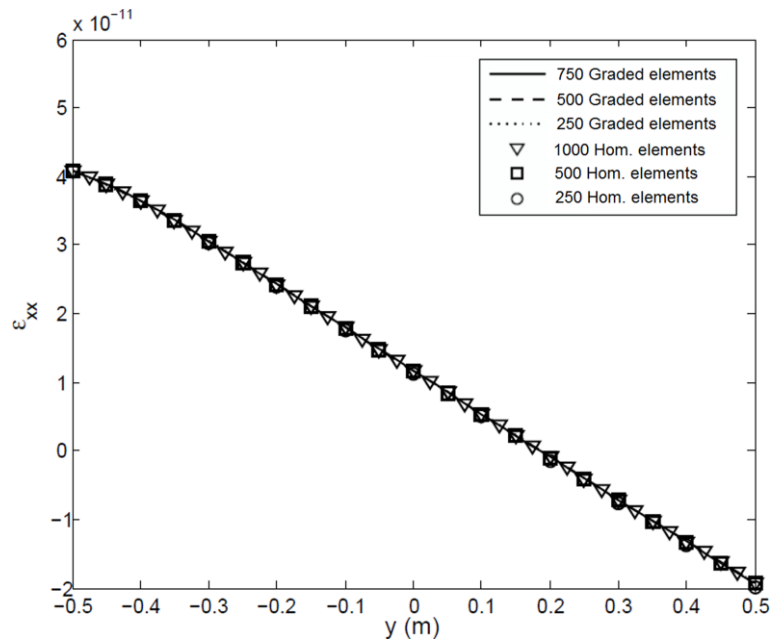

Fig. 3.23. The comparison of the axial strain along the beam thickness at $x = 0.5h$ for $\boldsymbol{\beta h = 1.25}$ between the obtained solutions by using graded elements and homogeneous elements

3.2.3 Indentation of a flat rigid punch to a FGM substrate

The last example designed to compare the reliability and accuracy of the solution obtained by using homogeneous and graded elements is related to the indentation of a flat rigid punch to a FGM substrate as exhibited in Fig. 3.24.
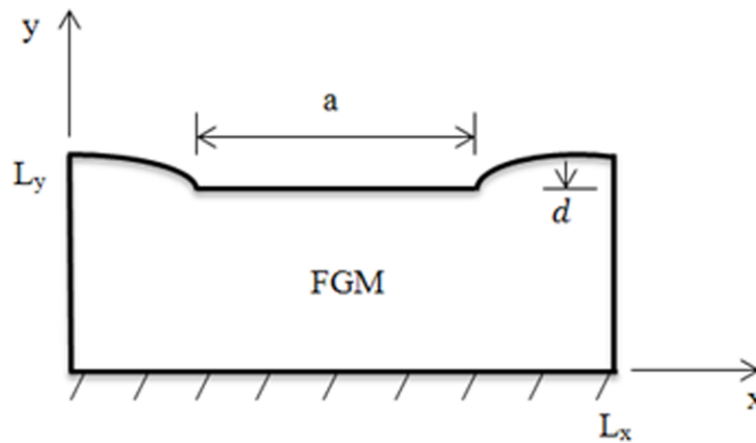
Fig. 3.24. A FGM substrate indented by a flat rigid punch

Imagine a FGM substrate with width $L_x = 2\,m$ and height $L_y = 1\,m$ indented by a flat rigid punch with the indentation depth of $d = 0.1\,mm$ (Fig. 3.24 exaggerate the deformation at the surface of the FGM). The elastic constants of the FGM substrate is supposed to vary exponentially in the y direction, and a reference value of 200 GPa is considered for the Young's modulus at the bottom, while the Poisson's ratio v has the constant value of 0.3 everywhere. The material gradient index represented by βL_y takes the value of zero for a homogeneous substrate and three other values as $1.5, 2$ and 2.5 for FGM substrates. The problem is solved under the plane strain condition. A path located at $x = 1$ along the y direction from the bottom to the top surface of the FGM is considered for investigating the results. Since the selected path is not close to the contact tips, the model can be meshed uniformly in order to provide a simple correlation between solutions reached by different numbers of homogeneous and graded elements.

Table 3.4. Meshing information for the model meshed with the 9- node graded and homogeneous elements

Total number elements	100	150	200	250	500	750	1000
Elements in each column	2	3	4	5	10	15	20
Elements in each row	50	50	50	50	50	50	50
Total number of nodes	505	707	909	1111	2121	3131	4141
DOFs	1010	1414	1818	2222	4242	6262	8282

The distribution of normal stresses and strains along the defined path are depicted for a range of material gradient indexes βL_y from 0 to 2.5 in Figs. 3.25 and 3.26. In contrast with the second example which displayed different stress profiles and similar strain profiles for homogeneous materials and FGMs, in this case the similarity between trends of stress can be observed in Fig. 3.25, while the distinction in profiles of strain distribution is clearly shown in Fig. 3.26. This issue is investigated in Fig. 3.27 which shows that despite some slight distinctions, stresses almost converge with the same number of elements.

On the other hand, the considerable difference between profiles of strain in homogeneous materials and FGMs leads to the distinction of solutions by homogeneous and graded elements. This issue is assessed by inspecting the strain convergence as illustrated in Fig. 3.28. It shows that although strains achieved by graded elements converge with 100 elements, for homogeneous elements the convergence happens with much greater number of elements. Table 3.5 indicates the percentage error at selected nodes caused by modelling the problem with homogeneous elements. It is interesting to see that 95% error occur in the element solution for strains at the middle of the path when employing 100 elements.
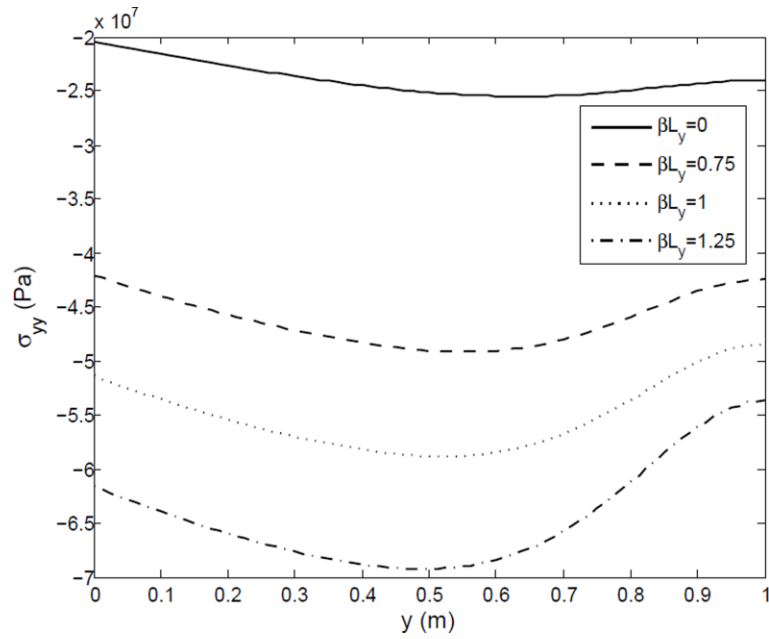
Fig. 3.25. The normal stress contour along the defined path for different indexes of material gradient
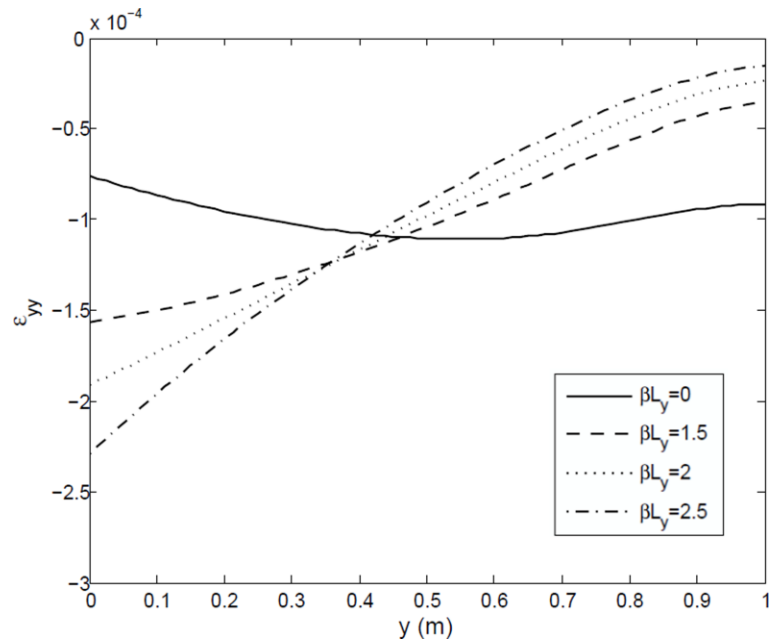
Fig. 3.26. The normal strain contour along the defined path for different indexes of material gradient
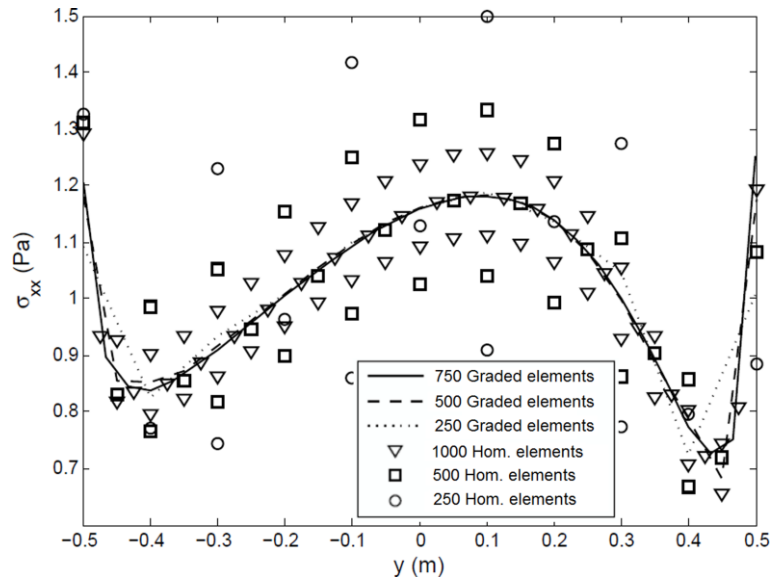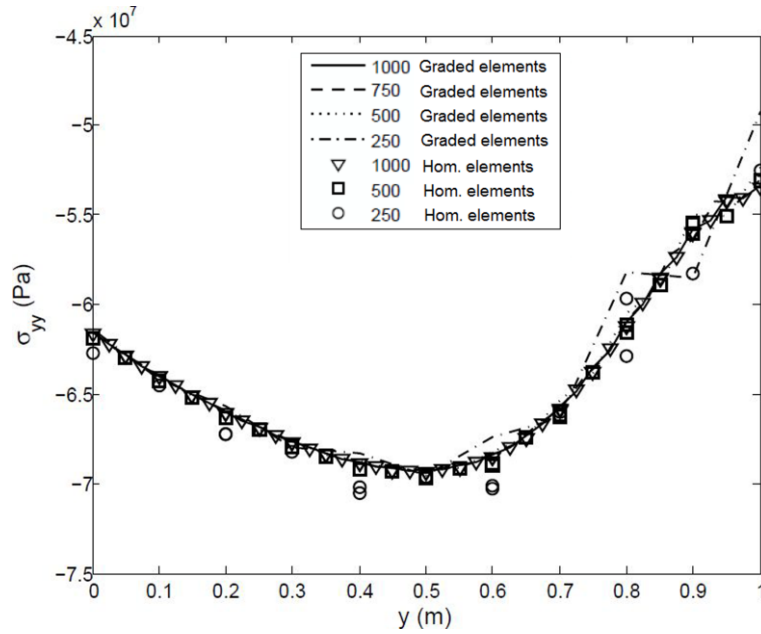
Fig. 3.27. The comparison of the normal stress along the defined path for $\beta L_y = 2.5$ between the obtained solutions by using graded elements and homogeneous elements
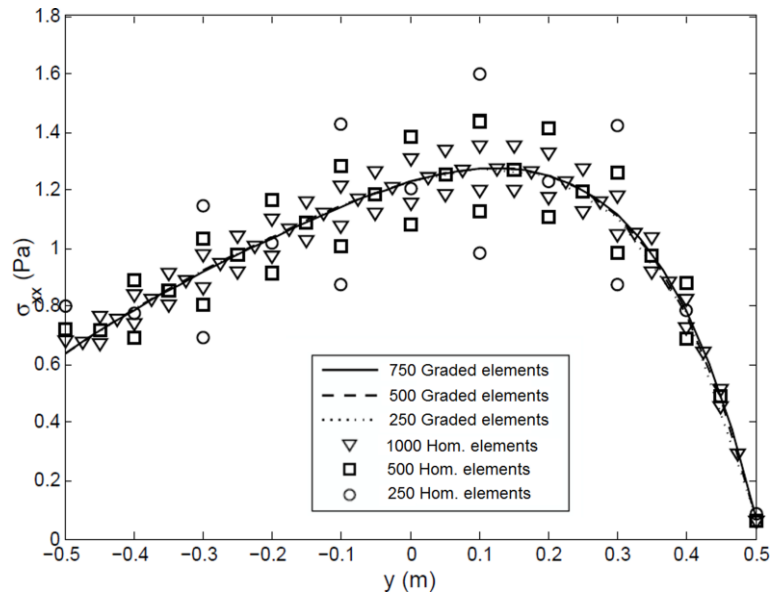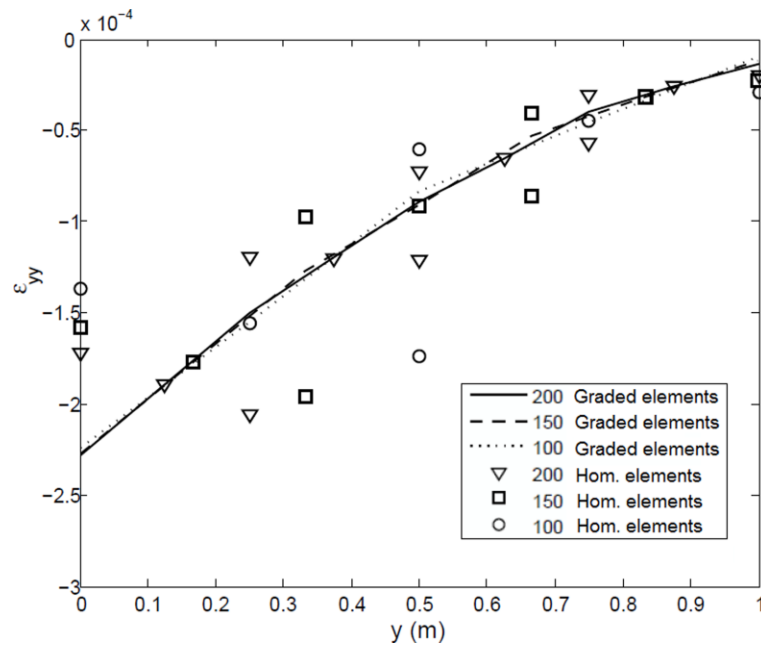

Fig. 3.28. The comparison of the normal strain along the defined path for $\beta L_y = 2.5$ between the obtained solutions by using graded elements and homogeneous elements

Table 3.5. The percentage of error for the axial strain through the defined path for $\beta L_y = 2.5$ obtained by using various numbers of homogeneous elements

	100 normal elements				
	$y = 0$	$y = 0.5$			$y = 1$
	39.92	95.07			52.07
	150 normal elements				
Error %	$y = 0$	$y = 0.33$		$y = 0.66$	$y = 1$
	30.46	51.28		51.43	16.48
	200 normal elements				
	$y = 0$	$y = 0.25$	$y = 0.5$	$y = 0.75$	$y = 1$
	24.45	38.02	35.50	45.91	7.27

3.3 Graded regular FEs for modelling dynamic problems

The FE formulation derived in section 3.1 expresses the static equilibrium condition of the FE assemblage. In these equilibrium conditions, the external loading may vary with time, which also causes displacements to vary with time. In such a case, Eq. (3.22) is a statement of equilibrium for any specific point in time. These solutions are valid under the quasi-static condition. However, if the loads vary rapidly with time, inertia forces become important. These inertia forces need to be considered to solve a real dynamic problem. They can be included as body forces. Assuming that the element accelerations are approximated in a similar way as used for displacements in Eq. (3.7), the contribution of the inertia forces to the equation of motion appear as, (Molavi Nojumi and Wang 2017b)

$$[M]\{\ddot{u}\} + [K]\{u\} = \{f\}, \tag{3.25}$$

in which $\{u\}$ and $\{f\}$ are time dependent vectors. The matrix $[M]$ is the global mass matrix, which is defined as,

$$M = \sum_m \int_{V^e} \rho \, N^T N \, dV^e, \tag{3.26}$$

where V^e is the volume of element, the index m is the element counter, and ρ represents the mass density.

In the case of FGMs, mass density as a material property changes based on the coordinate position. As a result, the distribution of the mass density over a graded element with n nodes can be considered by using Eq. (3.17) as,

$$\rho = \sum_{i=1}^{n} N_i \, \rho_i. \tag{3.27}$$

Thus, the global mass matrix for the FGM can be represented as,

$$M = \sum_m \int_{V^e} \left(\sum_{i=1}^{n} N_i \, \rho_i \right) N^T N \, dV^e, \tag{3.28}$$

Eq. (3.25) represents a system of second order linear differential equations which can be solved by using a proper finite difference technique. Two suggested solutions for such a system of equations are namely direct integration and mode superposition methods. In the direct integration method the equation of motion is numerically integrated with a step-by-step procedure, and it is not transformed to a new form before the integration. A simple idea which works in this method is satisfying the equation of motion at separate time intervals Δt apart.

There exists several traditional direct integration methods such as the central difference, Houbolt, Wilson θ, and Newmark methods. From the aforementioned methods each one has a specific advantage over the other methods upon considering the accuracy, time-step size, and the effort

required for working out the problem. The central difference method has been widely applied to the dynamical equations as an effective scheme. In this method, accelerations and velocities are written in the form of,

$$\ddot{u}_t = \frac{1}{\Delta t^2}(u_{t-\Delta t} - 2\,u_t + u_{t+\Delta t}),$$
(3.29)

$$\dot{u}_t = \frac{1}{2\Delta t}(u_{t+\Delta t} - u_{t-\Delta t}).$$
(3.30)

Displacements at the time "$t + \Delta t$" will be represented by considering the equation of motion at time "t" as,

$$[M]\{\ddot{u}\}_t + [K]\{u\}_t = \{f\}_t.$$
(3.31)

By substituting the acceleration and velocity from Eqs. (3.29) and (3.30) into Eq. (3.31), the equation of motion takes the following form.

$$\left(\frac{1}{\Delta t^2}[M]\right)\{u\}_{t+\Delta t} = \{f\}_t - \left([K] - \frac{2}{\Delta t^2}[M]\right)\{u\}_t - \left(\frac{1}{\Delta t^2}[M]\right)\{u\}_{t-\Delta t}.$$
(3.32)

After constructing the mass and stiffness matrices for the FGM structure as explained before, the initial values of displacements $\{u\}_0$, velocities $\{\dot{u}\}_0$, and accelerations $\{\ddot{u}\}_0$, need to be used in Eq. (3.32) in order to find $\{u\}_{\Delta t}$. It should be noted that knowing the initial displacements, initial accelerations can be calculated from Eq. (3.25). At the first step when $t = 0$, the term $\{u\}_{-\Delta t}$ is included in Eq. (3.32) which can be calculated as,

$$\{u\}_{-\Delta t} = \{u\}_0 - \Delta t\,\{\dot{u}\}_0 + \frac{\Delta t^2}{2}\{\ddot{u}\}_0$$
(3.33)

Finally, the problem will be solved by handling a set of algebraic equations in the matrix form.

As an important consideration in the use of the central difference scheme, it should be noted that the time step Δt should be smaller than a critical value Δt_{cr} which can be calculated from the mass and stiffness properties of the complete element assemblage. This condition expresses that,

$$\Delta t \leq \Delta t_{cr} = \frac{T_n}{\pi},$$

(3.34)

where T_n is the smallest period of the FE assemblage with n degrees of freedom.

3.4 Investigation of the performance of regular graded elements in dynamic problems

Consider a linear elastic isotropic FGM beam whose material properties vary along the x axis. The beam is loaded by a dynamic concentrated horizontal force applied to the middle of its free side as indicated in Fig. 3.29. It is assumed that Young's modulus and mass density vary exponentially while the Poisson's ratio remains constant.
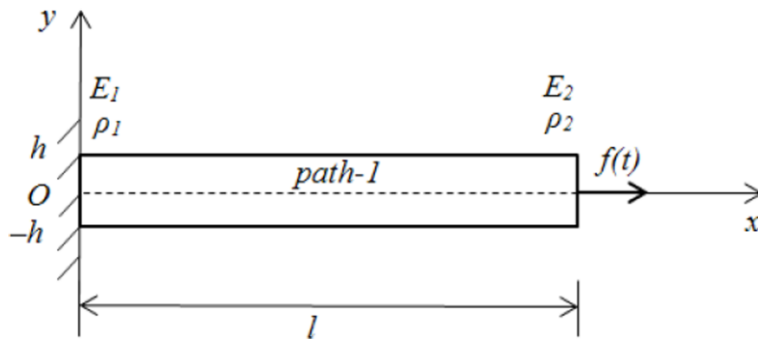
Fig. 3.29. A FGM beam under dynamical concentrated force at the middle of its free side

3.4.1 Verification of the dynamic solution obtained using regular graded elements

In order to evaluate the accuracy of the solution achieved by using the suggested graded elements, the dynamic solution is compared with the results obtained by simulating the problem

with the FEM software Ansys. For this purpose, the material gradient index is set to zero, i.e. the material is assumed to be homogeneous everywhere in the beam. The dynamic loading which represents one period of sinusoidal function is shown in Fig. 3.30. The information about parameters, meshing and time steps are mentioned in tables 3.6 and 3.7. It is worthy to mention that the loading frequency, meshing and time steps are adjusted in such a way that they are consistent with the restrictions regarding choosing the proper time steps as mentioned in Eq. (3.34).
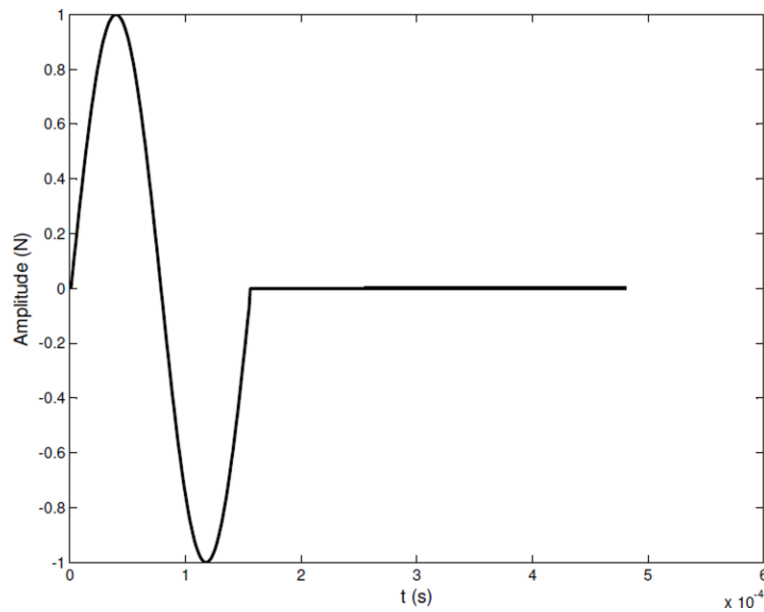
Fig. 3.30. Illustration of the applied sinusoidal load to the model

Table 3.6. Introducing parameters used in the model

l (m)	h (m)	E_2/E_1	ρ_2/ρ_1	E_1 (GPa)	ρ_1 (kg/m³)	ν	$f(t)$ (N)	f (Hz)
5	1	1	1	70	2700	0.3	$1\sin(2\pi f \times t)$	6420

Table 3.7. The meshing and time step information used in the model

Time step Δt (μs)	Time interval (ms)	Total number of elements	Element length (m)
1	0 - 0.48	500 (50×10)	0.1

A path is defined along the axis of the structure as shown in Fig. 3.29. Results are compared along this path. The horizontal component of displacement u_x at different locations on the considered path is plotted over time in Fig. 3.31. In addition, distribution of u_x along the considered path is shown at different times in Fig. 3.32. It is observed that the answers obtained by the written program in Matlab for using graded elements are in good agreement with the numerical outputs of the Ansys software. It should be pointed that there is no 9-node quadrilateral element in commercial FEM software Ansys. Thus, the simulation performed with Ansys involves the use of 8-node quadrilateral elements (plane 183).
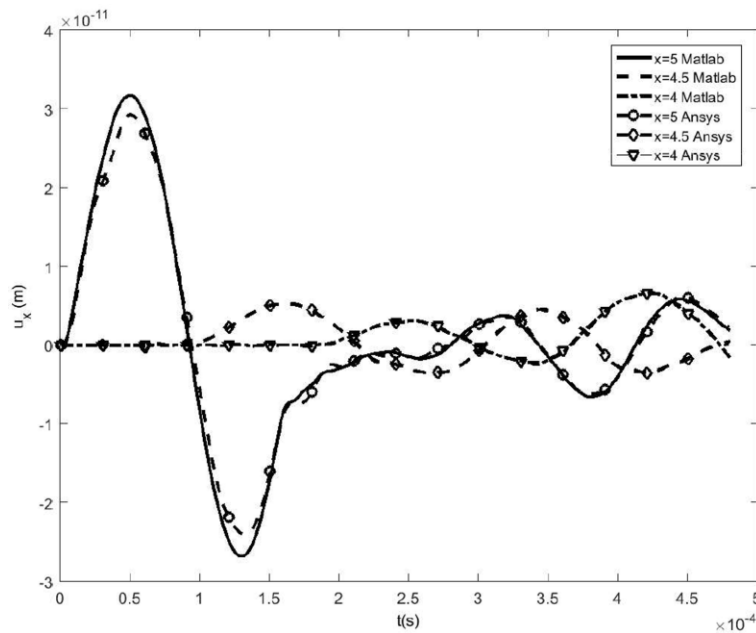
Fig. 3.31. Verification of the time history solution for $\boldsymbol{u_x}$ at different points along the considered path
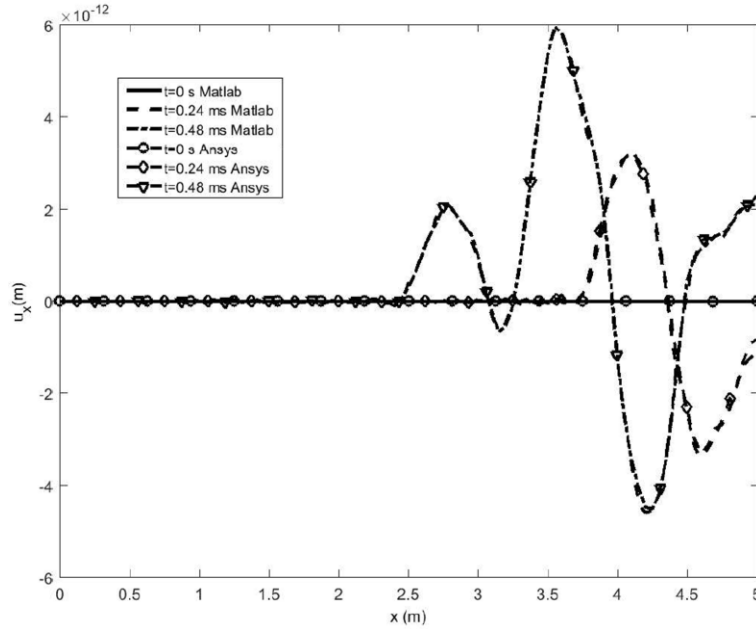
Fig. 3.32. Verification of the solution for distribution of $\boldsymbol{u}_x$ at different times along the defined path

3.4.2 Comparison between the regular graded and homogeneous elements in dynamic problem

The performance of the regular graded and homogeneous elements is compared in a specific problem under the dynamic loading. Consider a FGM structure as shown in Fig. 3.29 with properties and meshing information mentioned in tables 3.8 and 3.9. As expected, it is observed that when homogeneous elements are used, with refining the mesh, the answer approaches to the solution achieved with the graded elements. For this case, results obtained by graded and homogeneous elements are in a reasonable agreement. However, the required number of homogeneous elements is much greater than the number of graded elements needed for accurate solution, showing that graded elements are more efficient for modelling dynamic problems in FGMs. This issue is clearly depicted in the solution for ε_x along the defined pass at the middle of beam thickness in Fig. 3.33.

Table 3.8. Introducing material properties and parameters used in the FGM model

l (m)	h (m)	E_2/E_1	ρ_2/ρ_1	E_1 (GPa)	ρ_1 (kg/m³)	ν	$f(t)$ (N)	f (Hz)
2	1	20	3	70	2700	0.3	1sin(2πf × t)	3210

Table 3.9. The meshing and time step information used in the model

Time step Δt (μs)	Time interval (ms)	Total number of elements	Element length (m)	Element widths (m)
1	0 - 0.16	100 (10×10)	0.2	0.1
1	0 - 0.16	200 (20×10)	0.1	0.1
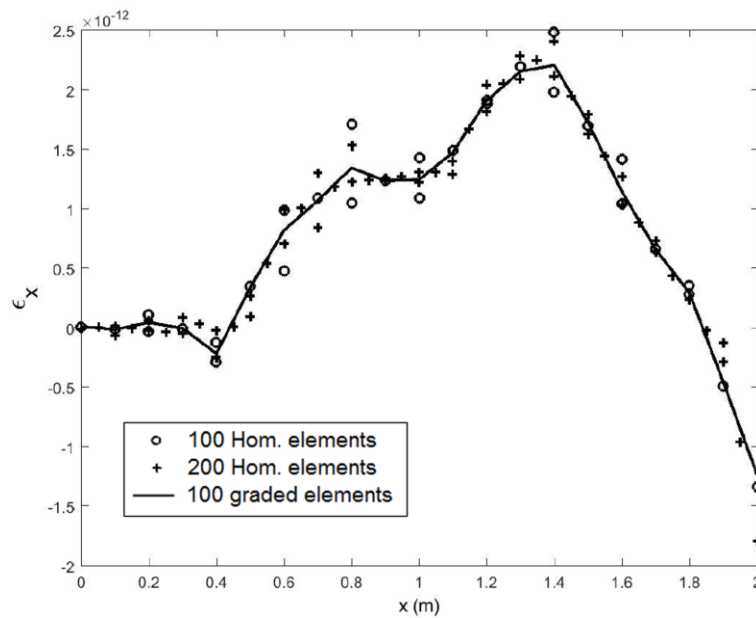
Fig. 3.33. The comparison of the FEM solution for the axial strain ε_x along the defined pass between graded and homogeneous elements

Graded elements always show reasonable distribution of field variables when convergence is achieved. Depending on the loading conditions homogeneous elements may perform differently, for example the stresses in FGM beam under simple tension and strains in a FGM substrate indented by a flat rigid punch show wrong trend of variation at the element level when homogeneous elements are used.

Chapter 4

Analysis of Crack Problems in Functionally Graded Materials Using Regular Graded Finite Elements

This chapter represents a comprehensive study on the application of regular graded finite elements to the analysis of linear elastic isotropic nonhomogeneous plates containing crack. A graded 9-node multiple isoparametric quadrilateral element is developed, in which both elastic and thermal properties vary at the element level. This 9-node element provides precise description of the variation of material properties. A set of simulations are performed for modelling edge-crack problems in functionally graded materials (FGMs) and FGM layers sandwiched between two homogeneous media under thermomechanical loading by using this graded element. The validity of the solution is confirmed by comparing with existing solutions. It was shown that compared with conventional homogeneous finite elements the current model is more reliable for modelling crack problems in FGMs. The influence of the steady state temperature distribution as well as material gradient on the crack tip local fields and fracture parameters, such as stress intensity factors, mode mixity, and energy release rate are studied.

4.1 Graded regular FEs for modelling crack problems under thermomechanical loading

The stress in an elastic FGM under thermomechanical loading can then be calculated using the Hooke's law,

$$\{\sigma\} = [D(x,y)]\{\varepsilon^e\} = [D(x,y)](\{\varepsilon\} - \{\varepsilon^t\}), \tag{4.1}$$

where $[D(x,y)], \{\varepsilon^e\}, \{\varepsilon^t\}$, and $\{\varepsilon\}$ are the constitutive elastic matrix, elastic strain, thermal strain, and total strain, respectively. Thermal strain is given by,

$$\{\varepsilon^t\} = \begin{Bmatrix} \alpha(x,y)T(x,y) \\ \alpha(x,y)T(x,y) \\ 0 \end{Bmatrix}, \tag{4.2}$$

whereas, α is the coefficient of thermal expansion and T is the temperature difference measured from a reference temperature.

Since thermomechanical properties of FGMs vary continuously with the coordinate position, it is essential to consider this variation of material properties through the element level as given by Eq. (3.17) in order to have an accurate estimation for thermoelastic problems. So, coefficients of thermal expansion $\alpha(x,y)$ will be represented in the following form,

$$\alpha = \sum_{i=1}^{n} N_i \alpha_i, \tag{4.3}$$

and the elastic matrix $[D(x,y)]$ will be formed based on Eq. (3.18).

By using the principle of minimum potential energy the equilibrium equation for a graded element can be obtained and written in the general form,

$$[K]\{u\} = \{f^m\} + \{f^t\}, \tag{4.4}$$

where, $[K]$, $\{f^m\}$ and $\{f^t\}$ are the element stiffness matrix given by Eq. (3.23), mechanical and thermal loading vectors, respectively. Mechanical loading can be implied based on the vector of applied forces $[F]$ as mentioned in Eq. (3.20), while the thermal loading representing fictitious forces due to the thermal expansion is given based on the thermal strain vector $\{\varepsilon^t\}$.

$$\{f^t\} = \int_{A_e} [B]^T [D(x,y)]\{\varepsilon^t\}dA. \tag{4.5}$$

In order to calculate the thermal strain, temperature field should be determined. In general, the heat flow through the unit area, q, in a FGM can be represented as,

$$q = -k(x,y)\left(\frac{\partial T}{\partial x}\hat{\imath} + \frac{\partial T}{\partial y}\hat{\jmath}\right), \tag{4.6}$$

where $k(x,y)$ is the thermal conductivity which changes based on the coordinate position in FGMs. In the current study, it is assumed that the cracked FGM plate is insulated on its vertical surfaces, while its bottom and top faces are maintained at different temperatures. Also, there exists a uniform heat generation of Q which is the same for each control volume considered in the model and consistent with the constant temperatures at the bottom and top faces. The variation of the thermal conductivity within the FGM is assumed to be in the y direction as,

$$k(y) = \left(\frac{-Q}{T_{bottom}\delta}\right)y + k_0, \tag{4.7}$$

where k_0 is the value of the thermal conductivity at the bottom surface, and δ is the parameter defined as,

$$\delta = \frac{T_{top} - T_{bottom}}{H \, T_{bottom}}, \tag{4.8}$$

where H is the plate height.

The heat equation under the steady state condition is,

$$\frac{\partial}{\partial y}\left(k(y)\frac{\partial T}{\partial y}\right) + Q = 0. \tag{4.9}$$

The obtained temperature field from Eq. (4.9) will be used to calculate the thermal loading vector. Finally, upon assembling the elements with the introduced formulation, a system of algebraic equations will be obtained for calculating the displacement field.

4.2 Numerical results and discussion

4.2.1 Computational model

In this part the concept of regular graded finite element is used to study the fracture behaviour of a linear elastic isotropic nonhomogeneous plate with an edge crack under the mechanical and thermal loading. In simulations different thicknesses of a FGM medium sandwiched between two homogeneous materials are considered. Material properties considered for the model are mentioned in table 4.1. First, consider a FGM plate with an edge crack under mechanical and thermal loading as shown in Fig. 4.1. Material properties at the bottom and top surfaces of the model correspond to phase 1 and phase 2, respectively, and vary linearly in the y direction. The width and height of the plate, and crack length are W, H, and a, respectively, with the H/W and a/W ratios being 1.31, and 0.5 in sequence. It is supposed that the plate is under uniform tensile

loading of σ_{yy} = 3.17 MPa and the bottom and top faces are maintained at constant temperatures

T_{bottom} and T_{top}, respectively. Numerical results are obtained for cases when $\Delta T = T_{top} - T_{bottom}$ = 0, 250, 500, 750, and 1000°K. Assuming that T_{bottom} = 273.15°K, the heat

generation value Q considered for each case of ΔT is mentioned in Table 4.2. Fine mesh near the

crack tip is used in order to obtain fracture parameters such as mode I and II SIFs, mode mixity,

energy release rates, and stress fields near the crack tip. Table 4.3 represents the element size

used for meshing the model at areas labelled in Fig. 4.1. The mesh is symmetric with respect to

horizontal and vertical axes passing through the crack tip.

Table 4.1. Material properties of the two phases considered for the FGM model

	E (GPa)	ν	α (/°K)×10⁻⁶	k ($W/m.°K$)
Phase 1	66	0.25	24	205
Phase 2	291	0.17	8.1	18

Table 4.2. Heat generation value considered for each temperature difference in the FEM model

$\Delta T°K$	0	250	500	750	1000
Q (kW/m^3)	0	275	550	825	1100
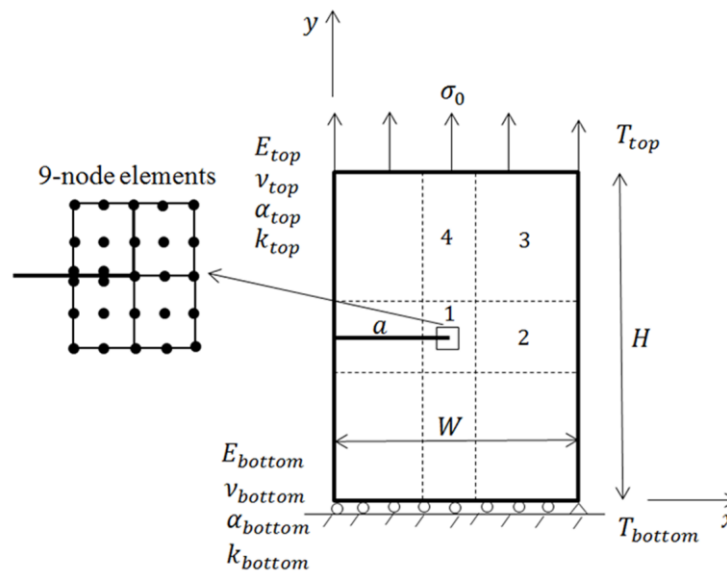
Fig. 4.1. Geometry and boundary conditions of the edge crack problem in a FGM plate

Table 4.3. Meshing information for the model meshed with graded quadrilateral 9-node elements

No. of elements	No. of nodes	Area	$\Delta x_{element}/W$	$\Delta y_{element}/H$
		1	0.002	0.002
19600	79101	2	0.02	0.002
		3	0.02	0.02
		4	0.002	0.02

4.2.2 Calculation of the SIF using fine mesh of regular graded elements

The SIF for the crack problem can be calculated using the stress information around the crack front. The singular stress field around the crack tip is represented in Eq. (4.10) in which r is the distance measured from the crack tip. It was reported that when $r/a \leq 0.1$, Eq. (4.10) is accurately governed except the case when the crack size is very small (Tan 1998; Whitney and Nuismer 1974). Also, it was shown that SIFs can be accurately calculated using the stress information at the interval $0 \leq r/a \leq 0.125$ (Papila and Haftka 2003). Fig. 4.2 illustrates an example of the distribution of the normal component of stress ahead of the crack for the FGM plate with no temperature difference at the bottom and top boundaries of the model. This information is obtained based on the nodal values for stresses in the above mentioned FEM model. By fitting the data obtained from the FEM to Eq. (4.10), SIFs can be calculated as the slope of the curve shown in Fig. 4.3.

$$\sigma_{yy} = \frac{K_I}{\sqrt{2\pi r}} \qquad (4.10)$$
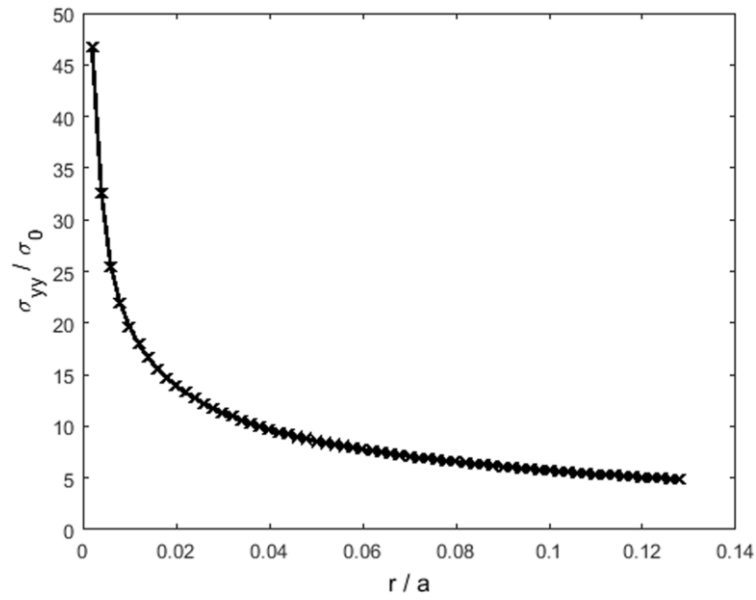
Fig. 4.2. Distribution of the normal stress near the crack tip in the FGM plate under mode I loading
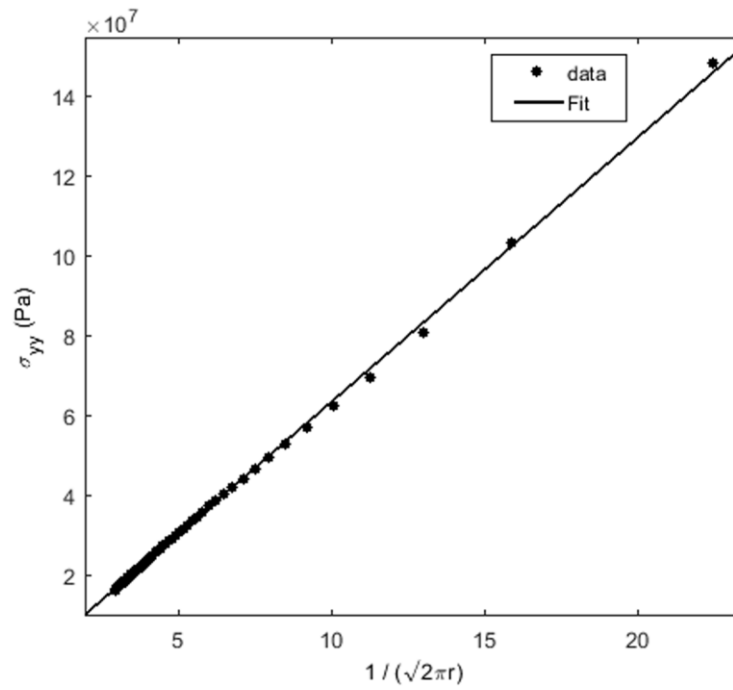
Fig. 4.3. Curve fitting over the stress values near the crack tip for calculating SIF

4.2.3 Comparison between the graded element solution and existing solutions

The validity of numerical results obtained with 9-node quadrilateral graded elements is demonstrated in comparison with existing solutions. At first, by setting the material property gradient index equal to zero, it is assumed that the whole plate is homogeneous. Using the solution reached by the weight function technique which considers the geometry effect (Fett 1998) SIF is calculated and compared with the current model.

Secondly, the thermal loading is added, and a temperature difference of $\Delta T = T_{top} - T_{bottom} = 500°K$ is applied to the model. The problem is simulated using the FEM software Ansys employing 78400 quadrilateral 4-node elements (PLANE182) which corresponds to the total number of 9-node graded elements in the current work. Table 4.4 provides the meshing information used by Ansys in areas labeled in Fig. 4.1.

Table 4.4. Meshing information for the model meshed with Ansys using PLANE181 elements

No. of elements	No. of nodes	Area	$\Delta x_{element}/W$	$\Delta y_{element}/H$
78400	79101	1	0.001	0.001
		2	0.01	0.001
		3	0.01	0.01
		4	0.001	0.01

Finally, the crack problem in the FGM plate has been considered. For this condition, K_I obtained with regular 9-node graded elements is compared with K_I obtained by the new graded singular element introduced in (Molavi Nojumi and Wang 2017a). The problem is modelled in accordance with the properties considered in the reference work ($E_{top}/E_{bottom} = 7, a/W = 0.5,$ without thermal loading).

The comparison of the normalized SIF between the current model and existing solutions including weight function technique, FEM solution with Ansys software, and a new graded

singular element is shown in table 4.5. The results agree well with the references, which demonstrate the accuracy of the solution obtained with 9-node quadrilateral graded elements.

Table 4.5. Comparison between the graded element solution and existing solutions

Homogeneous plate			
	Analytical solution (Fett 1998)	Current model	Error %
$K_I/\sigma_0\sqrt{\pi a}$	2.9100	2.9263	0.56
Homogeneous plate with temperature distribution			
	Ansys	Current model	Error %
$K_I/\sigma_0\sqrt{\pi a}$	1.7993	1.8697	3.91
FGM plate			
	Graded singular element (Molavi Nojumi and Wang 2017)	Current model	Error %
$K_I/\sigma_0\sqrt{\pi a}$	3.0039	3.0065	0.09

4.2.4 Investigation of the SIFs for the cracked nonhomogeneous plate under mechanical and thermal loading

In this section, SIFs obtained based on the procedure explained before in section *4.2.2*, are used to study the fracture behaviour of nonhomogeneous plates. Two categories have been considered to investigate the influence of the material gradient and loading on the SIFs in the nonhomogeneous cracked plate. First, the whole plate is supposed to be a FGM as indicated in Fig. 4.4a. Various temperature differences at the bottom and top faces are considered to obtain the influence of the thermal loading. Secondly, it is assumed that the plate contains a FGM layer sandwiched between two homogeneous materials as shown in Fig. 4.4b. Then, by changing the thickness of the FGM layer, *h*, the effect of the material gradient index is studied. It should be noted that for this case material properties are continuous at boundaries of the FGM layer.
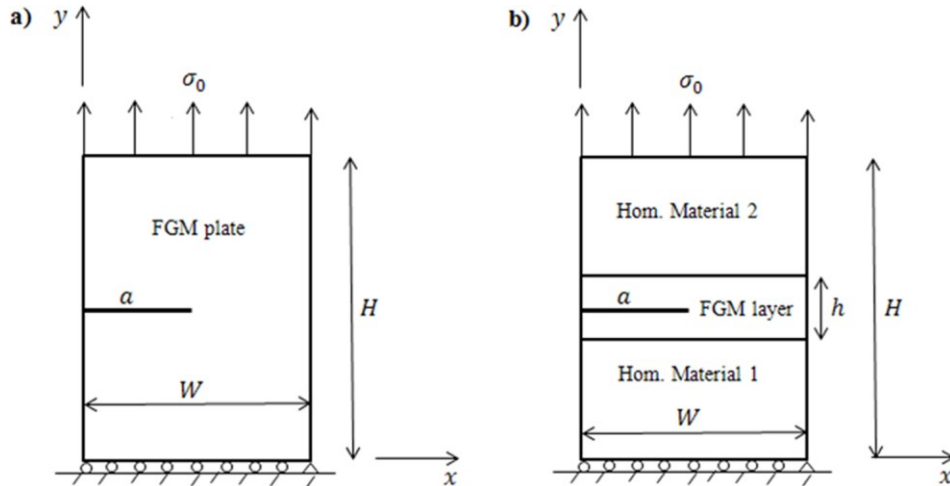
Fig. 4.4. Geometry of the considered model for a) cracked FGM plate and b) cracked FGM layer sandwiched between two different homogeneous materials

4.2.4.1 Cracked FGM plate

Normalized SIFs ($K_I/\sigma_0\sqrt{\pi a}$ and $K_{II}/\sigma_0\sqrt{\pi a}$), mode mixity ($\Psi/\Psi_{\Delta T=1000}$; $\Psi = \tan^{-1}(K_{II}/K_I)$), and energy release rate ($G/G_{\Delta T=1000}$; $G = (K_I^2 + K_{II}^2)/E_{tip}$) calculated for the FGM plate under different loadings are mentioned in Table 4.6. As a special case when material gradient index is zero, results are represented for the homogeneous plate with the phase 1 material properties. It is observed that the mode I SIF (K_I) decreases with increasing temperature difference for homogeneous plate. Whereas, the mode II SIF (K_{II}) rises with increasing temperature difference. Also, results show that the coupling between K_I and K_{II} without thermal loading is almost zero as predicted by the analytical solution. However, the higher the thermal loading, the stronger the mode mixity. Normalized energy release rate decreases from $\Delta T = 0°K$ to $\Delta T = 250°K$, and shows an increasing trend up to $\Delta T = 1000°K$. These changes can be explained by considering the induced shear stresses in the model as the temperature difference increases.

On the other hand, when the material gradient index is not zero, fracture parameters illustrate different behaviour from the homogeneous plate. At first, unlike the homogeneous plate, the computed K_I drastically increases with the higher thermal loading. Also, higher values of K_{II} and mode mixity in comparison with the homogeneous plate points to the stronger coupling between K_I and K_{II}. This phenomenon can be justified by considering the influence of the change of material properties in addition to the thermal loading on inducing shear stress in the model due to the coupling between normal and shear stresses in FGMs. In addition, normalized energy release rates are smaller for the FGM plates.

Table 4.6. Normalized SIFs, mode mixity and energy release rate for the cracked homogeneous and FGM plate under different temperature gradients

Homogeneous plate					
$\Delta T\,^\circ$K	0	250	500	750	1000
$\dfrac{K_I}{\sigma_0\sqrt{\pi a}}$	2.926	2.398	1.870	1.342	0.814
$\dfrac{K_{II}}{\sigma_0\sqrt{\pi a}}$	0.042	0.994	1.945	2.897	3.849
$\dfrac{\Psi}{\Psi_{\Delta T=1000}}$	0.010	0.288	0.591	0.835	1
$\dfrac{G}{G_{\Delta T=1000}}$	0.553	0.435	0.470	0.659	1
FGM plate					
$\Delta T\,^\circ$K	0	250	500	750	1000
$\dfrac{K_I}{\sigma_0\sqrt{\pi a}}$	2.968	5.548	8.467	11.221	13.970
$\dfrac{K_{II}}{\sigma_0\sqrt{\pi a}}$	0.150	1.366	2.883	4.399	5.915
$\dfrac{\Psi}{\Psi_{\Delta T=1000}}$	0.126	0.603	0.819	0.933	1
$\dfrac{G}{G_{\Delta T=1000}}$	0.038	0.142	0.348	0.631	1

Local stress fields near the crack tip are described for the homogeneous and FGM plate under the mechanical and thermal loading in Figs. 4.5-4.13. Figs. 4.5-4.7 illustrates contours of normalized

stress σ_{yy}/σ_0 ahead of the crack tip for homogeneous plate without thermal loading, then homogeneous and FGM plate with temperature difference of $\Delta T = 1000°K$, respectively. Contours of normal stress are plotted for homogeneous material without thermal loading in Fig. 4.5. Increasing temperature difference in the homogeneous material, the profile of the stress distribution near the crack tip changes as indicated in Fig. 4.6. This change is mainly caused by the induced shear stress in the model. That is because the material at different positions tends to have different thermal extensions. Finally, contours of normal stress are drawn for the FGM plate with temperature difference of $\Delta T = 1000°K$ in Fig. 4.7. In this condition the coefficient of thermal expansion decreases in the y direction, which moderates the thermal extension. Consequently, the stress profile is more similar to the homogeneous material without temperature difference. However, the material symmetry is broken, and coupled modes of fracture exist. It is observed that contours of stress are tilted so that the lower parts are at farther distance from the crack tip. The same discussion can be repeated for other components of stress, σ_{xx}/σ_0 and σ_{xy}/σ_0 as plotted in Figs. 4.8-4.10 and Figs. 4.11-4.13, respectively.
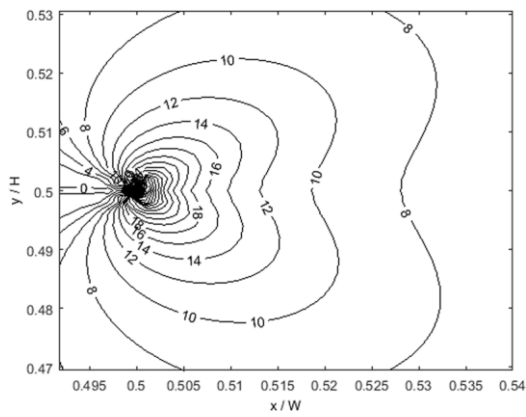
Fig. 4.5. Contours of normalized stress σ_{yy}/σ_0 ahead of the crack tip for homogeneous plate without thermal loading
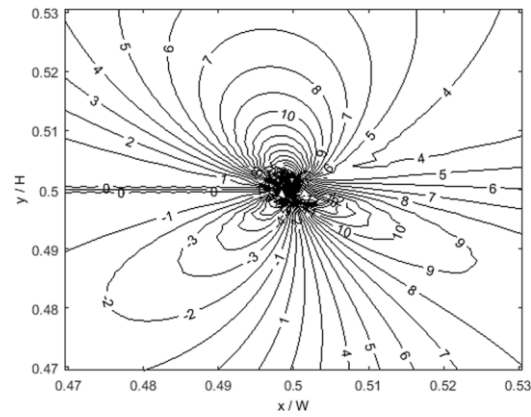
Fig. 4.6. Contours of normalized stress σ_{yy}/σ_0 ahead of the crack tip for homogeneous plate with thermal loading ($\Delta T = 1000^\circ K$)
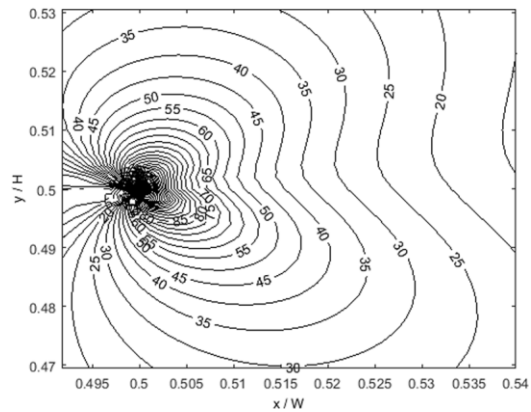
Fig. 4.7. Contours of normalized stress σ_{yy}/σ_0 ahead of the crack tip for FGM plate with thermal loading
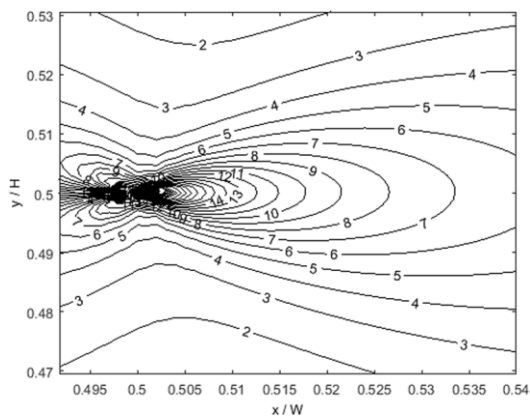
($\Delta T = 1000^\circ K$)

Fig. 4.8. Contours of normalized stress σ_{xx}/σ_0 ahead of the crack tip for homogeneous plate without thermal loading
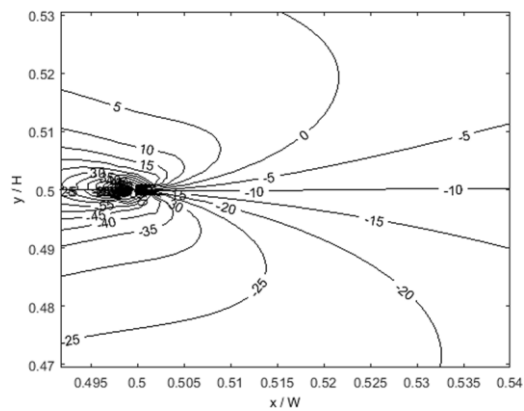
Fig. 4.9. Contours of normalized stress σ_{xx}/σ_0 ahead of the crack tip for homogeneous plate with thermal loading ($\Delta T = 1000^\circ K$)
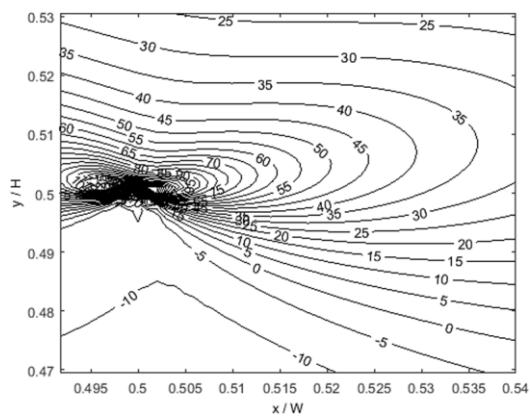
Fig. 4.10. Contours of normalized stress σ_{xx}/σ_0 ahead of the crack tip for FGM plate with thermal loading ($\Delta T = 1000^\circ K$)
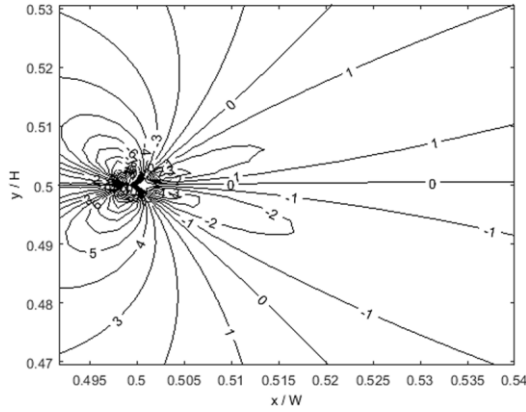
Fig. 4.11. Contours of normalized stress σ_{xy}/σ_0 ahead of the crack tip for homogeneous plate without thermal loading
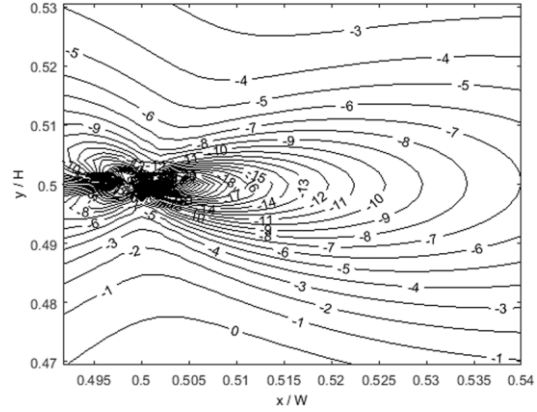
Fig. 4.12. Contours of normalized stress σ_{xy}/σ_0 ahead of the crack tip for homogeneous plate with thermal loading ($\Delta T = 1000°K$)
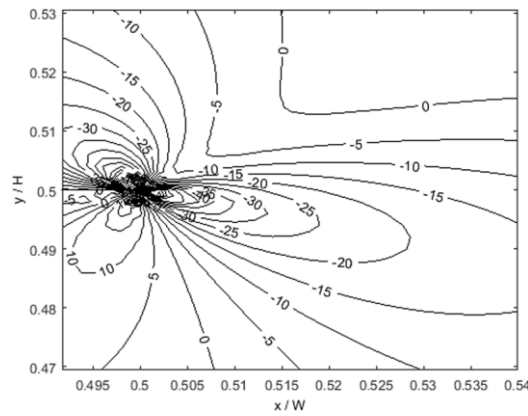
Fig. 4.13. Contours of normalized stress σ_{xy}/σ_0 ahead of the crack tip for FGM plate with thermal loading ($\Delta T = 1000°K$)

4.2.4.2 Cracked FGM layer sandwiched between two different homogeneous materials

In this section the configuration of the model has been switched to Fig. 4.4b. Different thicknesses of the FGM layer as $h/H = 0.2, 0.04,$ and 0.004 are considered with various temperature differences. It is assumed that the temperature difference happens through the FGM layer thickness, while the temperature is kept constant in each homogeneous medium. The

temperature distribution is assumed to be continuous so that there is no jump at the interface of the FGM layer and homogeneous media. Fracture parameters including SIFs, mode mixity, and energy release rates are computed for the new configuration and results are presented in table 4.7. Tables 4.6 and 4.7 show that mode II SIF is more sensitive to the material gradient when there is no thermal loading. This issue has also been reported in other researches (Gao et al. 2008; Molavi Nojumi and Wang 2017a). By considering a range of temperature differences it is observed that this phenomenon exists at the presence of the thermal loading as well. The key point is that when material gradient is sharp this pattern is reversed. In such a case mode I SIF becomes more sensitive to the material gradient. The comparison of K_I and K_{II} between $h/H = 0.04$ and $h/H = 0.004$ for different temperature differences clearly illustrates this fact. This phenomenon can be justified by noting that with increasing temperature difference, higher shear stresses will be induced in the model, consequently when the material gradient is sharp, these high values of K_{II} will influence K_I since they are coupled.

Local stress fields near the crack tip are described for the sandwiched FGM plates under the mechanical and thermal loading in Figs. 4.14-4.22. Contour plots are shown for the case that the temperature difference between the top and bottom surfaces is 1000°K. Figs. 4.14-4.16 illustrates normalized component of stress normal to the crack line σ_{yy}/σ_0. These stress contours are similar to those drawn for the case when whole plate is FGM as shown in Fig. 4.7. However, since the material gradient is higher in the FGM layer as its thickness becomes smaller; more deviation is observed from the symmetric condition. Contours of σ_{yy}/σ_0 are more deviated toward the softer material showing the crack intend to growth in that direction. The high density stress lines located inside the very thin FGM layer shown in Fig. 4.16 indicates that there exists stress concentration at the FGM layer in addition to the crack tip singularity. Figs. 4.17-4.19

correspond to contours of σ_{xx}/σ_0 near the crack tip. It is also clear from these figures that the density of stress lines is higher in FGM layer when its thickness decreases. In continuance contours of σ_{xy}/σ_0 are plotted in Figs. 4.20-4.22. It can be understood from these plots that as the thickness of the FGM layer decrease, profile of shear stress at crack front becomes more symmetric; however, away from the crack tip the symmetry of contours is broken.

Table 4.7. Normalized SIFs, mode mixity and energy release rate for the cracked FGM layer sandwiched between two different homogeneous materials

$h/H = 0.2$					
$\Delta T^\circ K$	0	250	500	750	1000
$\dfrac{K_I}{\sigma_0\sqrt{\pi a}}$	3.346	9.099	14.858	20.612	26.339
$\dfrac{K_{II}}{\sigma_0\sqrt{\pi a}}$	0.539	6.566	13.669	20.778	27.846
$\dfrac{\Psi}{\Psi_{\Delta T=1000}}$	0.196	0.769	0.915	0.971	1
$\dfrac{G}{G_{\Delta T=1000}}$	0.008	0.086	0.277	0.583	1
$h/H = 0.04$					
$\Delta T^\circ K$	0	250	500	750	1000
$\dfrac{K_I}{\sigma_0\sqrt{\pi a}}$	3.415	8.835	14.257	19.679	25.096
$\dfrac{K_{II}}{\sigma_0\sqrt{\pi a}}$	0.869	9.974	20.831	31.689	42.542
$\dfrac{\Psi}{\Psi_{\Delta T=1000}}$	0.240	0.815	0.935	0.978	1
$\dfrac{G}{G_{\Delta T=1000}}$	0.005	0.073	0.261	0.570	1
$h/H = 0.004$					
$\Delta T^\circ K$	0	250	500	750	1000
$\dfrac{K_I}{\sigma_0\sqrt{\pi a}}$	2.623	5.947	9.274	12.602	15.925
$\dfrac{K_{II}}{\sigma_0\sqrt{\pi a}}$	0.786	10.135	21.060	31.985	42.905
$\dfrac{\Psi}{\Psi_{\Delta T=1000}}$	0.240	0.856	0.951	0.984	1
$\dfrac{G}{G_{\Delta T=1000}}$	0.004	0.066	0.253	0.564	1
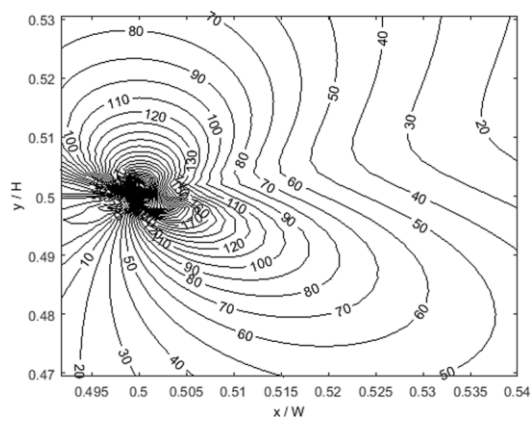
Fig. 4.14. Contours of normalized stress σ_{yy}/σ_0 ahead of the crack tip for sandwiched FGM layer between two different homogeneous materials with thermal loading $(h/H = 0.2, \Delta T = 1000^\circ K)$
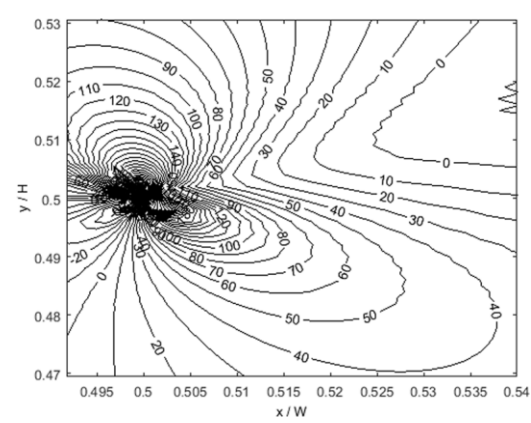
Fig. 4.15. Contours of normalized stress σ_{yy}/σ_0 ahead of the crack tip for sandwiched FGM layer between two different homogeneous materials with thermal loading $(h/H = 0.04, \Delta T = 1000^\circ K)$
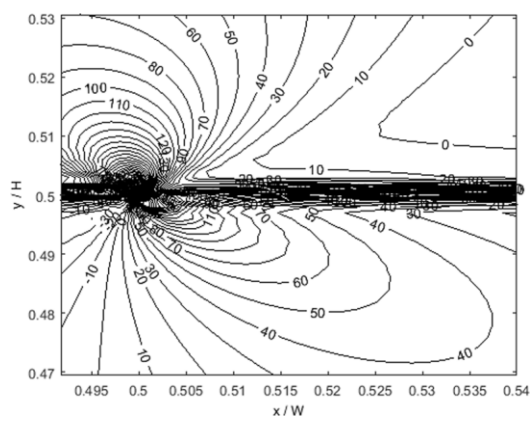
Fig. 4.16. Contours of normalized stress σ_{yy}/σ_0 ahead of the crack tip for sandwiched FGM layer between two different homogeneous materials with thermal loading $(h/H = 0.004, \Delta T = 1000^\circ K)$
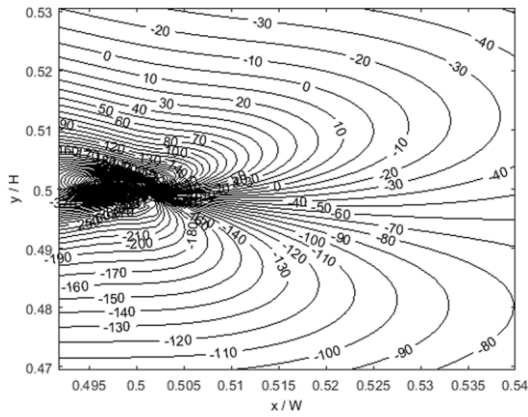
Fig. 4.17. Contours of normalized stress σ_{xx}/σ_0 ahead of the crack tip for sandwiched FGM layer between two different homogeneous materials with thermal loading ($h/H = 0.2, \Delta T = 1000^\circ K$)
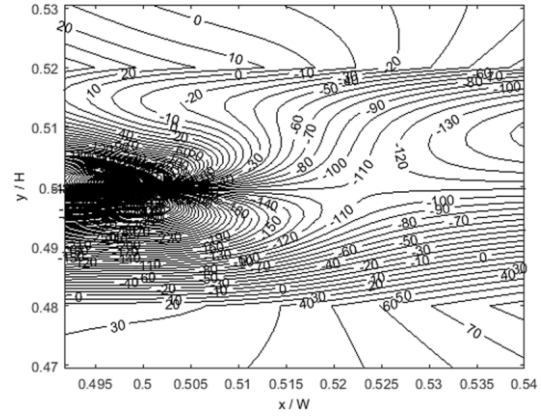
Fig. 4.18. Contours of normalized stress σ_{xx}/σ_0 ahead of the crack tip for sandwiched FGM layer between two different homogeneous materials with thermal loading ($h/H = 0.04, \Delta T = 1000^\circ K$)
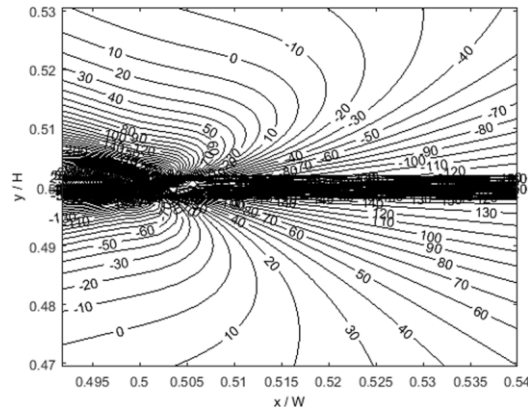
Fig. 4.19. Contours of normalized stress σ_{xx}/σ_0 ahead of the crack tip for sandwiched FGM layer between two different homogeneous materials with thermal loading ($h/H = 0.004, \Delta T = 1000^\circ K$)
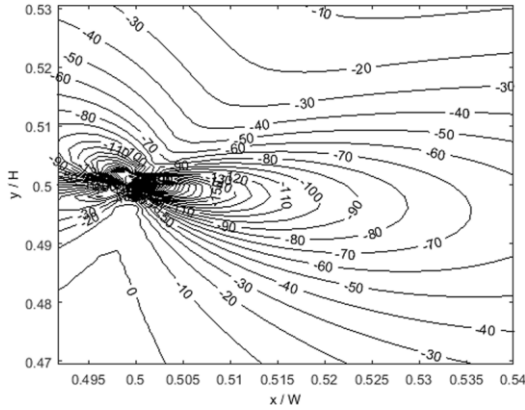
Fig. 4.20. Contours of normalized stress σ_{xy}/σ_0 ahead of the crack tip for sandwiched FGM layer between two different homogeneous materials with thermal loading ($h/H = 0.2, \Delta T = 1000°K$)
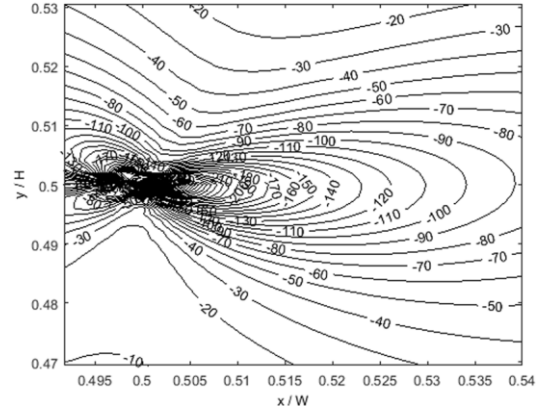
Fig. 4.21. Contours of normalized stress σ_{xy}/σ_0 ahead of the crack tip for sandwiched FGM layer between two different homogeneous materials with thermal loading ($h/H = 0.04, \Delta T = 1000°K$)
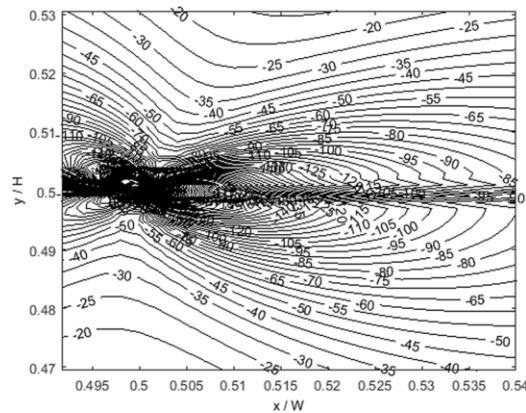
Fig. 4.22. Contours of normalized stress σ_{xy}/σ_0 ahead of the crack tip for sandwiched FGM layer between two different homogeneous materials with thermal loading ($h/H = 0.004, \Delta T = 1000°K$)

4.2.5 Comparison of the SIFs between sandwiched cracked FGM layers and bimaterial interface crack problem

SIFs obtained using graded elements are compared between sandwiched cracked FGM layers with different thicknesses and the bi-material interface crack problem under pure mechanical loading. Although both Young's modulus and Poisson's ratio has been considered as variable

material properties in simulations, but, here the comparison is set based on the Young's modulus gradient index. Figs. 4.23 and 4.24 show that with increasing the material gradient index (decreasing the thickness of the FGM layer) K_I and K_{II} becomes closer to corresponding values obtained for the bi-material interface crack problem, respectively.
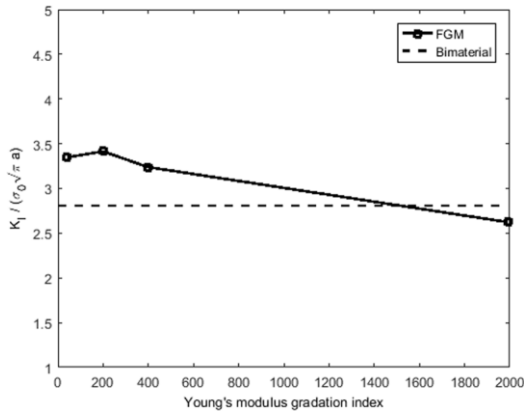
Fig. 4.23. The variation of K_I with Young's modulus gradient index
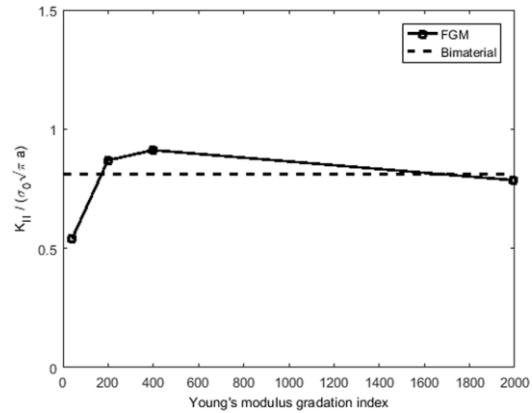
Fig. 4.24. The variation of K_{II} with Young's modulus gradient index

4.2.6 Challenging conventional homogeneous elements for modelling FGM crack problems

As explained in the finite element formulation part, conventional homogeneous elements possess a unique material property all over the element. As a result in modelling FGMs using conventional homogeneous elements a forced jump of material properties occurs at neighboring elements. Such an inappropriate characteristic will influence the solution for field variables. On the other hand, graded elements consider the inherent change of material properties at the element level. Consequently, a smooth distribution of material properties will be provided through the model. Some typical examples are mentioned in (Molavi Nojumi & Wang, 2016) for comparison between homogeneous and graded elements. Here, another example is presented corresponding to the cracked FGM layer sandwiched between two different homogeneous

materials. Since the material gradient happens in a limited small distance, there will be considerable mismatch between neighboring element properties in the FGM layer modelled with conventional elements. Consider the extreme case when $h/H = 0.004$ and $\Delta T = 1000°K$ for the model shown in Fig. 4.4b. At first, the problem is solved using graded quadrilateral 9-node elements whose validity is confirmed in comparison with existing solutions mentioned section *4.2.3*. The meshing information is given in table 4.3. Secondly, the problem is solved using homogeneous quadrilateral 9-node elements with the same meshing information. Normalized values for K_I and K_{II} obtained from homogeneous and graded element solution are indicated in Table 4.8. Although, results agree well for K_{II}, however, the considerable error happening for K_I is a good example showing conventional homogeneous elements are not reliable especially when sharp material gradient exists.

Table 4.8. Comparison of the SIFs for the sandwiched cracked FGM layer obtained with graded and homogeneous elements

	Graded element	Homogeneous element	Error %
$\dfrac{K_I}{\sigma_0\sqrt{\pi a}}$	15.925	19.769	24.14
$\dfrac{K_{II}}{\sigma_0\sqrt{\pi a}}$	42.905	43.712	1.88

Chapter 5

A New Graded Singular Finite Element for Crack Problems in Functionally Graded Materials[*]

A new graded singular finite element is proposed for analyzing crack problems in linear elastic isotropic functionally graded materials (FGMs) with spatially varying elastic parameters. The general formulation of the suggested singular element is obtained by analyzing the crack-tip stress field using the Westergaard stress function method. The general shape function is generated by integrating the strains obtained from the stress function. The stiffness matrix for the singular element is then determined using the principle of minimum potential energy. Using the displacement continuity between the singular and the adjacent regular elements, stiffness matrices are assembled. This new element is characterized by containing both singular and higher order terms, which provides more precise description of the crack-tip fields. The validity of the new element is demonstrated by comparing with existing solutions. This element is implemented for simulating crack problems in FGMs whose elastic properties vary normal to the crack line. Stress intensity factors (SIFs), energy release rates, levels of non-singular stresses, and stress distributions near the crack-tip are investigated. Numerical results reveal that the

---

[*] This chapter is published as (Molavi Nojumi and Wang 2017)

introduced graded singular element is more efficient than conventional finite elements as it provides more accurate description of the crack-tip field.

5.1 Crack-tip fields in FGMs

Consider the crack-tip stress field in linearly elastic isotropic FGM in which elastic constants change normal to the crack line as shown in Fig. 5.1, where the origin of the coordinate system is located at the crack-tip. The current study is focused on the case where the material gradation direction (y) is perpendicular to the crack alignment (x), i.e., $E(y) = E_0(1 + \delta_y y)$, to evaluate interface-like crack and the mixed-mode fracture. The Poisson's ratio is assumed to be a constant across the material. An asymptotic analysis using the Westergaard stress function approach has been conducted (Jain, Rousseau, and Shukla 2004). In general, three dimensional stress distribution may occur near the crack tip (Rosakis and Ravi-Chandar 1986). In the current study, the thickness of the plate is considered large enough to maintain plane strain condition at the crack tip. The compatibility equation can be expressed under plane strain condition, as

$$\left(1 + \delta_y y\right)^2 \nabla^2 (\nabla^2 F) - 2\delta_y \left(1 + \delta_y y\right) \frac{\partial}{\partial y} (\nabla^2 F) + 2\delta_y{}^2 (\nabla^2 F) - \frac{2\delta_y{}^2}{(1 - v)} \frac{\partial^2 F}{\partial x^2} = 0. \tag{5.1}$$
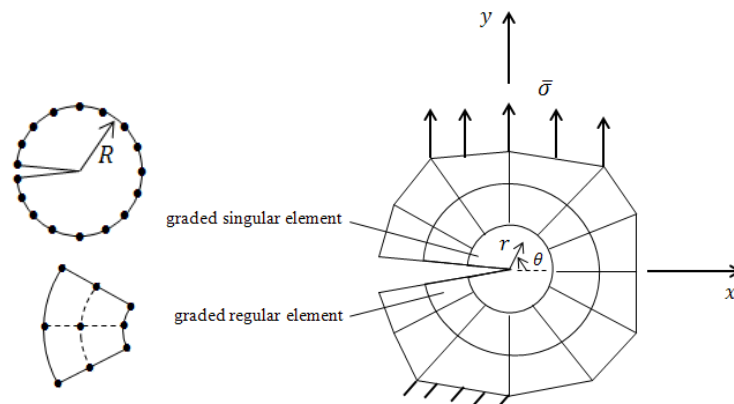
Fig. 5.1. Schematic illustration of the FEM modelling of the crack problem in FGMs.

where ∇^2 is the Laplace operator. E_0 and δ_y are the Young's modulus at the crack tip and the material non-homogeneity index, respectively, while F represents the Westergaard stress

function. After a transformation using scaled coordinates $\eta_1 = x/\varepsilon$, and $\eta_2 = y/\varepsilon$, this stress function can be expressed as,

$$F(\varepsilon\eta_1, \varepsilon\eta_2) = \sum_{m=0}^{\infty} \varepsilon^{\left(m+\frac{3}{2}\right)} \phi_m(\eta_1, \eta_2) + \sum_{n=0}^{\infty} \varepsilon^{(n+2)} \psi_n(\eta_1, \eta_2), \tag{5.2}$$

where ε is the scaling factor to fill the whole considered field. The first series in the supposed stress function, including ϕ_m stands for the singular part whereas the second series, involving ψ_n represents the non-singular terms. Substituting this stress function, Eq. (5.2), into the compatibility equation, Eq. (5.1), results in the following equation,

$$\sum_{m=0}^{\infty} \left\{ \varepsilon^{\left(m+\frac{3}{2}\right)} \nabla^2 (\nabla^2 \phi_m) + \varepsilon^{\left(m+\frac{5}{2}\right)} \left[2\delta_y \eta_1 \nabla^2 (\nabla^2 \phi_m) - 2\delta_y \frac{\partial}{\partial \eta_1} (\nabla^2 \phi_m) \right] \right.$$

$$+ \varepsilon^{\left(m+\frac{7}{2}\right)} \left[\delta_y^2 \eta_1^2 \nabla^2 (\nabla^2 \phi_m) - 2\delta_y^2 \eta_1 \frac{\partial}{\partial \eta_1} (\nabla^2 \phi_m) + 2\delta_y^2 (\nabla^2 \phi_m) \right.$$

$$\left. \left. - 2\delta_y^2 (1+v) \frac{\partial^2 \phi_m}{\partial \eta_2^2} \right] \right\}$$

$$+ \sum_{n=0}^{\infty} \left\{ \varepsilon^{(n+2)} \nabla^2 (\nabla^2 \psi_n) + \varepsilon^{(n+3)} \left[2\delta_y \eta_1 \nabla^2 (\nabla^2 \psi_n) - 2\delta_y \frac{\partial}{\partial \eta_1} (\nabla^2 \psi_n) \right] \right. \tag{5.3}$$

$$+ \varepsilon^{(n+4)} \left[\delta_y^2 \eta_1^2 \nabla^2 (\nabla^2 \psi_n) - 2\delta_y^2 \eta_1 \frac{\partial}{\partial \eta_1} (\nabla^2 \psi_n) + 2\delta_y^2 (\nabla^2 \psi_n) \right.$$

$$\left. \left. - 2\delta_y^2 (1+v) \frac{\partial^2 \psi_n}{\partial \eta_2^2} \right] \right\} = 0.$$

By equating the terms corresponding to each power of ε to zero, a set of differential equations are obtained.

$$\nabla^2(\nabla^2\phi_m) + \left[2\delta_y\eta_1\nabla^2(\nabla^2\phi_{m-1}) - 2\delta_y\frac{\partial}{\partial\eta_1}(\nabla^2\phi_{m-1})\right]$$

$$+ \left[\delta_y^2\eta_1^2\nabla^2(\nabla^2\phi_{m-2}) - 2\delta_y^2\eta_1\frac{\partial}{\partial\eta_1}(\nabla^2\phi_{m-2}) + 2\delta_y^2(\nabla^2\phi_{m-2})\right.$$

$$\left.- 2\delta_y^2(1+\nu)\frac{\partial^2\phi_{m-2}}{\partial\eta_2^2}\right] = 0, \quad m = 0, 1, 2, \ldots \tag{5.4}$$

$$\nabla^2(\nabla^2\psi_n) + \left[2\delta_y\eta_1\nabla^2(\nabla^2\psi_{n-1}) - 2\delta_y\frac{\partial}{\partial\eta_1}(\nabla^2\psi_{n-1})\right]$$

$$+ \left[\delta_y^2\eta_1^2\nabla^2(\nabla^2\psi_{n-2}) - 2\delta_y^2\eta_1\frac{\partial}{\partial\eta_1}(\nabla^2\psi_{n-2}) + 2\delta_y^2(\nabla^2\psi_{n-2})\right.$$

$$\left.- 2\delta_y^2(1+\nu)\frac{\partial^2\psi_{n-2}}{\partial\eta_2^2}\right] = 0, \quad n = 0, 1, 2, \ldots \tag{5.5}$$

where terms with negative index (m or n) will be considered to be zero. For $m = n = 0$,

$$\nabla^2(\nabla^2\phi_0) = 0, \nabla^2(\nabla^2\psi_0) = 0, \tag{5.6}$$

and when $m = n = 1$,

$$\nabla^2(\nabla^2\phi_1) + 2\delta_y\eta_1\nabla^2(\nabla^2\phi_0) - 2\delta_y\frac{\partial}{\partial\eta_1}(\nabla^2\phi_0) = 0,$$

$$\tag{5.7}$$

$$\nabla^2(\nabla^2\psi_1) + 2\delta_y\eta_1\nabla^2(\nabla^2\psi_0) - 2\delta_y\frac{\partial}{\partial\eta_1}(\nabla^2\psi_0) = 0.$$

The differential equations for a higher power of ε always contain lower order solutions, rather than the well-known bi-harmonic equation governing homogeneous materials. These equations are solved in a recursive manner. Details of the solution are available in reference (Jain, Rousseau, and Shukla 2004).

Using the general solution developed for F, Eq. (5.2), and transforming (η_1, η_2) back to (x, y) coordinates, the stress field σ_{xx} and σ_{yy} for our current model can be expressed in the following form with the series in Eq. (5.2) being truncated at $m, n = 1$.

$$\sigma_{xx} = \sum_{n=0}^{1} [Re\{P_n\} - yIm\{P_n'\} + 2Im\{R_n\} + yRe\{R_n'\} + 2Re\{Q_n\} + yIm\{Q_n'\} + Im\{S_n\}$$

$$+ yRe\{S_n'\}] + \delta_y [Im\{\widetilde{P_0}\} + 2yRe\{P_0\} - \frac{y^2}{2}Im\{P_0'\} - Re\{\widetilde{R_0}\} + 2yIm\{R_0\}$$

$$+ \frac{y^2}{2}Re\{R_0'\} + Im\{\widetilde{Q_0}\} + 2yRe\{Q_0\} - \frac{y^2}{2}Im\{Q_0'\} - Re\{\widetilde{S_0}\} + 2yIm\{S_0\}$$

$$+ \frac{y^2}{2}Re\{S_0'\}], \tag{5.8}$$

$$\sigma_{yy} = \sum_{n=0}^{1} [Re\{P_n\} + yIm\{P_n'\} - yRe\{R_n'\} + yIm\{Q_n'\} + Im\{S_n\} - yRe\{S_n'\}] +$$

$$\delta_y \left[\frac{y^2}{2}Im\{P_0'\} - \frac{y^2}{2}Re\{R_0'\} + \frac{y^2}{2}Im\{Q_0'\} - \frac{y^2}{2}Re\{S_0'\} \right]. \tag{5.9}$$

In the above relations, Re and Im represent real and imaginary parts of a complex functions. P_n, Q_n, R_n and S_n, are introduced as,

$$P_n = A_n z^{n-1/2}, \qquad Q_n = B_n z^n, \qquad R_n = C_n z^{n-1/2}, \qquad S_n = D_n z^n, \tag{5.10}$$

where $z = x + iy$ and A_n, B_n, C_n, D_n are real constants to be determined. The ($'$) and ($\sim$) signs in the formulation mean derivative and integration with respect to the complex variable z, respectively.

Using the Hooke's law the strain field can be calculated, with material variation being a linear function of y, and the Poisson's ratio being a constant,

$$\varepsilon_{xx} = \frac{1-v^2}{E(y)}\left[\sigma_{xx} - \frac{v}{1-v}\sigma_{yy}\right], \varepsilon_{yy} = \frac{1-v^2}{E(y)}\left[\sigma_{yy} - \frac{v}{1-v}\sigma_{xx}\right], \varepsilon_{xy} = \frac{1}{2G(y)}\sigma_{xy}. \tag{5.11}$$

The displacements can then be determined from

$$\varepsilon_{xx} = \frac{\partial u}{\partial x}, \quad \varepsilon_{yy} = \frac{\partial v}{\partial y}, \quad \varepsilon_{xy} = \frac{1}{2}\left(\frac{\partial u}{\partial y} + \frac{\partial v}{\partial x}\right). \tag{5.12}$$

which give, for the first two terms of the expansion series,

$$u = \int \frac{1}{E(y)} \left[\left[\sum_{n=0}^{1}\left[Re\{P_n\} - yIm\{P_n'\} + 2Im\{R_n\} + yRe\{R_n'\} + 2Re\{Q_n\} + yIm\{Q_n'\}\right.\right.\right.$$

$$+Im\{S_n\} + yRe\{S_n'\}\right] + \delta_y\left[Im\{\widetilde{P_0}\} + 2yRe\{P_0\} - \frac{y^2}{2}Im\{P_0'\} - Re\{\widetilde{R_0}\}\right.$$

$$+2yIm\{R_0\} + \frac{y^2}{2}Re\{R_0'\} + Im\{\widetilde{Q_0}\} + 2yRe\{Q_0\} - \frac{y^2}{2}Im\{Q_0'\} - Re\{\widetilde{S_0}\}$$

$$+2yIm\{S_0\} + \frac{y^2}{2}Re\{S_0'\}\right]\right] - v\left[\sum_{n=0}^{1}\left[Re\{P_n\} + yIm\{P_n'\} - yRe\{R_n'\} + yIm\{Q_n'\}\right.\right.$$

$$\left.+Im\{S_n\} - yRe\{S_n'\}\right] + \delta_y\left[\frac{y^2}{2}Im\{P_0'\} - \frac{y^2}{2}Re\{R_0'\} + \frac{y^2}{2}Im\{Q_0'\}\right.$$

$$\left.\left.\left.-\frac{y^2}{2}Re\{S_0'\}\right]\right]\right] dx. \tag{5.13}$$

$$v = \int \frac{1}{E(y)} [[\sum_{n=0}^{1} [Re\{P_n\} + yIm\{P_n'\} - yRe\{R_n'\} + yIm\{Q_n'\} + Im\{S_n\} - yRe\{S_n'\}]$$

$$+ \delta_y [\frac{y^2}{2} Im\{P_0'\} - \frac{y^2}{2} Re\{R_0'\} + \frac{y^2}{2} Im\{Q_0'\} - \frac{y^2}{2} Re\{S_0'\}] - v [\sum_{n=0}^{1} [Re\{P_n\} -$$

$$yIm\{P_n'\} + 2Im\{R_n\} + yRe\{R_n'\} + 2Re\{Q_n\} + yIm\{Q_n'\} + Im\{S_n\} + yRe\{S_n'\}] +$$

$$\delta_y [Im\{\widetilde{P_0}\} + 2yRe\{P_0\} - \frac{y^2}{2} Im\{P_0'\} - Re\{\widetilde{R_0}\} + 2yIm\{R_0\} + \frac{y^2}{2} Re\{R_0'\} +$$

$$Im\{\widetilde{Q_0}\} + 2yRe\{Q_0\} - \frac{y^2}{2} Im\{Q_0'\} - Re\{\widetilde{S_0}\} + 2yIm\{S_0\} + \frac{y^2}{2} Re\{S_0'\}]]] \, dy.$$

(5.14)

According to this solution, the stress, strain and displacement fields at the crack tip are described analytically in terms of the coordinate position and real unknown coefficients A_0, A_1, B_0, B_1, C_0, C_1, D_0, and D_1, from which a finite element formulation will be developed.

5.2 Finite Element formulation

5.2.1 Nodal displacements

Consider a singular graded element at the crack tip as illustrated in Fig. 5.1. Since the singular element should be able to represent the rigid body motion, the displacements u_0, v_0, and rotation φ_0 corresponding to the rigid body motion will be added to the displacement field obtained,

$$\begin{Bmatrix} U(r,\theta) \\ V(r,\theta) \end{Bmatrix} = \begin{Bmatrix} u(r,\theta) \\ v(r,\theta) \end{Bmatrix} + \begin{Bmatrix} u_0 - (rsin\theta)\varphi_0 \\ v_0 + (rcos\theta)\varphi_0 \end{Bmatrix},$$

(5.15)

where U and V are the x and y components of the total displacement. The first vector on the right hand side of Eq. (5.15) represents the displacement due to the deformation as discussed before, and the last vector is the rigid body displacement vector for the node located at the position (r, θ) on the boundary of the singular element. The displacement field through the singular

element can be expressed as a known coefficient matrix $[H]$ multiplied by the vector of unknowns $\{\alpha\}$,

$$\begin{Bmatrix} U \\ V \end{Bmatrix} = [H]\{\alpha\}, \tag{5.16}$$

where,

$$\{\alpha\}^T = \{A_0 \quad A_1 \quad \dots \quad D_0 \quad D_1 \quad u_0 \quad v_0 \quad \varphi_0\}, \tag{5.17}$$

$$[H] = \begin{bmatrix} h_{11} & h_{12} & \cdots & h_{18} & 1 & 0 & -rsin\theta \\ h_{21} & h_{22} & \cdots & h_{28} & 0 & 1 & rcos\theta \end{bmatrix}, \tag{5.18}$$

The coefficient matrix $[H]$ can be calculated from Eqs. (5.13) and (5.14) by numerical integration, in which h_{1j}, h_{2j} ($j = 1, \dots, 8$) can be easily obtained by appropriate arrangement of these equations in terms of unknowns $(A_0, A_1, \dots, D_1)$.

Considering all the included p nodes of the singular element along the boundary of the element of radius R, Eq. (5.18) takes the following form.

$$\begin{Bmatrix} U_1 \\ V_1 \\ \vdots \\ U_p \\ V_p \end{Bmatrix} = \begin{bmatrix} h_{11}^1 & h_{12}^1 & \cdots & h_{18}^1 & 1 & 0 & -Rsin\theta_1 \\ h_{21}^1 & h_{22}^1 & \cdots & h_{28}^1 & 0 & 1 & Rcos\theta_1 \\ \vdots & \vdots & \vdots & \vdots & \vdots & \vdots & \vdots \\ h_{11}^p & h_{12}^p & \cdots & h_{18}^p & 1 & 0 & -Rsin\theta_p \\ h_{21}^p & h_{22}^p & \cdots & h_{28}^p & 0 & 1 & Rcos\theta_p \end{bmatrix} \begin{Bmatrix} A_0 \\ A_1 \\ \vdots \\ D_0 \\ D_1 \\ u_0 \\ v_0 \\ \varphi_0 \end{Bmatrix}. \tag{5.19}$$

Eq. (5.19) can be represented in the compact form as,

$$\{\mathbf{U}_s\}_{2p \times 1} = [\mathrm{T}]_{2p \times q}\{\alpha\}_{q \times 1}. \tag{5.20}$$

where q is the total number of unknowns in the unknown vector $\{\alpha\}$. For the order considered

$q = 11$.

5.2.2 Shape function matrix

The unknown vector $\{\alpha\}$, as defined in Eq. (5.17), can be expressed in terms of the nodal

displacements of the singular element. From Eq. (5.20), $[T]^T\{\mathbf{U}_s\} = [T]^T[T]\{\alpha\}$ which leads to

$$\{\alpha\} = \left[[T]^T[T]\right]^{-1}[T]^T\{\mathbf{U}_s\} = [\boldsymbol{Q}]\{\mathbf{U}_s\}. \tag{5.21}$$

It should be mentioned that to ensure that the inversion of $\left[[T]^T[T]\right]$ exists, $2p$ should be greater

than or equal to q. For example, for the order considered, there exists 11 unknowns in the

unknown vector $\{\alpha\}$. Hence, at least 6 nodes along the boundary of the singular element are

needed.

For the case that material gradation direction (y) is perpendicular to the crack alignment (x),

substitution of the Eq. (5.21) into Eq. (5.16) leads to,

$$\begin{Bmatrix} U \\ V \end{Bmatrix} = [H][\boldsymbol{Q}]\{\mathbf{U}_s\} = [N]\{\mathbf{U}_s\}, \tag{5.22}$$

from which the displacement field in the singular element is expressed in terms of the nodal

displacements. As a result, the matrix $[N]$ represents the shape functions for the singular

element.

5.2.3 Stiffness matrix

By considering the strain-displacement relation, the strain field will be obtained in terms of the nodal displacements, as

$$\{\epsilon\} = \begin{Bmatrix} \epsilon_{xx} \\ \epsilon_{yy} \\ \epsilon_{xy} \end{Bmatrix} = \begin{bmatrix} \dfrac{\partial}{\partial x} & 0 \\ 0 & \dfrac{\partial}{\partial y} \\ \dfrac{\partial}{\partial y} & \dfrac{\partial}{\partial x} \end{bmatrix} \begin{Bmatrix} U \\ V \end{Bmatrix} = \begin{bmatrix} \dfrac{\partial}{\partial x} & 0 \\ 0 & \dfrac{\partial}{\partial y} \\ \dfrac{\partial}{\partial y} & \dfrac{\partial}{\partial x} \end{bmatrix} [N]\{\mathbf{U}_s\} = [B]\{\mathbf{U}_s\}. \tag{5.23}$$

By multiplying the elastic matrix to the strain vector, the stresses for the singular element will be obtained as follows:

$$\{\sigma\} = \begin{Bmatrix} \sigma_{xx} \\ \sigma_{yy} \\ \sigma_{xy} \end{Bmatrix} = \frac{E(y)}{(1+v)(1-2v)} \begin{bmatrix} 1-v & v & 0 \\ v & 1-v & 0 \\ 0 & 0 & \dfrac{1-2v}{2} \end{bmatrix} \begin{Bmatrix} \epsilon_{xx} \\ \epsilon_{yy} \\ \epsilon_{xy} \end{Bmatrix} = [D][B]\{\mathbf{U}_s\}. \tag{5.24}$$

Using Eqs. (5.23) and (5.24), the strain energy (V_S) in the singular element can be determined as

$$V_S = \frac{1}{2} \int_{A_s} \{\epsilon\}^T \{\sigma\} dA_S = \frac{1}{2} \{\mathbf{U}_s\}^T [\mathbf{K}_s]\{\mathbf{U}_s\} \tag{5.25}$$

where

$$[\mathbf{K}_s] = \int_{A_s} [B]^T [D][B] \, dA_S \tag{5.26}$$

For this singular element, the applied loads are at the nodes along the boundary which can be represented as a vector $\{F_S\}$, then the total potential energy of the element is,

$$\Pi_S = V_S - \{\mathbf{U}_s\}^T \{F_S\} = \frac{1}{2}\{\mathbf{U}_s\}^T [\mathbf{K}_s]\{\mathbf{U}_s\} - \{\mathbf{U}_s\}^T \{F_S\}. \tag{5.27}$$

The principle of minimum potential energy (Zienkiewicz & Taylor 2000) indicates that the variation of Π_S shown by $\delta\Pi_S$ equals to zero which results in

$$[\mathbf{K}_s]\{\mathbf{U}_s\} = \{F_S\} \tag{5.28}$$

where $[\mathbf{K}_s]$ is the stiffness matrix of the singular element.

5.2.4 Determination of the unknown coefficients

Consider a finite element model which is discretized by graded regular 9-node quadrilateral elements and a graded singular element shown in Fig. 5.1. For such a model, similar to Eq. (5.27), the potential energy of the whole system can be represented by the sum of the strain energy for both graded regular (V_R) and singular (V_S) elements minus the work done by the external loading ($\bar{\sigma}$),

$$\Pi = V_R + V_S - \int_\Gamma \{\mathbf{U}\}^T \{\bar{\sigma}\}\, dS, \tag{5.29}$$

$$V_R = \frac{1}{2}\{\mathbf{U}\}^T [\mathbf{K}]\{\mathbf{U}\}, \quad V_S = \frac{1}{2}\{\mathbf{U}_s\}^T [\mathbf{K}_s]\{\mathbf{U}_s\}. \tag{5.30}$$

In Eq. (5.30) $\{\mathbf{U}\}$ is the vector of all displacements at the nodes of the regular graded elements, and $[\mathbf{K}]$ is the stiffness matrix formed by these regular elements, given in chapter 3. The boundary value problem introduced in Eq. (5.19) can then be solved by equating the

displacement components at the boundary between the singular and other surrounding regular elements. For this purpose, the displacement field represented by regular elements $\{\mathbf{U}\}$ should be decomposed to two parts as the components with respect to interior displacement vector $\{\mathbf{U}_i\}$ and those located at the common boundary with the singular element $\{\mathbf{U}_b\}$. Thus, Eq. (5.29) takes the following form,

$$\Pi = \frac{1}{2}\begin{Bmatrix}\mathbf{U}_i\\\mathbf{U}_b\end{Bmatrix}^T \begin{bmatrix}\mathbf{K}_{ii} & \mathbf{K}_{ij}\\\mathbf{K}_{ji} & \mathbf{K}_{jj}\end{bmatrix}\begin{Bmatrix}\mathbf{U}_i\\\mathbf{U}_b\end{Bmatrix} + \frac{1}{2}\{\mathbf{U}_s\}^T[\mathbf{K}_s]\{\mathbf{U}_s\} - \int_\Gamma \{\mathbf{U}\}^T\{\bar{\sigma}\}\,dS. \tag{5.31}$$

The continuity of the displacement between the singular element and its surrounding graded regular elements leads to,

$$\{\mathbf{U}_b\} = \{\mathbf{U}_s\} = [\mathrm{T}]\{\alpha\}. \tag{5.32}$$

After assembling the stiffness matrices, it can be written as

$$\Pi = \frac{1}{2}\begin{Bmatrix}\mathbf{U}_i\\\alpha\end{Bmatrix}^T \begin{bmatrix}\mathbf{K}_{ii} & \mathbf{K}_{ij}T\\T^T\mathbf{K}_{ji} & T^T(\mathbf{K}_{jj} + \mathbf{K}_s)T\end{bmatrix}\begin{Bmatrix}\mathbf{U}_i\\\alpha\end{Bmatrix} - \int_\Gamma \{\mathbf{U}\}^T\{\bar{\sigma}\}\,dS. \tag{5.33}$$

Minimizing the potential energy, results in a set of algebraic equations,

$$\begin{bmatrix}\mathbf{K}_{ii} & \mathbf{K}_{ij}T\\T^T\mathbf{K}_{ji} & T^T(\mathbf{K}_{jj} + \mathbf{K}_s)T\end{bmatrix}\begin{Bmatrix}\mathbf{U}_i\\\alpha\end{Bmatrix} = \{\mathcal{F}\}, \tag{5.34}$$

where $\{\mathcal{F}\}$ represents the loading vector. After solving Eq. (5.34) all unknowns of the problem will be determined.

To determine the SIFs, consider the stress field near the crack tip. From Eq. (5.9),

$$\sigma_{yy} = Re\left\{\frac{A_0}{\sqrt{z}}\right\} + higher\ order\ terms \tag{5.35}$$

Therefore, the SIF for mode I is

$$K_I = \lim_{\text{mod}(z)\to 0}(\sqrt{2\pi z}\ \sigma_{yy}) = \sqrt{2\pi}A_0. \tag{5.36}$$

Similarly,

$$\sigma_{xy} = Re\left\{\frac{C_0}{\sqrt{z}}\right\} + higher\ order\ terms \tag{5.37}$$

$$K_{II} = \lim_{\text{mod}(z)\to 0}(\sqrt{2\pi z}\ \sigma_{xy}) = \sqrt{2\pi}C_0. \tag{5.38}$$

The mode mixity Ψ can be determined as,

$$\Psi = tan^{-1}\frac{K_{II}}{K_I}. \tag{5.39}$$

The energy release rate can also be calculated accordingly as,

$$G = \frac{K_I^2 + K_{II}^2}{E_{tip}}. \tag{5.40}$$

The nonsingular stress at the crack tip appears as $\sigma_{0x} = -2B_0$.

5.3 Results and discussion

5.3.1 Computational model

In order to probe the efficiency of the developed element for investigating fracture parameters in linear elastic isotropic FGMs with spatial variation of elastic constants, a set of examples representing an edge crack problem in FGMs, is shown in Fig. 5.2. Fig. 5.2 illustrates the geometry and discretized model including 52 graded regular 9-node isoparametric quadrilateral elements and one graded singular element containing 17 nodes. The width and height of the plate are W and H, respectively, with the H/W ratio being 1.31. A uniform tensile load of $\sigma_{yy} = 3.17$ MPa is applied to the top and bottom surfaces. Crack surfaces are traction free and the node located at $(x, y) = (W, H/2)$ is locked in x and y directions to remove rigid body motion. For the sake of convenience in description of the geometry and variation of elastic properties through the model, a reference coordinate system is located at the left lower corner of the model.

The introduced graded singular element with the linear elastic isotropic properties can be described by the number of unknown coefficients attained by truncating the series expansion for the stress function. The radius of the singular element (R) and the angle between adjacent nodes $(\Delta\theta)$ are other parameters which characterize the singular element. To ensure accuracy the size of the singular element is usually limited. In the current study R and $\Delta\theta$ are selected to be $R/a \leq 0.1$, and $\Delta\theta = 22.5°$ based on existing results (Tan 1998), which show that when the size of the singular element is $0.1a$ for a finite edge crack problem of length a subjected to mode I loading, accurate results can be obtained with about 2% error. The selection of the size of this singular element is also verified by evaluating the effect of different sizes of the singular element. Fig. 5.3 illustrates the variation of the normalized SIF for homogeneous and FGM

$(E_{top}/E_{bottom} = 2)$ plates with $a/W = 0.5$, and $\Delta\theta = 22.5°$ obtained with different sizes of the singular element with the other elements being adjusted accordingly. The variation in the normalized SIF is about 2%, compared with its average value. Numerical results are also compared with the analytical solution (Fett 1998) for homogeneous materials and the error is around 2% when $R/a \le 0.1$. Because of the excellent results shown, this size of the singular element will be used in the following discussion. Accordingly, the first two terms will be used in the series expansion in Eq. (5.2) which provides 11 unknowns for the singular element.
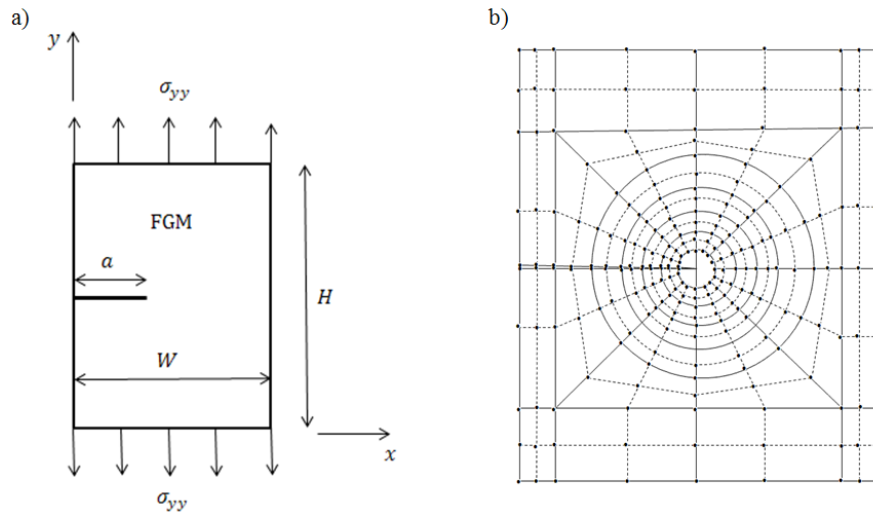
Fig. 5.2. Schematic illustration of a) geometry of the edge crack problem b) meshing of the model.
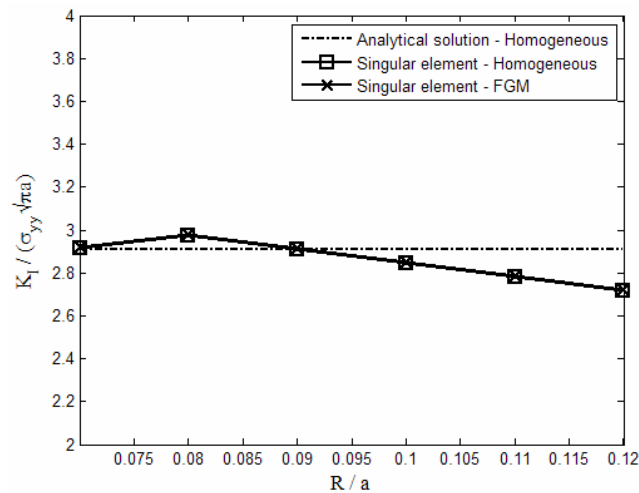
Fig. 5.3. Normalized stress intensity factor versus different sizes of the singular element.

5.3.2 Comparison between the graded singular element and existing solutions

At first, the validity of numerical results obtained with the graded singular element is demonstrated by comparing the normalized mode-I SIF for homogeneous materials with the solution provided by the weight function technique which considers the geometry effect (Fett 1998). Elastic properties attributed to the model are $E = 66.3$ GPa and $v = 0.23$. The boundary conditions are similar to what is illustrated in Fig. 5.2a. The determined coefficients involved in the singular element are given in table 5.1 for different a/W ratios. The SIF is determined from A_0 and compared with the analytical solution.

Table 5.1. Coefficients related to the stress function and normalized SIFs for different crack lengths in homogeneous structures.

a/W	$A_0 \times 10^{-6}$	$A_1 \times 10^{-6}$	$B_0 \times 10^{-6}$	$B_1 \times 10^{-6}$	$C_0 \times 10^{-6}$	$C_1 \times 10^{-6}$	$D_0 \times 10^{-6}$	$D_1 \times 10^{-6}$	$\dfrac{K_I}{\sigma_{yy}\sqrt{\pi a}}$			$\dfrac{K_{II}}{\sigma_{yy}\sqrt{\pi a}}$
									Current work	Analytical (Fett 1998)	Error%	
0.4	1.8630	-38.6163	4.9526	198.5094	0	0	0	0	2.3381	2.31	1.22	0
0.5	2.6505	-68.0597	9.0938	289.6431	0	0	0	0	2.9752	2.91	2.24	0
0.6	4.0584	-131.5868	15.8344	506.1866	0	0	0	0	4.1586	4.14	0.45	0

Secondly, consider the case that the material gradation is perpendicular to the crack line, and the rectangular FGM plate is under the same uniform tensile loading as indicated in Fig. 5.4. It is assumed that E_{top}/E_{bottom} equals to 7, where E_{bottom} and v are considered as 66.3 GPa and 0.23, respectively, and a/W ratio equals to 0.5.
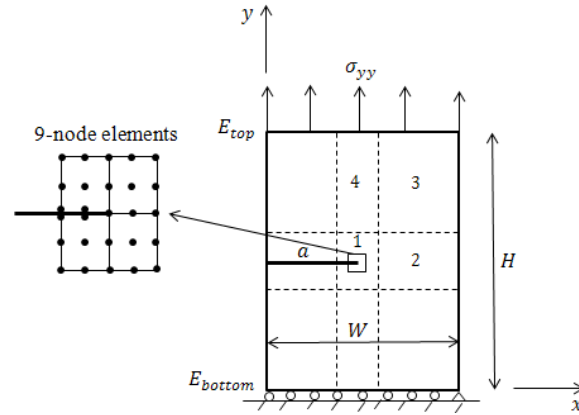
Fig. 5.4. The geometry, loading, and boundary conditions for an edge crack normal to the material gradation direction.

To compare the efficiency of new singular element with that of non-singular element for FGMs, the problem shown in Fig. 5.4 is solved using both elements. The model is meshed via non-singular graded quadrilateral 9-node elements. Table 5.2 represents the element size used for meshing the model at areas labeled in Fig. 5.4. The mesh is symmetric with respect to horizontal and vertical axes passing through the crack tip. The comparison between the solution using the dense mesh of non-singular elements and singular element approach is performed. The crack opening displacement is computed with these two approaches as shown in Fig. 5.5 in which x and R are the distance from the crack tip and singular element radius respectively. The convergence of the crack opening outputs using non-singular graded elements is checked with employing different element numbers in the model. It can be observed that solution approximately converges by utilizing 4900 elements. As indicated, results obtained with very fine mesh and singular element are in a good agreement which accredits the validity of the newly developed singular element.

Table 5.2. Meshing information for the model meshed with non-singular graded quadrilateral 9-node elements.

No. of elements	No. of nodes	Area	$\Delta x_{element}/W$	$\Delta y_{element}/H$
19600	79101	1	0.002	0.002
		2	0.02	0.002
		3	0.02	0.02
		4	0.002	0.02
4900	19951	1	0.004	0.004
		2	0.04	0.004
		3	0.04	0.04
		4	0.004	0.04
1600	6601	1	0.01	0.01
		2	0.04	0.01
		3	0.04	0.04
		4	0.01	0.04
400	1701	1	0.02	0.02
		2	0.08	0.08
		3	0.08	0.08
		4	0.02	0.08
256	1105	1	0.033	0.033
		2	0.08	0.033
		3	0.08	0.08
		4	0.033	0.033
No. of elements	No. of nodes	Area	$\Delta x_{element}/W$	$\Delta y_{element}/H$
64	297	1	0.05	0.05
		2	0.2	0.05
		3	0.2	0.2
		4	0.05	0.2
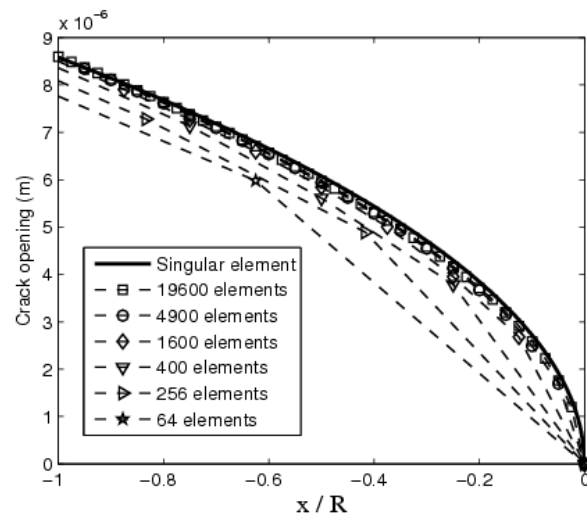
Fig. 5.5. Comparison of the crack tip opening obtained with using refined mesh of non-singular elements and singular element approach.

5.3.3 Fracture parameters obtained with the graded singular element

In table 5.3, unknown coefficients mentioned in the graded singular element formulation are computed for different values of the non-homogeneity parameter (δ_y) and normalized crack length (a/W) for the case shown in Fig. 5.4. Normalized SIFs are calculated from the determined unknowns. From these results, fracture parameters will be determined and analyzed.

Table 5.3. Coefficients related to the stress function and normalized SIFs for different crack lengths and non-homogeneity constant when material gradation direction is normal to the crack line.

a/W	$A_0 \times 10^{-6}$	$A_1 \times 10^{-6}$	$B_0 \times 10^{-6}$	$B_1 \times 10^{-6}$	$C_0 \times 10^{-6}$	$C_1 \times 10^{-6}$	$D_0 \times 10^{-6}$	$D_1 \times 10^{-6}$	$\dfrac{K_I}{\sigma_{yy}\sqrt{\pi a}}$	$\dfrac{K_{II}}{\sigma_{yy}\sqrt{\pi a}}$
$E_{top}/E_{bottom} = 1$										
0.4	1.8471	-36.5358	4.4388	193.9219	0	0	0	0	2.3181	0
0.5	2.6361	-65.5544	8.2761	287.1983	0	0	0	0	2.9590	0
0.6	4.0492	-129.6854	14.9043	508.8310	0	0	0	0	4.1492	0
$E_{top}/E_{bottom} = 2$										
0.4	1.8530	-37.3795	4.5654	195.4952	0.0428	-8.9866	-0.0756	17.3767	2.3255	0.0537
0.5	2.6425	-66.7073	8.4656	289.4179	0.0701	-12.9551	-0.0591	21.4092	2.9662	0.0787
0.6	4.0559	-131.2580	15.1820	513.3484	0.1202	-23.9767	0.5342	47.5245	4.1561	0.1232
$E_{top}/E_{bottom} = 5$										
0.4	1.8768	-40.5435	5.1788	216.6991	0.1207	-38.4357	1.7048	85.5099	2.3554	0.1515
0.5	2.6662	-70.7436	9.3638	318.6645	0.1895	-55.9500	2.4641	110.4208	2.9928	0.2127
0.6	4.0792	-136.2357	16.3979	560.3147	0.2589	-92.5089	4.8621	190.0632	4.1800	0.2653
$E_{top}/E_{bottom} = 7$										
0.4	1.8871	-41.7474	5.4672	234.1101	0.1334	-52.5682	2.7322	116.6342	2.3683	0.1674
0.5	2.6761	-72.1802	9.7817	342.7354	0.2092	-76.2221	3.9040	149.2357	3.0039	0.2348
0.6	4.0883	-137.8963	16.9391	598.0511	0.2720	-124.0657	7.1895	249.0894	4.1893	0.2787

5.3.3.1 Stress intensity factors

The variation of the normalized mode-I SIF against the dimensionless non-homogeneity factor $\delta_y H$ is shown in Fig. 5.6 for different (a/W) ratios. From this figure it can be understood that the mode-I SIF is less sensitive to the non-homogeneity parameter and slightly increases with increasing gradient index. On the other hand, as illustrated in Fig. 5.7 the normalized mode-II SIF is more sensitive to the material gradient, and increases significantly with increasing gradient index, however, its rate of growth decreases for higher non-homogeneity constants.
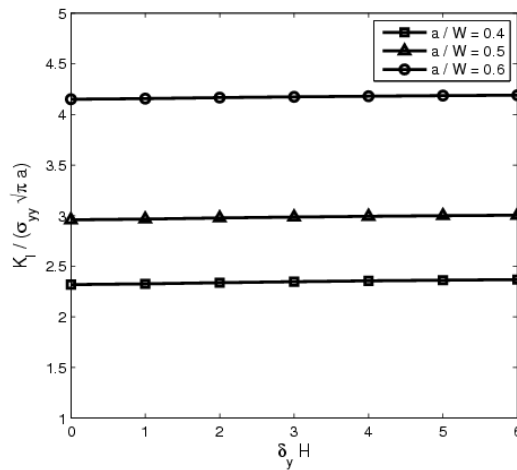
Fig. 5.6. Variation of the normalized mode-I SIF vs dimensionless non-homogeneity parameter for $a/W = 0.4, 0.5, 0.6$.
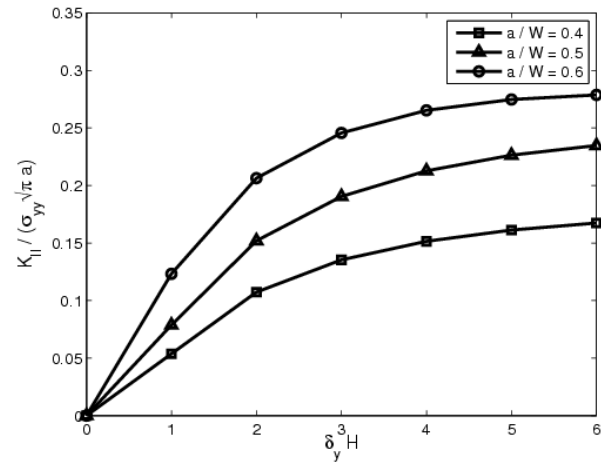
Fig. 5.7. Variation of the normalized mode-II SIF vs dimensionless non-homogeneity parameter for $a/W = 0.4, \ 0.5, \ 0.6$.

The mode mixity defined by Eq. (5.39) for various a/W ratios is plotted in Fig. 5.8 in which mode mixity Ψ is normalized by the value for the case when $\delta_y H = 6$. It is revealed that normalized mode mixity approaches to a specific value when the gradation index is sufficiently great. It is also observed that normalized mode mixity differs very slightly between $a/W = 0.4, 0.5$ while it becomes stronger for a longer crack as shown for $a/W = 0.6$.
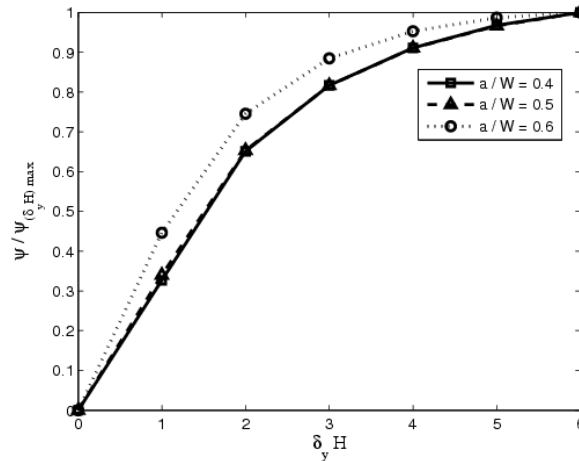
Fig. 5.8. Normalized mode mixity against dimensionless non-homogeneity parameter for $a/W = 0.4,\ 0.5,\ 0.6$.

5.3.3.2 Energy release rate

The change of energy release rate calculated from SIFs and normalized by the corresponding values for homogeneous materials is represented in Fig. 5.9. As shown, with increasing dimensionless non-homogeneity the normalized energy release rate drops drastically so that for $\delta_y H = 6$ it is 74% smaller than that of the homogeneous material. This trend is mainly caused by the increase of the crack tip Young's modulus at the denominator of the fraction in Eq. (5.40) for computing the energy release rate.
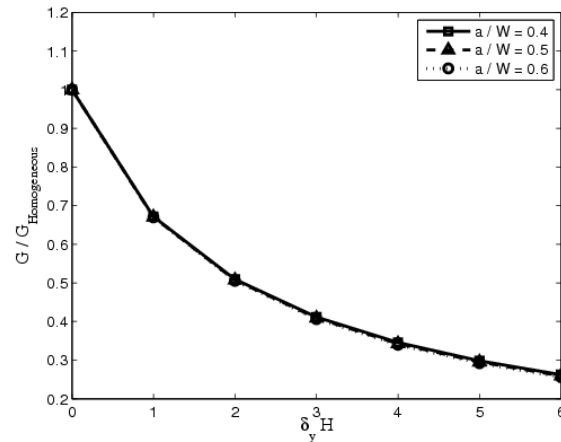
Fig. 5.9. Normalized energy release rate against dimensionless non-homogeneity parameter for $a/W = 0.4, \ 0.5,$

0.6.

5.3.3.3 Non-singular stress at the crack tip (T-stress)

The role of the non-singular stress, σ_{0x}, also known as T-stress is important in discussing the mixed mode crack growth, the crack path stability, crack tip constraint, and toughness. Negative values of σ_{0x} represents a shielding effect. The variation of the normalized σ_{0x} versus the material gradient index is plotted in Fig. 5.10. It is observed that normalized σ_{0x} increases with the increase of the non-homogeneity index. The physical interpretation of this issue is that with higher material gradient index, the shielding effect becomes stronger. Furthermore, the smaller values of σ_{0x} obtained for longer cracks can be explained by the reduction in crack growth stability.
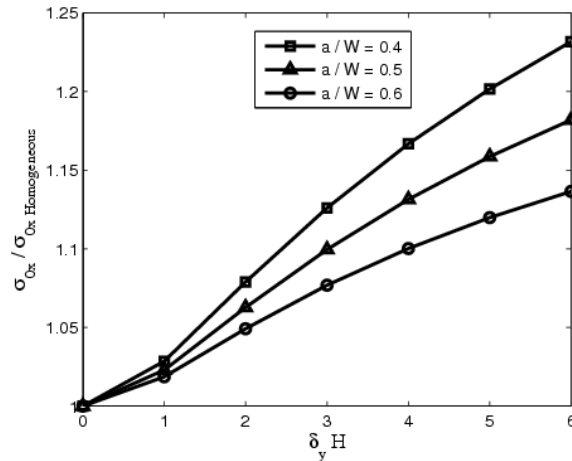
Fig. 5.10. Normalized constant non-singular stress σ_{0x} against dimensionless non-homogeneity parameter for

$$a/W = 0.4, \ 0.5, \ 0.6.$$

5.3.3.4 Contribution of higher order terms in the crack tip stress field

To evaluate the contribution of higher order terms, the effect of $A_1, B_1, C_1,$ and D_1 on the stress field ahead of the crack are calculated separately and shown in Figs. 5.11-5.14 for the case that $E_{top}/E_{bottom} = 7$ and $a/W = 0.5$. The physical meaning of these coefficients is related to the stress caused by the higher order terms in the stress function, which provide more accurate description of the crack tip field.
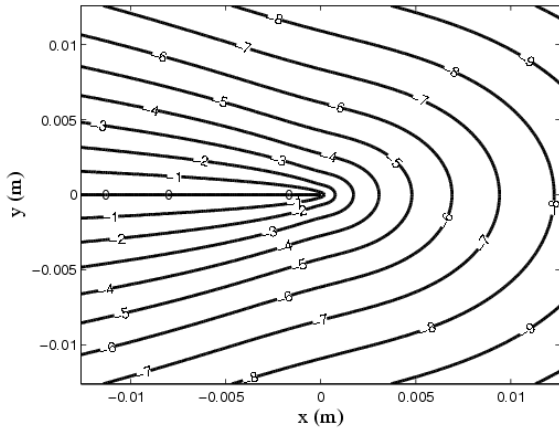
Fig. 5.11. Contribution of higher order terms corresponding to A_1 in the stress field σ_{xx} (MPa) at the crack tip.
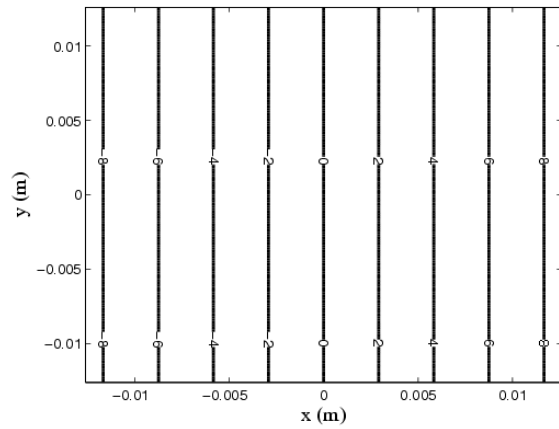
Fig. 5.12. Contribution of higher order terms corresponding to B_1 in the stress field σ_{xx} (MPa) at the crack tip.
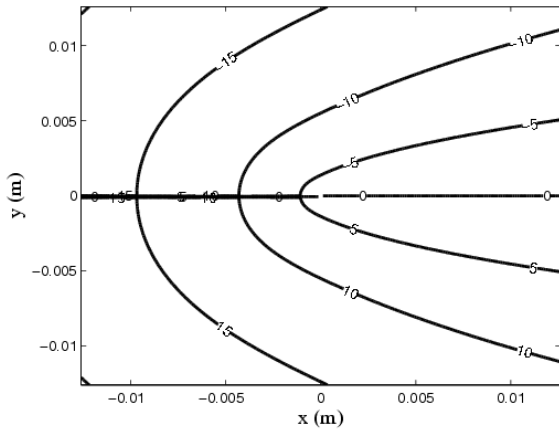
Fig. 5.13. Contribution of higher order terms corresponding to C_1 in the stress field σ_{xx} (MPa) at the crack tip.
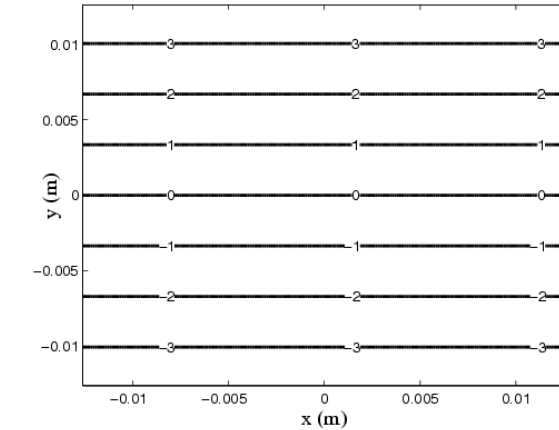
Fig. 5.14. Contribution of higher order terms corresponding to D_1 in the stress field σ_{xx} (MPa) at the crack tip.

The variation of elastic property will result in non-singular higher order terms in the stress field, which is proportional to δ_y, as in Eq. (5.8). These higher order terms are dominant in distinction of the solution for homogeneous materials and FGMs. Figs. 5.15-5.18 indicate the stress due to these higher order term. The contribution of $A_0, B_0, C_0,$ and D_0 on these higher order terms is computed and represented respectively.
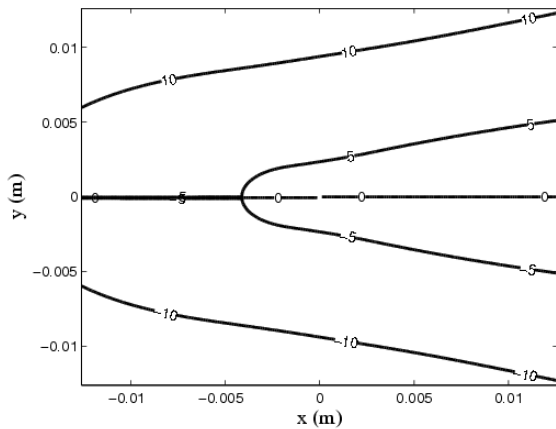
Fig. 5.15. Higher order non-singular σ_{xx} (MPa) at the

crack tip corresponding to A_0.
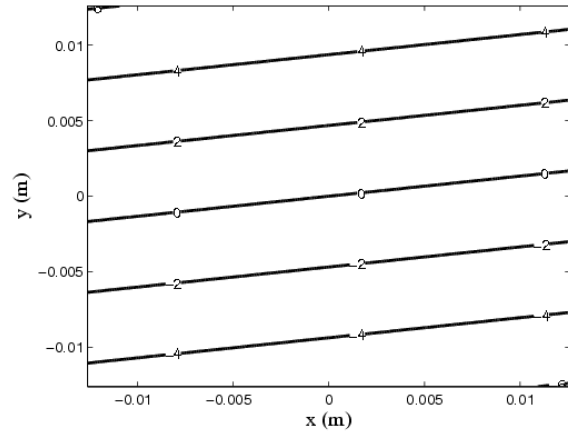
Fig. 5.16. Higher order non-singular σ_{xx} (MPa) at the

crack tip corresponding to B_0.
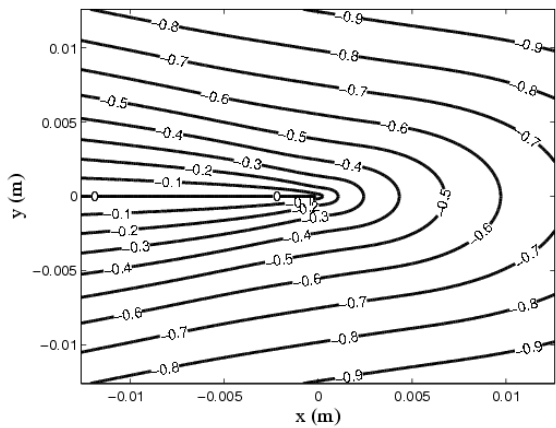
Fig. 5.17. Higher order non-singular σ_{xx} (MPa) at the

crack tip corresponding to C_0.
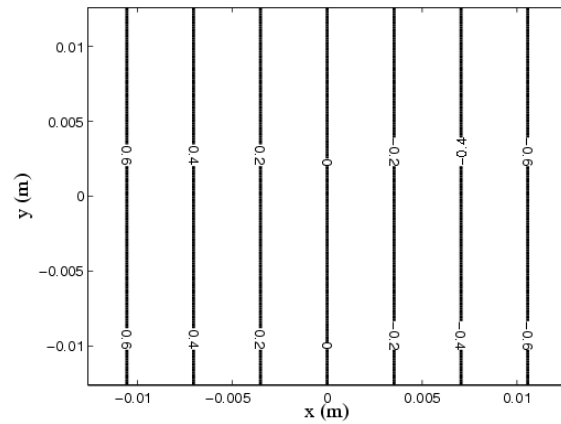
Fig. 5.18. Higher order non-singular σ_{xx} (MPa) at the

crack tip corresponding to D_0.

4.3.3.5 Contours of stress near the crack tip

The stress field ahead of the crack can be described by drawing contours of stress for

homogeneous and graded materials with a/W ratio being 0.5 in Figs. 5.19-5.24. As indicated by

the figures, the stress distribution around the crack tip is symmetric with respect to the crack line

for homogeneous materials; however, in the case of graded materials due to the break of material

symmetry, contours of stress do not remain symmetric. These figures reveal that the structure of contours is unaffected at very close distances to the crack tip for graded materials; nevertheless, the singular field changes significantly away from the crack tip owing to the contribution of the higher order terms.

The developed singular element is aimed at stationary cracks, focusing on accurately evaluating the local stress field near crack tips in FGMs. The element will also be suitable for steady state growth but remeshing of other elements is necessary. For fast crack propagation, i.e. dynamic problems, the singular element can be used but the element size needs to be sufficiently small to reduce discrepancy caused by ignoring the inertial effect in the current singular element.

Contours of maximum principal stress are computed and drawn in Figs. 5.25 and 5.26 for homogeneous and FGMs, respectively, to evaluate the effect of material variation. These figures provide detailed information about the direction of the maximum stress, which differs from that of homogeneous materials. As illustrated in Fig. 5.26 contours of constant maximum principal stress tilt toward the compliant side in FGMs.
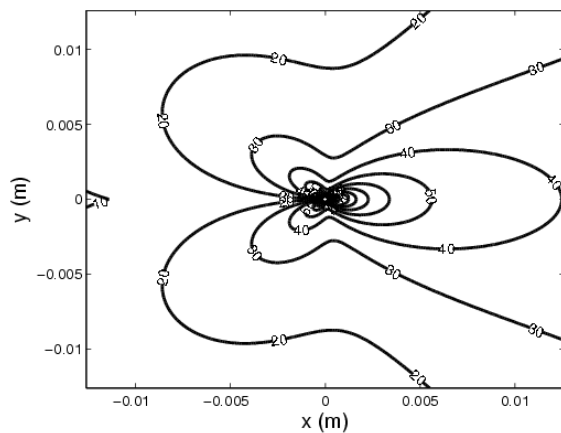
Fig. 5.19. Contours of σ_{xx} (MPa) near the crack tip for homogeneous material ($E_{top}/E_{bottom} = 1$).
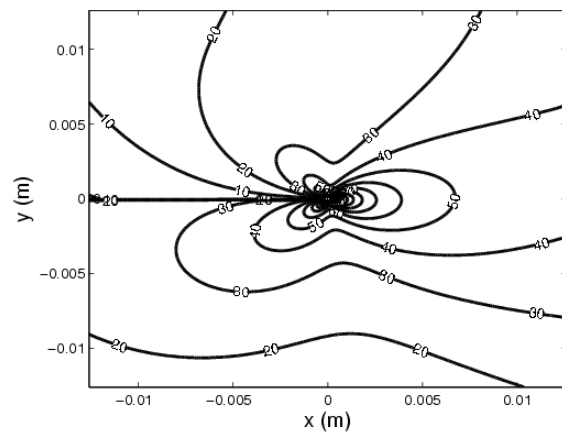
Fig. 5.20. Contours of σ_{xx} (MPa) near the crack tip for graded material ($E_{top}/E_{bottom} = 7$).
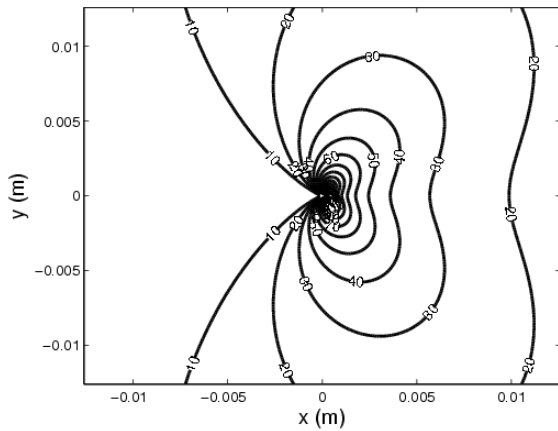
Fig. 5.21. Contours of σ_{yy} (MPa) near the crack tip for homogeneous material ($E_{top}/E_{bottom} = 1$).
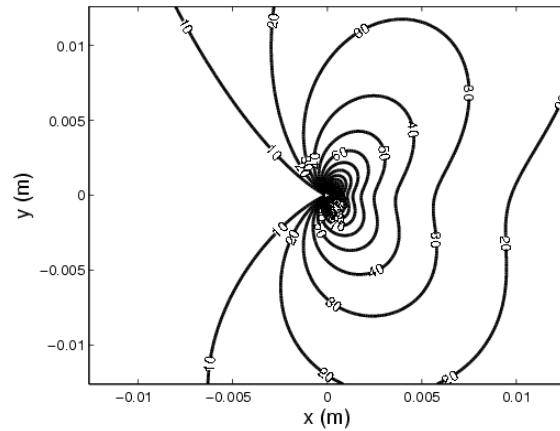
Fig. 5.22. Contours of σ_{yy} (MPa) near the crack tip for graded material ($E_{top}/E_{bottom} = 7$).
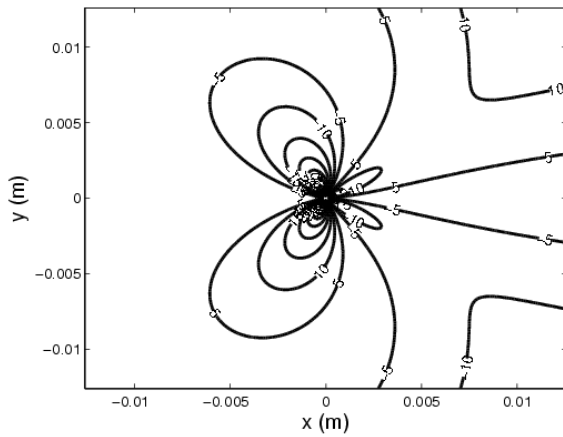
Fig. 5.23. Contours of σ_{xy} (MPa) near the crack tip for homogeneous material ($E_{top}/E_{bottom} = 1$).
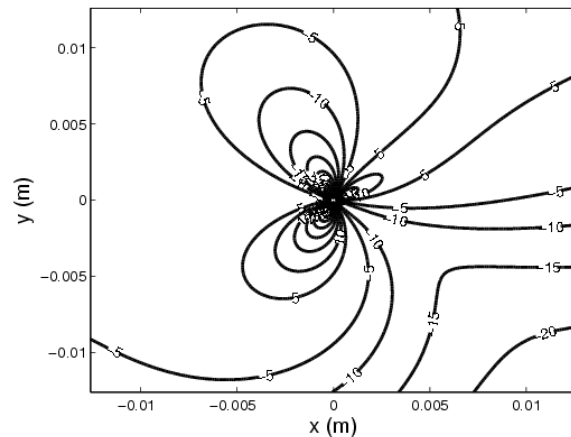
Fig. 5.24. Contours of σ_{xy} (MPa) near the crack tip for graded material ($E_{top}/E_{bottom} = 7$).
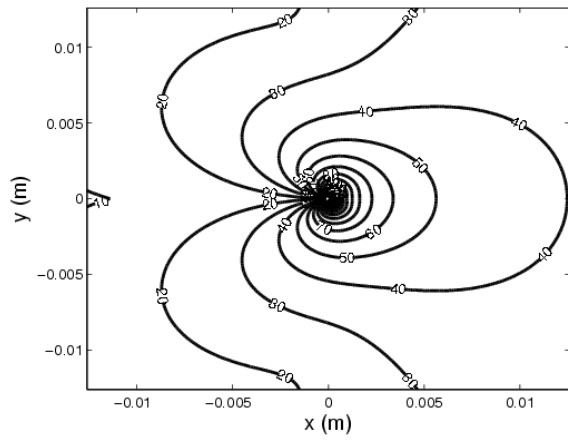
Fig. 5.25. Contours of maximum principal stress (σ_{max}) (MPa) near the crack tip for homogeneous material ($E_{top}/E_{bottom} = 1$).

Fig. 5.26. Contours of maximum principal stress ($\boldsymbol{\sigma_{max}}$) (MPa) near the crack tip for graded material ($\boldsymbol{E_{top}/E_{bottom} = 7}$).

Chapter 6

Dynamic Analysis of Crack Problems in Functionally Graded Materials Using a New Graded Singular Finite Element[*]

In this chapter the graded singular element developed in chapter 5 is used for studying dynamic crack problems in linear elastic isotropic functionally graded materials (FGMs) with spatially varying elastic parameters. Details of the FEM formulation are mentioned in chapter 5. The stiffness and consistent mass matrices for the singular element are determined based on the principle of minimum potential energy and kinetic energy of the element, respectively. The global stiffness and mass matrices are then generated by assembling matrices for the singular and adjacent regular elements by considering the displacement continuity at their common boundary. The results from the current method are compared with existing solutions to evaluate the accuracy of the technique. A set of simulations are performed using this element for analyzing dynamic crack problems in FGMs whose elastic properties vary normal to the crack line. Compared with traditional elements, the proposed element includes higher order terms in addition to the singular term, which leads to accurate description of the stress field near the crack

---

[*] This chapter is published as (Molavi Nojumi and Wang 2018)

tip. It also significantly reduces the calculation time needed in comparison with using very fine mesh of traditional elements. With the use of the singular element, no post processing technique is required for calculating fracture parameters such as stress intensity factors, energy release rate, and mode mixity.

6.1 Crack-tip fields in FGMs

Consider the crack tip stress field under the plane strain condition in linearly elastic isotropic FGM in which elastic constants vary in the direction perpendicular to the crack line (y-direction) as shown in Fig. 6.1, where the origin of the coordinate system is located at the crack tip. The material constants may vary exponentially, linearly or in other general forms. The focus of the current work is on the crack tip field and the area of interest for the crack tip element is relatively small in comparison with the size of the crack. Therefore, only the zeroth and the first order variations of the material constants, which are the most important terms for the crack tip field, are included in the formulation of the crack tip field, which provide a simple yet general description of the graded material property. For the case that material gradation direction (y) is perpendicular to the crack alignment (x), the Young's modulus and mass density can be expressed as,

$$E(y) = E_0(1 + \delta_E y), \tag{6.1}$$

$$\rho(y) = \rho_0(1 + \delta_\rho y), \tag{6.2}$$

where E_0, ρ_0, δ_E and δ_ρ are the Young's modulus and mass density at the coordinate center and the elastic and density gradient indexes, respectively. The Poisson's ratio is assumed to be a constant in the material.

Under general dynamic loading, the dynamic behaviour of elastic FGMs as governed by the equation of motion, in absence of body forces, can be described as,

$$\nabla \cdot \boldsymbol{\sigma} = \rho(y)\ddot{\boldsymbol{u}}, \tag{6.3}$$

where ∇, $\boldsymbol{\sigma}$ and $\boldsymbol{u}$ are the del operator, the stress and displacement, respectively. The stress-strain relation is governed by

$$\{\sigma\} = \begin{Bmatrix} \sigma_{xx} \\ \sigma_{yy} \\ \sigma_{xy} \end{Bmatrix} = \frac{E(y)}{(1+v)(1-2v)} \begin{bmatrix} 1-v & v & 0 \\ v & 1-v & 0 \\ 0 & 0 & \frac{1-2v}{2} \end{bmatrix} \begin{Bmatrix} \epsilon_{xx} \\ \epsilon_{yy} \\ 2\epsilon_{xy} \end{Bmatrix}, \tag{6.4}$$

and

$$\{\epsilon\} = \begin{Bmatrix} \epsilon_{xx} \\ \epsilon_{yy} \\ 2\epsilon_{xy} \end{Bmatrix} = \begin{bmatrix} \frac{\partial}{\partial x} & 0 \\ 0 & \frac{\partial}{\partial y} \\ \frac{\partial}{\partial y} & \frac{\partial}{\partial x} \end{bmatrix} \begin{Bmatrix} u \\ v \end{Bmatrix}. \tag{6.5}$$

It is well-understood that the stress field at the crack tip will be square-root singular (Delale and Erdogan 1983; Erdogan 1995). Correspondingly, the displacement and stress near the crack tip can be generally expanded in polar coordinates (r, θ) (Jain, Rousseau, and Shukla 2004; Molavi Nojumi and Wang 2017a) as

$$u_i = \sum_{n=0}^{\infty} r^{\left(n+\frac{1}{2}\right)} f_{in}^u(\theta, E, v) + \sum_{n=0}^{\infty} r^{(n+1)} g_{in}^u(\theta, E, v), (i = 1,2) \tag{6.6}$$

$$\sigma_{ij} = \sum_{n=0}^{\infty} r^{\left(n-\frac{1}{2}\right)} f_{ijn}^{\sigma}(\theta, E, v) + \sum_{n=0}^{\infty} r^{(n)} g_{ijn}^{\sigma}(\theta, E, v), (i, j = 1, 2) \tag{6.7}$$

where r represents the distance from the crack tip. In general, f_{in}^{u}, g_{in}^{u}, f_{ijn}^{σ} and g_{ijn}^{σ} are functions depending on the material property and the coordinate position. The zero order in Eqs. (6.6) and (6.7) represents the singular field at the crack tip and the first order represents a higher order term. If only zero and first order are considered, the displacement and stress fields become,

$$u_i = r^{\left(\frac{1}{2}\right)} f_{i0}^{u}(\theta, E, v) + r^{\left(\frac{3}{2}\right)} f_{i1}^{u}(\theta, E, v) + r g_{i0}^{u}(\theta, E, v), \tag{6.8}$$

$$\sigma_{ij} = r^{\left(\frac{-1}{2}\right)} f_{ij0}^{\sigma}(\theta, E, v) + r^{\left(\frac{1}{2}\right)} f_{ij0}^{\sigma}(\theta, E, v) + g_{ij0}^{\sigma}(\theta, E, v). \tag{6.9}$$

The higher order terms for linear stress have also been ignored.

Substituting Eqs. (6.8) and (6.9) into the equation of motion, it can be observed that the order of r at the right hand side is higher than that at the left hand side. Therefore, at the crack tip (as r approaches zero), the contribution of the inertia term at the right hand side of the equation can be ignored and a quasi-static condition is achieved. As a result, for the stress field near the crack tip, static analysis can be conducted. The static compatibility equation can then be expressed as (Jain, Rousseau, and Shukla 2004),

$$(1 + \delta_E y)^2 \nabla^2 (\nabla^2 F) - 2\delta_E (1 + \delta_E y) \frac{\partial}{\partial y} (\nabla^2 F) + 2\delta_E{}^2 (\nabla^2 F) - \frac{2\delta_E{}^2}{(1-v)} \frac{\partial^2 F}{\partial x^2} = 0. \tag{6.10}$$

where, F is the Westergaard stress function, with stress components being given by

$$\sigma_{xx} = \frac{\partial^2 F}{\partial y^2}; \ \ \sigma_{yy} = \frac{\partial^2 F}{\partial x^2}; \ \ \sigma_{xy} = -\frac{\partial^2 F}{\partial x \partial y} \tag{6.11}$$
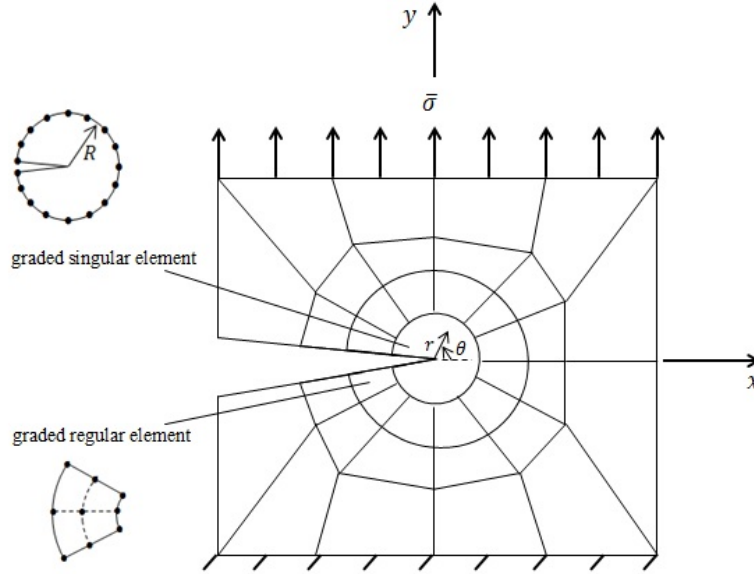
Fig. 6.1. Schematic illustration of the FEM modelling of the crack problem in FGMs

The procedure of extracting the stress and strain fields using an asymptotic analysis incorporated with the Westergaard stress function is explained in chapter 5. The resulting displacements corresponding to the zero and first orders in the expansion, can be represented, near the crack tip, as

$$u = \int \frac{1}{E(y)} \left[\left[\sum_{n=0}^{1} \left[Re\{P_n\} - yIm\{P_n'\} + 2Im\{R_n\} + yRe\{R_n'\} \right] + 2Re\{Q_0\} \right. \right.$$

$$+ \delta_E \left[Im\{\widetilde{P_0}\} + 2yRe\{P_0\} - \frac{y^2}{2} Im\{P_0'\} - Re\{\widetilde{R_0}\} + 2yIm\{R_0\} + \frac{y^2}{2} Re\{R_0'\} \right. \tag{6.12}$$

$$+ Im\{\widetilde{Q_0}\} + 2yRe\{Q_0\} - Re\{\widetilde{S_0}\} \right] \right] - v \left[\sum_{n=0}^{1} \left[Re\{P_n\} + yIm\{P_n'\} \right. \right.$$

$$-yRe\{R'_n\}] + \delta_E \left[\frac{y^2}{2} Im\{P'_0\} - \frac{y^2}{2} Re\{R'_0\}\right]]] \, dx.$$

$$v = \int \frac{1}{E(y)} [[\sum_{n=0}^{1} [Re\{P_n\} + yIm\{P'_n\} - yRe\{R'_n\}] + \delta_E [\frac{y^2}{2} Im\{P'_0\} - \frac{y^2}{2} Re\{R'_0\}]$$

$$-v \left[\sum_{n=0}^{1} [Re\{P_n\} - yIm\{P'_n\} + 2Im\{R_n\} + yRe\{R'_n\}] + 2Re\{Q_0\} + \delta_E[Im\{\widetilde{P_0}\} + \right.$$

$$2yRe\{P_0\} - \frac{y^2}{2} Im\{P'_0\} - Re\{\widetilde{R_0}\} + 2yIm\{R_0\} + \frac{y^2}{2} Re\{R'_0\} + Im\{\widetilde{Q_0}\}$$

$$+2yRe\{Q_0\} - Re\{\widetilde{S_0}\}]]] \, dy.$$

(6.13)

In the above relations, Re and Im represent real and imaginary parts of complex functions. P_0, P_1, R_0, R_1, Q_0 and S_0 are given by

$$P_0 = A_0 z^{-1/2}, P_1 = A_1 z^{+1/2}, Q_0 = B_0, R_0 = C_0 z^{-1/2}, R_1 = C_1 z^{+1/2}, S_0 = D_0, \qquad (6.14)$$

where $z = x + iy$ and $A_0, A_1, B_0, C_0, C_1, D_0$ are real constants to be determined. The ($'$) and ($\sim$) signs in the formulation mean derivative and integration with respect to the complex variable z, respectively.

According to this solution, the stress, strain and displacement fields at the crack tip are described analytically in terms of the coordinates and real unknown coefficients A_0, A_1, B_0, C_0, C_1 and D_0, from which a finite element formulation is developed.

6.2 Finite Element formulation

6.2.1 Shape function of the singular element and stiffness matrix

Consider a singular graded element of radius R at the crack tip as illustrated in Fig. 6.1. Since the singular element should be able to represent the rigid body motion, displacements u_0, v_0, and rotation φ_0 corresponding to the rigid body motion of the singular element are added to the displacement field obtained,

$$\begin{Bmatrix} U(r,\theta) \\ V(r,\theta) \end{Bmatrix} = \begin{Bmatrix} u(r,\theta) \\ v(r,\theta) \end{Bmatrix} + \begin{Bmatrix} u_0 - (rsin\theta)\varphi_0 \\ v_0 + (rcos\theta)\varphi_0 \end{Bmatrix}, \tag{6.15}$$

where U and V are the x and y components of the total displacement. (r, θ) are the polar coordinates located at the crack tip. The first vector on the right hand side of Eq. (6.15) represents the displacement due to the deformation as discussed before, and the last vector is the rigid body displacement vector at the position (r, θ). Based on Eq. (6.15), the displacement field in the singular element can then be expressed in terms of a known coefficient matrix $[H]$ multiplied by a vector of unknowns $\{\alpha\}$,

$$\begin{Bmatrix} U \\ V \end{Bmatrix} = [H]\{\alpha\}, \tag{6.16}$$

where,

$$\{\alpha\}^T = \{A_0 \quad A_1 \quad B_0 \quad C_0 \quad C_1 \quad D_0 \quad u_0 \quad v_0 \quad \varphi_0\}, \tag{6.17}$$

$$[H] = \begin{bmatrix} h_{11} & h_{12} & \cdots & h_{16} & 1 & 0 & -rsin\theta \\ h_{21} & h_{22} & \cdots & h_{26} & 0 & 1 & rcos\theta \end{bmatrix}. \tag{6.18}$$

The coefficient matrix $[H]$ represents the distribution of displacements in terms of the unknown vector $\{\alpha\}$. The elements of $[H]$ are determined by substituting Eq. (6.14) into Eqs. (6.12), (6.13), (6.15) and identifying terms corresponding to each elements of $\{\alpha\}$. As shown in these equations, determination of $[H]$ involves integration of both singular and non-singular terms. The singularity can be easily removed by integration by parts. For example, h_{21} is given by

$$h_{21} = \int \frac{1}{E(y)}\left[(Re\{P_0\} + yIm\{P_0'\}) + \delta_E\left(\frac{y^2}{2}Im\{P_0'\}\right)\right] -$$

(6.19)

$$v\left[(Re\{P_0\} - yIm\{P_0'\}) + \delta_E\left(Im\{\widetilde{P_0}\} + 2yRe\{P_0\} - \frac{y^2}{2}Im\{P_0'\}\right)\right]dy,$$

in which $Re\{P_0\}$ term is singular. The singularity can be removed by considering

$$\int \frac{1}{E(y)}Re\{P_0\}dy = \int \frac{1}{E_0(1 + \delta_E y)}Re\{P_0\}dy$$

(6.20)

$$= \frac{1}{E_0(1 + \delta_E y)}Im\{\widetilde{P_0}\} + \int \frac{\delta_E}{E_0(1 + \delta_E y)^2}Im\{\widetilde{P_0}\}dy,$$

with the second term being the integration of a non-singular function and,

$$Im\{\widetilde{P_0}\} = Im\{2A_0\, z^{1/2}\} = 2A_0\, Im\left\{r^{1/2}\left(cos\left(\frac{\theta}{2}\right) + i\, sin\left(\frac{\theta}{2}\right)\right)\right\}$$

(6.21)

$$= 2A_0\, r^{1/2}\, sin\left(\frac{\theta}{2}\right) = 2A_0\left(\sqrt{x^2 + y^2}\right)^{1/2} sin\left(\frac{arctan(\frac{y}{x})}{2}\right).$$

Therefore, the calculation of h_{21} will only involve integration of non-singular functions containing the general term $1/E(y)$. The Gauss integration method is selected to complete the numerical integration because it is easy to use and is accurate in interpolating polynomials. Other elements of matrix $[H]$ are similarly determined.

The unknown vector $\{\alpha\}$ can be related to the nodal displacements $\{\mathbf{U}_s\}$ of the singular element at the boundary nodes. As discussed in chapter 5, $\{\alpha\}$ can be expressed as,

$$\{\alpha\}_{q\times 1} = [Q]_{q\times 2p}\{\mathbf{U}_s\}_{2p\times 1}, \tag{6.22}$$

where q is the total number of unknowns in the unknown vector $\{\alpha\}$ and p is the number of nodes included in the singular element. As a result, the displacement inside the singular element can be expressed in terms of $\{\mathbf{U}_s\}$ as

$$\begin{Bmatrix} U \\ V \end{Bmatrix} = [H][\boldsymbol{Q}]\{\mathbf{U}_s\} = [N]\{\mathbf{U}_s\}. \tag{6.23}$$

The matrix $[N]$ represents the shape functions for the singular element, from which the strain in the singular element can be determined as

$$\{\epsilon\} = \begin{bmatrix} \dfrac{\partial}{\partial x} & 0 \\ 0 & \dfrac{\partial}{\partial y} \\ \dfrac{\partial}{\partial y} & \dfrac{\partial}{\partial x} \end{bmatrix} [N]\{\mathbf{U}_s\} = [B]\{\mathbf{U}_s\}. \tag{6.24}$$

Using Eq. (6.24), the strain energy (V_S) in the singular element can be calculated as

$$V_s = \frac{1}{2}\int_{A_s} \{\epsilon\}^T\{\sigma\}dA_s = \frac{1}{2}\{\mathbf{U}_s\}^T[\mathbf{K}_s]\{\mathbf{U}_s\}, \tag{6.25}$$

where,

$$[\mathbf{K}_s] = \int_{A_s} [B]^T[D][B]\, dA_s \tag{6.26}$$

is the stiffness matrix of the singular element.

6.2.2 Consistent mass matrix

Taking time derivative of the displacements given in Eq. (6.23) the velocity vector will be obtained as

$$\begin{Bmatrix} \dot{U} \\ \dot{V} \end{Bmatrix} = [H][\mathbf{Q}]\{\dot{\mathbf{U}}_s\}. \tag{6.27}$$

The kinetic energy of the singular element can then be calculated as,

$$T_s = \frac{1}{2}\int \rho(y)\left[\dot{U}^2 + \dot{V}^2\right]dA, \tag{6.28}$$

in which $\rho(y)$, representing the mass density, is a linear function of y. Eq. (6.28) can be rewritten in the form of

$$T_s = \frac{1}{2}\int \rho(y)\{\dot{U} \quad \dot{V}\}\begin{Bmatrix} \dot{U} \\ \dot{V} \end{Bmatrix}dA. \tag{29}$$

Substituting the velocity vector from Eq. (6.27) into Eq. (6.29) leads to

$$T_s = \frac{1}{2}\{\dot{\mathbf{U}}_s\}^T \int \rho(y)[\mathbf{Q}]^T[H]^T[H][\mathbf{Q}]\, dA.\{\dot{\mathbf{U}}_s\} = \frac{1}{2}\{\dot{\mathbf{U}}_s\}^T[M_s]\{\dot{\mathbf{U}}_s\}, \tag{6.30}$$

where $[M_s]$ is the consistent mass matrix given by

$$[M_s] = \int \rho(y)[\mathbf{Q}]^T[H]^T[H][\mathbf{Q}]\, dA. \tag{6.31}$$

It should be mentioned that the current method can be directly extended to use lumped mass matrices. The main concern in the current study is the performance of the singular element in dealing with dynamic problems, instead of the efficiency of the calculation. Therefore the consistent mass matrix is used to reduce potential influence from the simplification of the mass matrix.

6.2.3. Equation of motion

In the current finite element analysis, in addition to the singular element, graded regular 9-node quadrilateral elements will also be used for other areas of the graded material as shown in Fig. 6.1. The strain energy and kinetic energy corresponding to the regular and singular graded elements can be determined as,

$$V_R = \frac{1}{2}\{\mathbf{U}\}^T[\mathbf{K}]\{\mathbf{U}\}, \quad V_S = \frac{1}{2}\{\mathbf{U}_s\}^T[\mathbf{K}_s]\{\mathbf{U}_s\}, \tag{6.32}$$

$$T_R = \frac{1}{2}\{\dot{\mathbf{U}}\}^T[\mathbf{M}]\{\dot{\mathbf{U}}\}, \quad T_S = \frac{1}{2}\{\dot{\mathbf{U}}_s\}^T[\mathbf{M}_s]\{\dot{\mathbf{U}}_s\}. \tag{6.33}$$

in which $\{\mathbf{U}\}$ and $\{\dot{\mathbf{U}}\}$ are the nodal displacement and velocity vectors for regular elements. $[\mathbf{M}]$ and $[\mathbf{K}]$ are the mass and stiffness matrices for regular elements. Corresponding parameters for

the singular element are indicated by subscript 's'. The Lagrangian of the system can then be written as,

$$L = T - V = \left[\frac{1}{2}\{\dot{U}\}^T[M]\{\dot{U}\} + \frac{1}{2}\{\dot{U}_s\}^T[M_s]\{\dot{U}_s\}\right]$$

$$- \left[\frac{1}{2}\{U\}^T[K]\{U\} + \frac{1}{2}\{U_s\}^T[K_s]\{U_s\}\right].$$

(6.34)

Displacement continuity between the singular and surrounding regular elements should be satisfied. To establish this continuity the displacement vector for regular elements should be divided to two parts, i.e. in the interior and along the boundary of the singular element. Those components located at the interior part of the model are indicated by index 'i', and those located at the boundary of the singular element by index 'b',

$$\{U\} = \begin{Bmatrix} U_i \\ U_b \end{Bmatrix}.$$

(6.35)

Correspondingly, the mass and stiffness matrices for regular elements should also be partitioned and, as a result, the Lagrangian takes the following form.

$$L = \left[\frac{1}{2}\begin{Bmatrix} \dot{U}_i \\ \dot{U}_b \end{Bmatrix}^T \begin{bmatrix} M_{ii} & M_{ij} \\ M_{ji} & M_{jj} \end{bmatrix} \begin{Bmatrix} \dot{U}_i \\ \dot{U}_b \end{Bmatrix} + \frac{1}{2}\{\dot{U}_s\}^T[M_s]\{\dot{U}_s\}\right]$$

$$- \left[\frac{1}{2}\begin{Bmatrix} U_i \\ U_b \end{Bmatrix}^T \begin{bmatrix} K_{ii} & K_{ij} \\ K_{ji} & K_{jj} \end{bmatrix} \begin{Bmatrix} U_i \\ U_b \end{Bmatrix} + \frac{1}{2}\{U_s\}^T[K_s]\{U_s\}\right].$$

(6.36)

The singular and regular elements will be assembled by considering the continuity of displacements at corresponding nodes located at the boundary of the singular element, such that

$$\{\mathbf{U}_b\} = \{\mathbf{U}_s\} = [\mathrm{T}]\{\alpha\}. \tag{6.37}$$

Thus, the Lagrangian becomes

$$L = \frac{1}{2}\begin{Bmatrix}\dot{\mathbf{U}}_\iota \\ \dot{\alpha}\end{Bmatrix}^T \begin{bmatrix} \boldsymbol{M}_{ii} & \boldsymbol{M}_{ij}\mathbf{T} \\ \mathbf{T}^T\boldsymbol{M}_{ji} & \mathbf{T}^T(\boldsymbol{M}_{jj} + \mathbf{M}_s)\mathbf{T} \end{bmatrix} \begin{Bmatrix}\dot{\mathbf{U}}_\iota \\ \dot{\alpha}\end{Bmatrix} - \frac{1}{2}\begin{Bmatrix}\mathbf{U}_i \\ \alpha\end{Bmatrix}^T \begin{bmatrix} \boldsymbol{K}_{ii} & \boldsymbol{K}_{ij}\mathbf{T} \\ \mathbf{T}^T\boldsymbol{K}_{ji} & \mathbf{T}^T(\boldsymbol{K}_{jj} + \mathbf{K}_s)\mathbf{T} \end{bmatrix} \begin{Bmatrix}\mathbf{U}_i \\ \alpha\end{Bmatrix}. \tag{6.38}$$

Supposing the dynamic loading vector to be $\{\mathcal{F}(t)\}$, the Lagrangian equations appears as,

$$\frac{d}{dt}\frac{\partial L}{\partial \dot{q}_\iota} - \frac{\partial L}{\partial q_i} = \mathcal{F}_i(t), \tag{6.39}$$

in which $q_i = \{\mathbf{U}_i \quad \alpha\}^T$ represents unknowns. Substituting Eq. (6.38) into Eq. (6.39) results in

the equation of motion for the finite element model,

$$\begin{bmatrix} \boldsymbol{M}_{ii} & \boldsymbol{M}_{ij}\mathbf{T} \\ \mathbf{T}^T\boldsymbol{M}_{ji} & \mathbf{T}^T(\boldsymbol{M}_{jj} + \mathbf{M}_s)\mathbf{T} \end{bmatrix} \begin{Bmatrix}\ddot{\mathbf{U}}_\iota \\ \ddot{\alpha}\end{Bmatrix} + \begin{bmatrix} \boldsymbol{K}_{ii} & \boldsymbol{K}_{ij}\mathbf{T} \\ \mathbf{T}^T\boldsymbol{K}_{ji} & \mathbf{T}^T(\boldsymbol{K}_{jj} + \mathbf{K}_s)\mathbf{T} \end{bmatrix} \begin{Bmatrix}\mathbf{U}_i \\ \alpha\end{Bmatrix} = \{\mathcal{F}(t)\}. \tag{6.40}$$

6.2.4 Solution of the equation of motion

The equation of motion extracted for the linear dynamic response of the system of finite

elements can be represented in the abstract form of

$$[M^*]\{\ddot{X}\} + [K^*]\{X\} = \{\mathcal{F}\}, \tag{6.41}$$

where M^* and K^* are the global mass and stiffness matrices for the finite element assemblage

shown in Eq. (6.40). The first term in the left hand side of Eq. (6.41) represents the inertia force

and the second term corresponds to the elastic force, induced in the system due to the applied external loading.

Eq. (6.41) represents a system of second order linear differential equations. In the current work the direct integration method in which a step by step integration procedure is applied has been selected to solve the dynamic equation. Among different schemes of the direct integration method each one has specific advantages and disadvantages considering factors such as accuracy, selection of the time step size, computational cost, and implementation convenience. The constant-average-acceleration Newmark method has been used for the numerical integration since it provides the possibility to get the unconditionally stable integration.

In the Newmark method the equation of motion is satisfied at time step $t + \Delta t$ when determining displacements, velocities, and accelerations at time $t + \Delta t$, i.e.

$$[M^*]\{\ddot{X}\}_{t+\Delta t} + [K^*]\{X\}_{t+\Delta t} = \{\mathcal{F}\}_{t+\Delta t}. \tag{6.42}$$

Displacements and velocities update in each time step based on the following procedure,

$$\{\dot{X}\}_{t+\Delta t} = \{\dot{X}\}_t + \left[(1-\bar{\delta})\{\ddot{X}\}_t + \bar{\delta}\{\ddot{X}\}_{t+\Delta t}\right]\Delta t, \tag{6.43}$$

$$\{X\}_{t+\Delta t} = \{X\}_t + \{\dot{X}\}_t \Delta t + \left[\left(\frac{1}{2}-\bar{\alpha}\right)\{\ddot{X}\}_t + \bar{\alpha}\{\ddot{X}\}_{t+\Delta t}\right]\Delta t^2. \tag{6.44}$$

where $\bar{\alpha}$ and $\bar{\delta}$ are parameters that control the accuracy and stability of the integration. In the current study $\bar{\alpha} = 0.25$ and $\bar{\delta} = 0.5$ are used, which make the integration unconditionally stable (Bathe 1982).

After solving equation of motion, the time history of unknown coefficients involved in the singular element formulation will be obtained.

The dynamic stress field near the crack tip can then be expressed as,

$$\sigma_{yy}(x, y, t) = Re\left\{\frac{A_0(t)}{\sqrt{x^2 + y^2}}\right\} + higher\ order\ terms \tag{6.45}$$

$$\sigma_{xy}(x, y, t) = Re\left\{\frac{C_0(t)}{\sqrt{x^2 + y^2}}\right\} + higher\ order\ terms \tag{6.46}$$

The dynamic SIFs for mode I and mode II can be explicitly determined as

$$K_I(t) = \lim_{x \to 0}(\sqrt{2\pi x}\ \sigma_{yy}(x, 0, t)) = \sqrt{2\pi}A_0(t), \tag{6.47}$$

$$K_{II}(t) = \lim_{x \to 0}(\sqrt{2\pi x}\ \sigma_{xy}(x, 0, t)) = \sqrt{2\pi}C_0(t). \tag{6.48}$$

The nonsingular stress at the crack tip appears as $\sigma_{0x}(t) = -2B_0(t)$.

6.3 Results and discussion

6.3.1 Computational model

In order to investigate the efficiency of the developed graded singular element for analyzing dynamic crack problems in linear elastic isotropic FGMs a set of examples corresponding to a central crack in a rectangular FGM plate under dynamic loading is presented. The width and height of the plate are $W = 20\ (mm)$ and $H = 40\ (mm)$, respectively. The crack size is $2a = 4.8\ (mm)$. Constant-slope-front step function with magnitude of $\sigma_0 = 0.4$ (GPa) is considered as the general form of the dynamic loading as shown in Fig. 6.2.
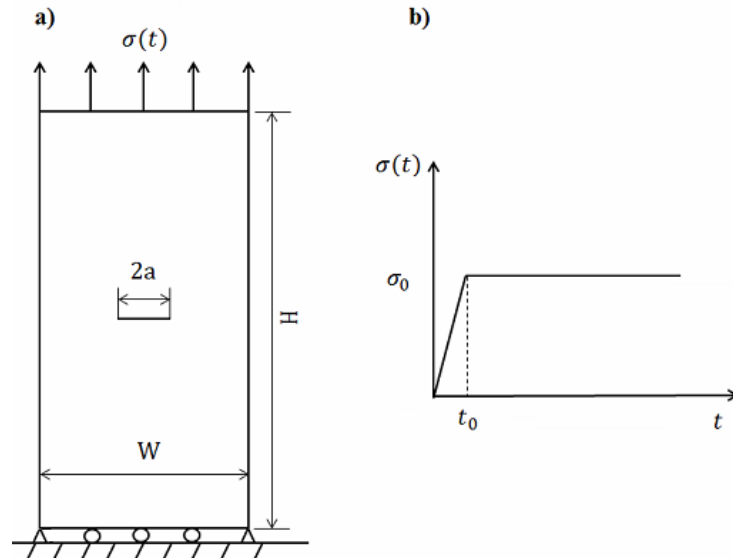
Fig. 6.2. Schematic illustration of a) geometry of the central crack problem b) dynamic loading of the model

In order to determine the proper mesh size of regular elements with the considered loading, a simple problem shown in Fig. 6.3, has been considered in which a uniform plate is subjected to the load shown in Fig. 6.2b at the left boundary, and has zero shear stress and zero vertical displacement at the upper and lower boundaries. As a result, the plate is deformed uniformly in the vertical direction. The solution obtained at point 'A' located $12 \ (mm)$ from the loaded side at the middle line is depicted in Fig. 6.4 for a total time of $t = 15 \ (\mu s)$ for the case that $t_0 = 2.5 \ (\mu s)$. Element sizes of $4 \ (mm), 2 \ (mm), 1 \ (mm)$ and $0.5 \ (mm)$ in the horizontal direction are used and the convergence of results for these selected element sizes is observed. Also, a good agreement exists between the finite element model and the analytical solution.
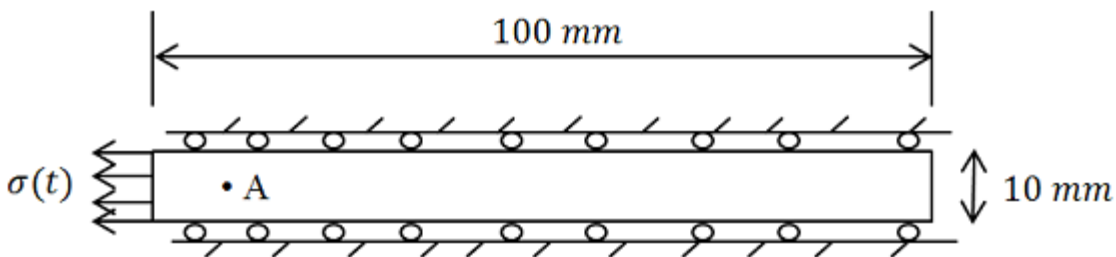
Fig. 6.3. Geometry and loading conditions of dynamic problem without crack for determining the regular mesh size
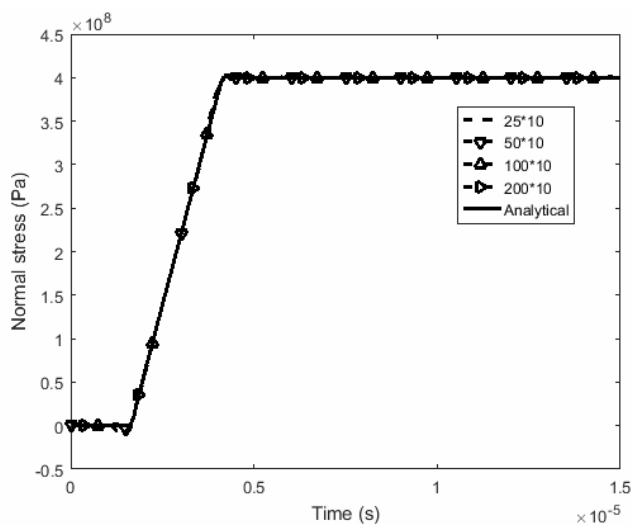
Fig. 6.4. Time history of the normal stress at point 'A' obtained using different element numbers and compared with the analytical solution

The original model shown in Fig. 6.2 is then meshed using the proper regular element sizes, which are within the considered range of the element size. Since the model is symmetric only half of the plate is meshed as shown in Fig. 6.5. The meshed model includes 134 regular graded 9-node isoparametric quadrilateral elements and one graded singular element containing 17 nodes uniformly distributed at its boundary.
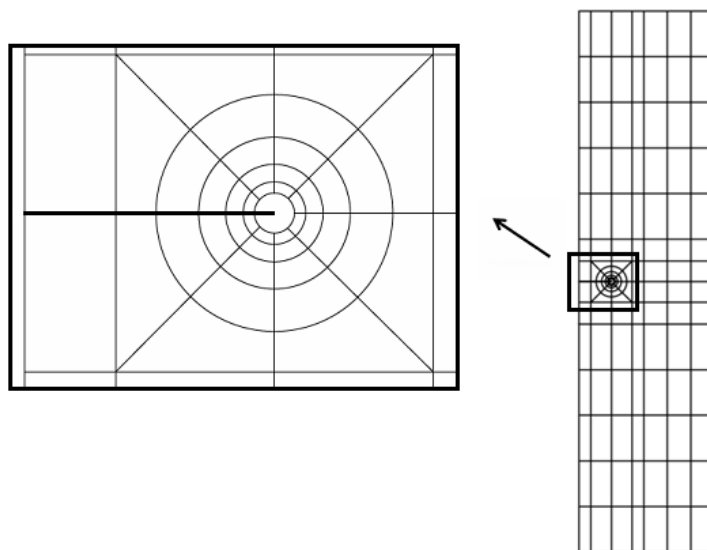
Fig. 6.5. Meshing of the FGM plate

6.3.2 Comparison between the results from graded singular element and existing solutions

In order to demonstrate the accuracy of the solution obtained with the proposed graded singular element, comparisons are performed with existing solutions using finite difference method (Y. M. Chen 1974) and finite element method (Tan 1998). The considered model for the comparison is a homogeneous plate with the same geometry explained for the computational model. Material properties are assumed to be $\mu = 76.923$ (GPa), $\nu = 0.3$, and $\rho = 5$ (Mg/m^3) (Y. M. Chen 1974). The chosen time step is $\Delta t = $3e-8 (s) while the total solution time is 15 (μs). Normalized dynamic SIFs are calculated for the cracked plate under the rectangular step function loading using the graded singular element and compared with the results provided by Chen (Y. M. Chen 1974) and Tan (Tan 1998) in Fig. 6.6. A good agreement is observed. The same model is also considered under the constant-slope-front step function loading shown in Fig. 6.2b ($t_0 = $ 5 (μs)), and dynamic SIFs obtained with the graded singular element are compared with the solution given by Tan (Tan 1998) in Fig. 6.7. A good agreement is also observed. It has been reported that when the size of the singular element (R) is within the range of $R/a \leq 0.1$, the SIF is accurate unless the crack length is very small (Whitney and Nuismer 1974; Tan 1998; Molavi Nojumi and Wang 2017a). In the current examples, the singular element size is selected as $R/a = 0.04$. In addition, to ensure the accuracy of the solution with the chosen time step, smaller time step have been employed as $\Delta t/2$ which proved the convergence of results. Because $R/a = 0.04$ provides good agreement with existing solutions, this size of the singular element and time step will be used in the following discussion.
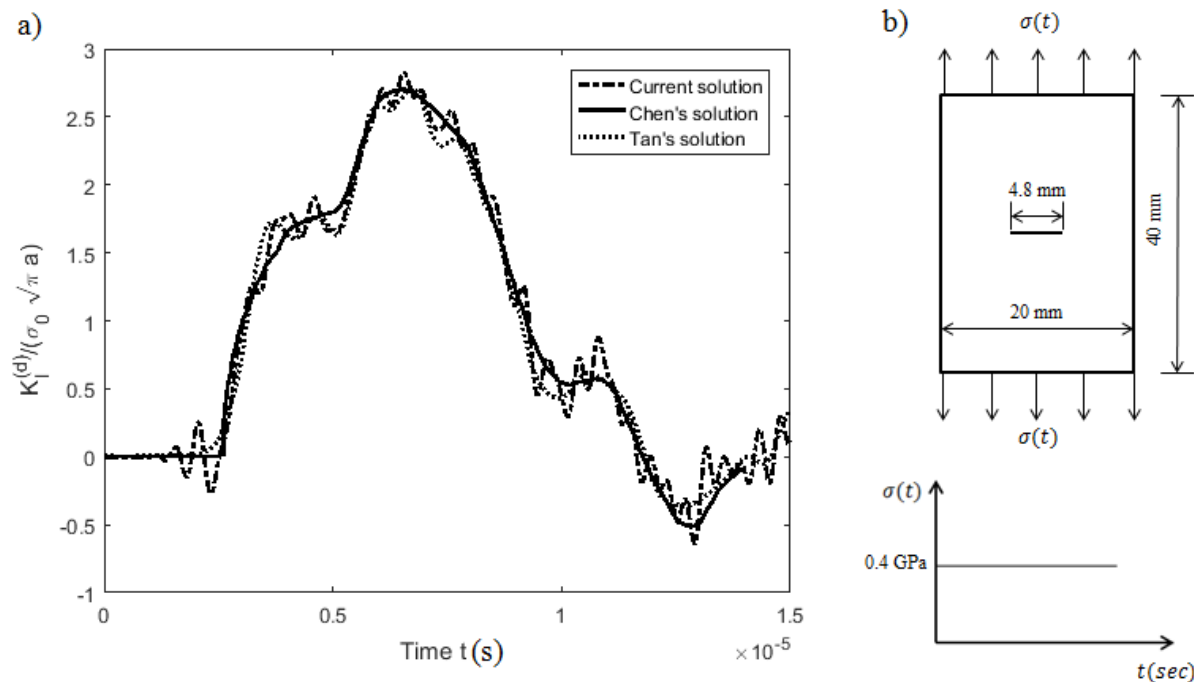
Fig. 6.6. a) Comparison of the dynamic SIFs obtained using the finite difference method (Y. M. Chen 1974), finite element method (Tan 1998) and current solution b) loading condition
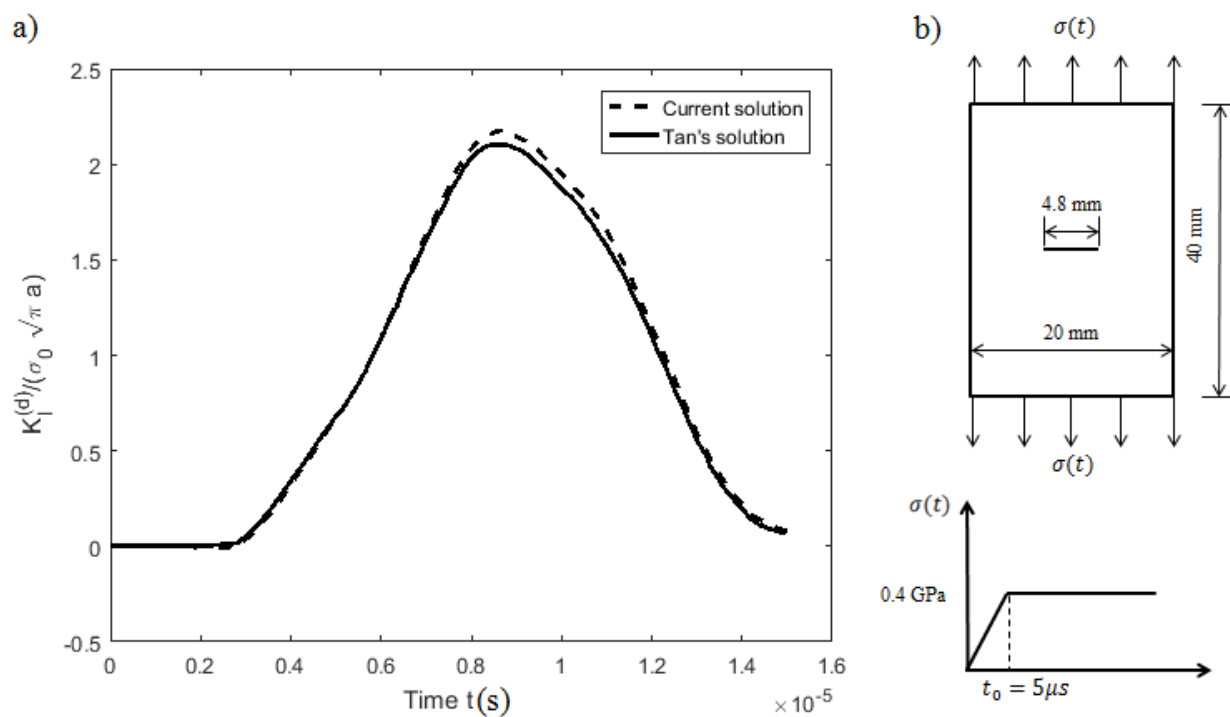
Fig. 6.7. a) Comparison of the dynamic SIFs obtained using the finite element method suggested by Tan (Tan 1998) and current solution b) loading condition

6.3.3 Dynamic fracture parameters obtained using the graded singular element

For FGMs, the influence of the variation of material properties and loading conditions on the dynamic fracture parameters is important. These parameters can be obtained explicitly by solving the equation of motion as explained in section *6.2.4* for the general case where material properties vary with position. In continuance, the role of material gradient and loading on the dynamic fracture behaviour of the FGM model will be investigated. In the following simulations the Poisson's ratio is assumed to be a constant $v = 0.3$. The values of the Young's modulus and the density at the bottom surface of the model are assumed to be $E_0 = 70$ (GPa) and $\rho_0 = 2700$ (kg/m^3). For the case where the Young's modulus and the density at the top surface of the model are $E_1 = 7E_0$ and $\rho_1 = \rho_0$ respectively, the problem is solved for the constant-slope-front step function loading $(t_0 = 2.5$ $(\mu s))$ with boundary conditions shown in Fig. 6.2. The dynamic SIFs and σ_{0x} are then explicitly obtained from determined values of A_0, C_0 and B_0, respectively. Time history of the fracture parameters are illustrated in Fig. 6.8. Typical results for the moments $t = 4.74, 10.95$ and 16.17 (μs) which correspond to three peak points of the mode-I dynamic SIF (K_I^d) are shown in table 6.1.
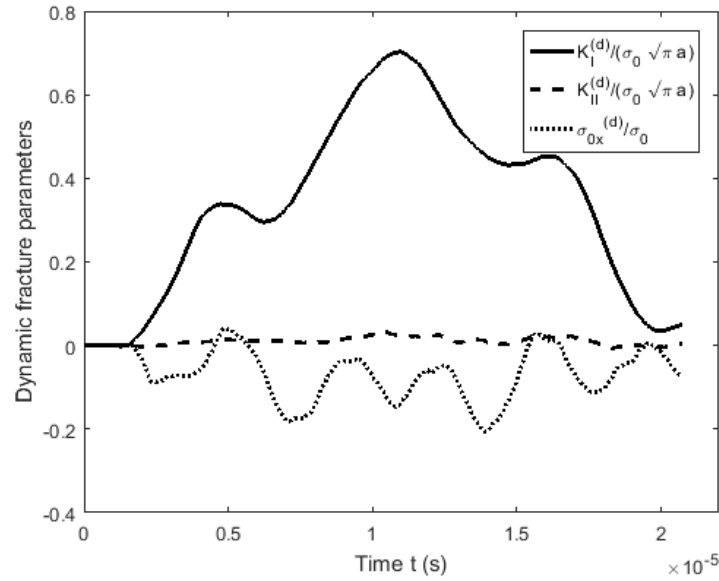
Fig. 6.8. Time history of fracture parameters under constant-slope-front step function loading ($t_0 = 2.5\ (\mu s), E_1 = 7E_0$ and $\rho_1 = \rho_0$)

Table 6.1. Determination of normalized dynamic SIFs and the nonsingular stress at the crack tip at peak points of the mode-I SIF when $E_1/E_0 = 7$ and $\rho_1/\rho_0 = 1$ under the constant-slope-front step function loading

$t\ (\mu s)$	$A_0 \times 10^{-6}$	$B_0 \times 10^{-6}$	$C_0 \times 10^{-6}$	$\dfrac{\sigma_{0x}^d}{\sigma_0}$	$\dfrac{K_I^d}{\sigma_0\sqrt{\pi a}}$	$\dfrac{K_{II}^d}{\sigma_0\sqrt{\pi a}}$
4.74	4.687	-6.057	0.192	0.030	0.338	0.014
10.95	9.735	28.174	0.343	-0.141	0.703	0.025
16.17	6.273	-3.168	0.285	0.016	0.453	0.021

6.3.4 The influence of the elastic gradient on the dynamic SIF

The effect of the variation of elastic properties on transient dynamic SIF is evaluated when the constant-slope-front step function loading ($t_0 = 2.5\ (\mu s)$) is applied to the model. Fig. 6.9 shows the variation of K_I^d when the load is applied at the stiffer side of the FGM plate, and Fig. 6.10 shows the corresponding result when the load is applied at the softer side. For results in Fig. 6.9,

E_0 is kept to be a constant ($E_0 = 70$ (GPa)) and E_1 changes based on the elastic gradient. It can be observed that the gradient of elastic property affects K_I^d so that with increasing elastic gradient, K_I^d becomes smaller and reaches its maximum value faster. For the cases shown in Fig. 6.10, $E_1 = 70$ (GPa) and E_0 changes based on the elastic gradient. In these cases where the softer side of the FGM plate is loaded, the magnitude of K_I^d increases drastically.
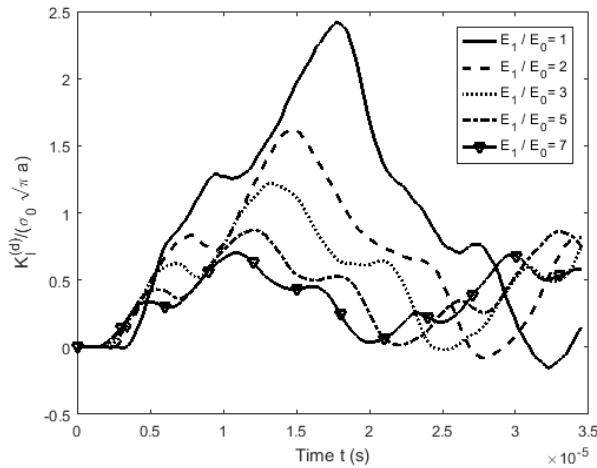
Fig. 6.9. Transient dynamic mode-I SIF obtained for different ratios of E_1/E_0 when the stiffer side is loaded ($E_0 = 70$ (GPa), $\rho_0 = \rho_1 = 2700$ (kg/m³))
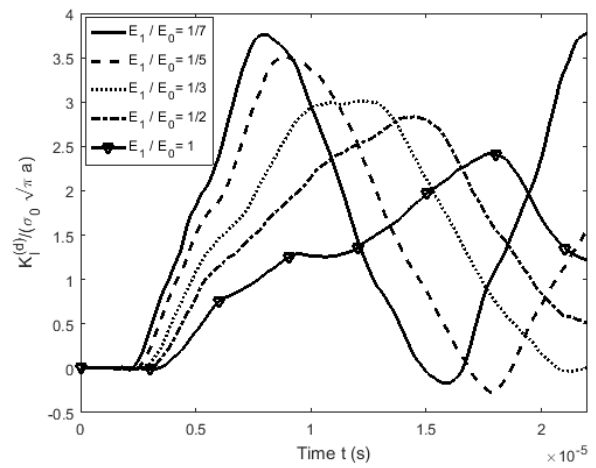
Fig. 6.10. Transient dynamic mode-I SIF obtained for different ratios of E_1/E_0 when the softer side is loaded ($E_1 = 70\ (GPa)$, $\rho_0 = \rho_1 = 2700\ (kg/m^3)$)

6.3.5 The influence of the density gradient on the dynamic SIF

The role of the density gradient on the dynamic fracture parameters is investigated when the constant-slope-front step function loading ($t_0 = 2.5\ (\mu s)$) is applied to the model. Figs. 6.11 and 6.12 show the effect of density variation on K_I^d when the load is applied at the higher and lower density sides, respectively. Fig. 6.11 is for the case where $\rho_1/\rho_0 \geq 1$, with $\rho_0 = 2700\ (kg/m^3)$ and ρ_1 changing based on the density gradient. It is observed that the density gradient influence the time history of K_I^d through wave speed. Also, it is illustrated that maximum values of K_I^d

increase slightly with increasing density gradient. When the lower density side of the FGM plate is loaded ($\rho_1/\rho_0 \leq 1$) as shown in Fig. 6.12, ρ_1 is kept to be 2700 (kg/m^3) and ρ_0 changes based on the density gradient. As expected, the change of density gradient affects the time history of K_I^d, but show insignificant effect on the maximum value of K_I^d.
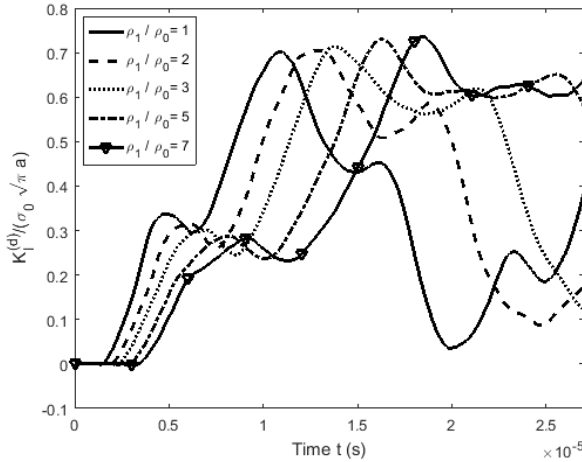
Fig. 6.11. Transient dynamic mode-I SIF obtained for different ratios of ρ_1/ρ_0 when the higher density side is loaded ($\rho_0 = 2700$ (kg/m^3), $E_1 = 7E_0$)
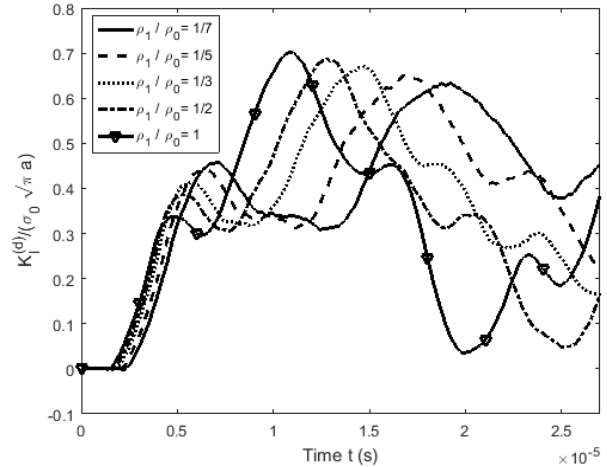
Fig. 6.12. Transient dynamic mode-I SIF obtained for different ratios of ρ_1/ρ_0 when the higher density side is loaded ($\rho_1 = 2700$ (kg/m^3), $E_1 = 7E_0$)

6.3.6 The influence of the loading on the dynamic fracture parameters

The influence of the loading on the K_I^d is investigated by changing the slope of the ramp at the beginning part of the loading shown in Fig. 6.2b. Fig. 6.13 indicates the dynamic response of the cracked FGM plate when $E_1 = 7E_0$ and $\rho_1 = 2\rho_0$. The slope of the ramp is changed by selecting different values of t_0 as $1.25, 2.5, 5$ and 7.5 (μs). It is observed that by decreasing the slope of the ramp the maximum values of K_I^d will be delayed and shows a reduction trend.
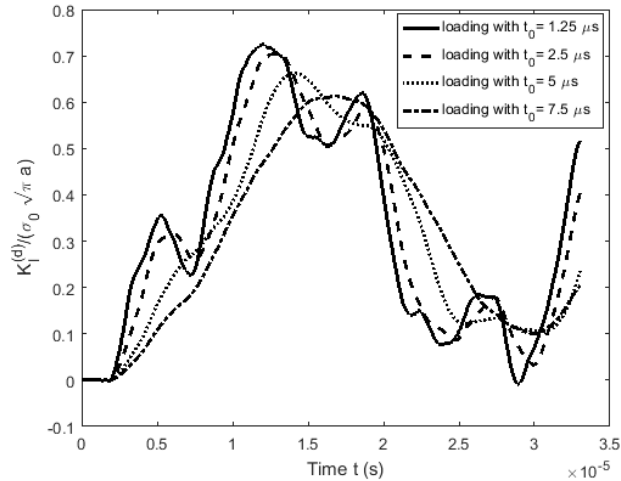
Fig. 6.13. Transient dynamic mode-I SIF obtained for different loadings when $E_1 = 7E_0$ and $\rho_1 = 2\rho_0$

6.3.7 Contours of stress near the crack tip

The contours of stress ahead of the crack are compared between the homogeneous and FGM plates in Figs. 6.14-6.19. This comparison is made based on the solution at $t = 6.12 \ (\mu s)$ when the plate is under the constant-slope-front step function loading with t_0 being 2.5 (μs). The material properties of the FGM are assumed to be $E_1/E_0 = 7$ and $\rho_1/\rho_0 = 2$ and homogeneous case corresponds to $E_1/E_0 = 1$ and $\rho_1/\rho_0 = 1$. The results clearly show that for the case of FGMs, the stress near the crack tip is less concentrated.
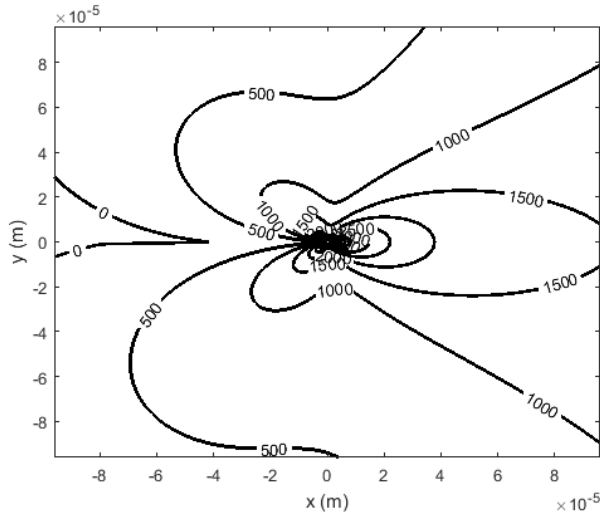
Fig. 6.14. Contours of σ_{xx} (MPa) near the crack tip for homogeneous material ($E_1/E_0 = 1$ and $\rho_1/\rho_0 = 1$) at $t = 6.12\ (\mu s)$
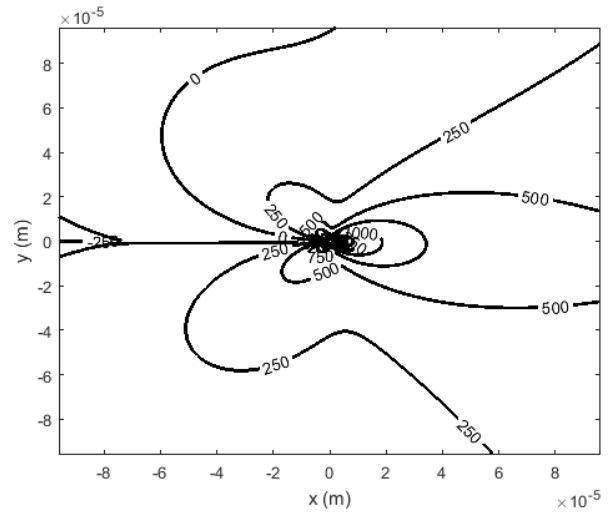
Fig. 6.15. Contours of σ_{xx} (MPa) near the crack tip for FGM ($E_1/E_0 = 7$ and $\rho_1/\rho_0 = 2$) at $t = 6.12\ (\mu s)$
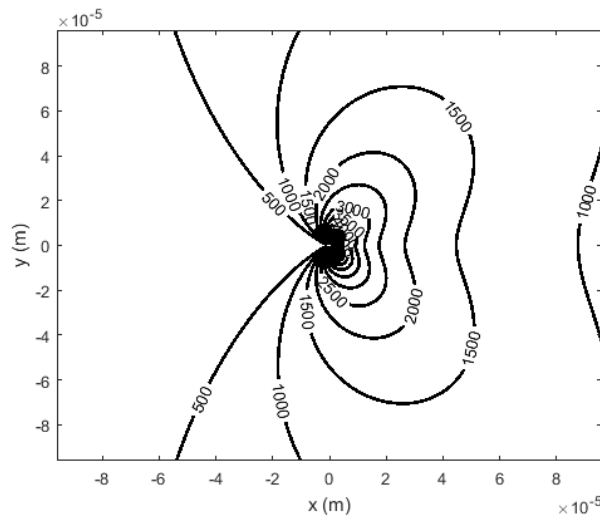
Fig. 6.16. Contours of σ_{yy} (MPa) near the crack tip for homogeneous material ($E_1/E_0 = 1$ and $\rho_1/\rho_0 = 1$) at $t = 6.12\ (\mu s)$
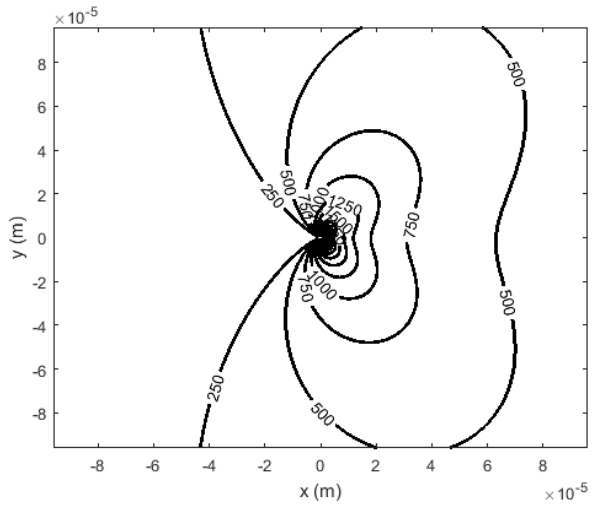
Fig. 6.17. Contours of σ_{yy} (MPa) near the crack tip for FGM ($E_1/E_0 = 7$ and $\rho_1/\rho_0 = 2$) at $t = 6.12\ (\mu s)$
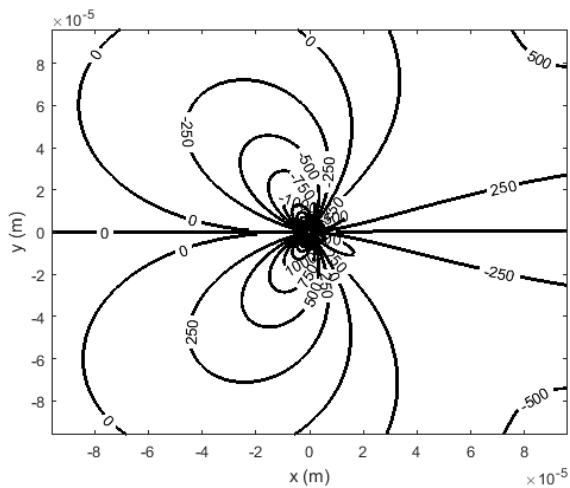
Fig. 6.18. Contours of σ_{xy} (MPa) near the crack tip for homogeneous material ($E_1/E_0 = 1$ and $\rho_1/\rho_0 = 1$) at $t = 6.12\ (\mu s)$
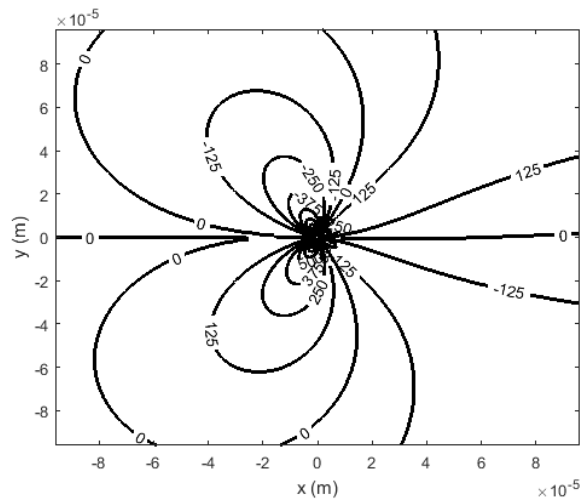
Fig. 6.19. Contours of σ_{xy} (MPa) near the crack tip for FGM ($E_1/E_0 = 7$ and $\rho_1/\rho_0 = 2$) at $t = 6.12\ (\mu s)$

Chapter 7

Conclusion and Future Works

7.1 Conclusions

7.1.1 Performance of regular graded elements against conventional elements in general elasticity problems

A new graded 9-node isoparametric quadrilateral element was used to investigate the structural behaviour of FGMs in three specific examples including a) the Saint-Venant principle in a FGM beam under simple tension, b) FGM beam under uniform bending, and c) indentation of a flat rigid punch to a FGM substrate, for quasi-static problems. Also, the dynamic problem corresponding to a FGM beam which is constrained at one side and loaded by a dynamic tensile force at the other side was considered. It was concluded that:

i)   The use of conventional homogeneous elements for modelling FGMs may cause significant errors except when a very fine mesh is applied which in turn decrease the efficiency of the solution.

ii)   This possible error in conventional elements is originated from the approximation made regarding the material property variation used in homogeneous elements. Graded elements always show reasonable distribution of field variables when convergence is achieved.   Depending on the loading conditions homogeneous elements may perform differently, for example the stresses in FGM beam under simple tension and strains in a FGM substrate indented by a flat rigid punch show wrong trend of variation at the element level when homogeneous elements are used.

7.1.2 Investigation of the crack problems in FGMs under thermomechanical loading using regular graded elements

A comprehensive study on the application of an improved regular graded finite element to the analysis of linear elastic isotropic nonhomogeneous plates containing crack under thermomechanical loading was performed. Sharp material and thermal gradient was considered by modelling a thin cracked FGM layer sandwiched between two different homogeneous media. It was concluded that:

i)   Homogeneous and FGM plates represent different fracture behaviour upon increasing the temperature difference applied to the model.

ii)   This dissimilarity is originated from the break of material symmetry and coupling between normal and shear stresses in FGMs.

iii)   When there is sharp gradient of temperature or a sharp change in material properties through the FGM layer, high shear stresses may be induced, which will be coupled with the normal stresses, and influence the stress intensity factors at the crack tip.

iv)   The graded elements are more reliable for modelling FGM crack problems, since the material gradient is included at the element level.

7.1.3 Developing a new graded singular element for quasi-static condition

A new graded singular finite element is developed for analyzing crack problems in linear elastic isotropic FGMs with spatially varying elastic parameters. This element was formulated using the analytical approach for determining the stress field near the crack tip by the mean of an asymptotic analysis coupled with the Westergaarde stress function. Special finite element formulation was adopted to express the nodal displacements in terms of the real unknown coefficients considered in the analytical solution. Shape function matrix was extracted, and the assemblage process of singular element with adjacent regular elements was accomplished by considering the displacement continuity at the boundary of the singular element. This novel element provides an efficient and reliable numerical tool for studying fracture of FGMs with following specific advantages:

i)   Accurate description of the crack tip stress field including higher order terms originated from the inherent material gradient at the crack tip can be obtained.

ii)   It eliminates the need to use of very fine mesh of regular elements near the crack area leading to less effort required for the solution which in turn increase the efficiency.

iii)   It is more convenient, since it does not require any post processing technique to reach fracture parameters such as stress intensity factors.

7.1.4 *The new graded singular element for dynamic problems*

To consider the effect of inertial forces for dynamic analysis of crack problems in FGMs, consistent mass matrix is formed and adopted to the finite element formulation. Using a convenient finite difference expression to approximate the accelerations and velocities in terms of the displacements, the equation of motion can be solved. This element keeps its advantageous properties such as precise description of the crack tip stress field with higher order terms, no need to any post processing technique, and high efficiency as the volume of calculations in each time step has been considerably decreased. This novel element was used to simulate the transient response of crack problems in rectangular FGM plates whose material properties varies linearly normal to the crack line. The FGM plate with central crack is constrained at one side and loaded by a tensile dynamic loading at the other side. It was concluded that:

i)   The gradient of elastic properties significantly influences the time history solution for stress intensity factors by affecting on both of the magnitude and phase of the solution.

ii)   The gradient of mass density significantly influences the time history solution for stress intensity factors. Its major effect is on the phase of solution, while the magnitude changes slightly.

iii)   Considering a constant-slope-front step function loading, it is found that the speed of loading significantly influence the time history solution for stress intensity factors. The faster the loading is applied, the higher stress intensity factors in shorter time will be resulted.

iv)   The stress field around the crack tip can be controlled by tailoring material properties using FGMs.

7.2 Thesis contribution

In this thesis a comprehensive numerical analysis is conducted to investigate the static and dynamic behaviour of linear elastic isotropic FGMs with the focus on fracture mechanics. The contribution can be summarized as,

i)   Comprehensive studies of graded elements are conducted for general analysis of static and dynamic behaviour of linear elastic isotropic FGMs by means of regular graded finite elements. Also, modelling crack problems in FGM plates and thin FGM layers under thermomechanical loading by using a new 9-node graded isoparametric element which considers the gradient of thermal and elastic properties at the element level was investigated. In addition, the use of conventional homogeneous elements for modelling FGMs in problems with and without crack was challenged by providing specific examples.

ii)   A new graded singular finite element for studying crack problems in FGMs was developed. Using this element enables the accurate determination of the singular

stress field at the crack tip with considering higher order terms emanating from the material gradient. This element eliminates the need to use very fine mesh of regular elements near the crack tip which results to higher efficiency. Furthermore, it does not require any post processing technique to determine the fracture parameters such as stress intensity factors. It provides a strong numerical tool for analyzing the influence of the material gradient, geometry, and loading conditions on the crack tip stress field, and fracture parameters.

iii)   The newly developed graded singular element was extended to cover dynamic crack problems in FGMs. The consistent mass matrix was constructed to account for the inertial forces caused by the dynamic loadings. Besides the high precision in determining the singular stress field at the crack tip and the straightforward way to obtain stress intensity factors, it remarkably reduce the computational effort required in each time step of the solution. This element was implemented to study the influence of the gradient of elastic properties, mass density, and loading on the crack tip stress field and fracture parameters.

7.3 Suggestions for future works

With conducting this research, it was found worthy to continue the studies on the following suggested topics:

i)   Using the graded singular element, examine the static and dynamic crack problems in FGMs for more general geometries, such as for cracks inclined to the material gradient direction, multiple cracks and interface cracks,

ii)   Investigate the viscoelastic fracture of FGMs using the graded singular element by constructing damping matrix based on the current stiffness and mass matrices,

iii)   Integrate the current graded singular element into commercial finite element software Ansys,

iv)   Examine the fracture behaviour of other advanced materials, such as functionally graded piezoelectric materials, by updating the current graded singular element.

References

Abrate, Serge. 2008. "Functionally Graded Plates Behave like Homogeneous Plates." *Composites Part B: Engineering* 39: 151–58. doi:10.1016/j.compositesb.2007.02.026.

Afsar, a. M., and J. I. Song. 2010. "Effect of FGM Coating Thickness on Apparent Fracture Toughness of a Thick-Walled Cylinder." *Engineering Fracture Mechanics* 77 (14). Elsevier Ltd: 2919–26. doi:10.1016/j.engfracmech.2010.07.001.

Aksoy, H.G., and E. Şenocak. 2009. "Wave Propagation in Functionally Graded and Layered Materials." *Finite Elements in Analysis and Design* 45 (12): 876–91. doi:10.1016/j.finel.2009.06.025.

Alibeigloo, A. 2016. "Thermo Elasticity Solution of Sandwich Circular Plate with Functionally Graded Core Using Generalized Differential Quadrature Method." *Composite Structure* 136. Elsevier Ltd: 229–40. doi:10.1016/j.compstruct.2015.10.012.

Allahyarzadeh, M H, M Aliofkhazraei, A R Sabour Rouhaghdam, and V Torabinejad. 2016. "Gradient Electrodeposition of Ni-Cu-W (Alumina) Nanocomposite Coating." *JMADE* 107. Elsevier Ltd: 74–81. doi:10.1016/j.matdes.2016.06.019.

Amor, Morched Ben, and Mohamed Hédi Ben Ghozlen. 2015. "Lamb Waves Propagation in Functionally Graded Piezoelectric Materials by Peano-Series Method." *Ultrasonics* 55. Elsevier B.V.: 10–14. doi:10.1016/j.ultras.2014.08.020.

Anlas, G, Mh Santare, and J Lambros. 2000. "Numerical Calculation of Stress Intensity Factors in Functionally Graded Materials." *International Journal of Fracture*, no. 1994: 131–43. doi:10.1023/A:1007652711735.

Bagheri, R., M. Ayatollahi, and E. Asadi. 2013. "Dynamic Fracture Analysis of Multiple Defects in an Imperfect FGM Coating-Substrate Layers." *International Journal of Mechanical Sciences* 75. Elsevier: 55–65. doi:10.1016/j.ijmecsci.2013.06.006.

Bao, G., and L. Wang. 1995a. "Multiple Cracking in Functionally Graded Ceramic/metal Coatings." *International Journal of Solids and Structures* 32 (19): 2853–71. doi:10.1016/0020-7683(94)00267-Z.

Bao, G, and L Wang. 1995b. "Multiple Cracking in Functionally Graded Ceramic/metal Coatings." *International Journal of Solids and Structures* 32 (19). Elsevier Science Ltd: 2853–71. doi:10.1016/0020-7683(94)00267-Z.

Bathe, K. J. 1982. "Finite Element Procedures in Engineering Analysis." New Jersey: Prentice-Hall, inc., Englewood Cliffs. doi:10.1115/1.3264375.

Bayesteh, Hamid, and Soheil Mohammadi. 2013. "XFEM Fracture Analysis of Orthotropic Functionally Graded Materials." *Composites Part B: Engineering* 44 (1). Elsevier Ltd: 8–25. doi:10.1016/j.compositesb.2012.07.055.

Belytschko, T, and T Black. 1999. "Elastic Crack Growth in Finite Elements." *International Journal for Numerical Methods in Engineering* 620 (July 1998): 601–20.

Belytschko, T, Y Y Lu, L Gu, and M Tabbara. 1995. "Element-Free Galerkin Methods for Static and Dynamic Fracture." *International Journal of Solids and Structures* 32 (17): 2547–70. doi:10.1016/0020-7683(94)00282-2.

Ben, Issam, Morched Ben, Mohamed Hédi, and Ben Ghozlen. 2015. "Effect of a Functionally Graded Soft Middle Layer on Love Waves Propagating in Layered Piezoelectric Systems." *Ultrasonics* 61. Elsevier B.V.: 145–50. doi:10.1016/j.ultras.2015.04.011.

Bernardo, G M S, F R Damásio, T A N Silva, and M A R Loja. 2016. "A Study on the Structural Behaviour of FGM Plates Static and Free Vibrations Analyses." *Composite Structure* 136.

Elsevier Ltd: 124–38. doi:10.1016/j.compstruct.2015.09.027.

Cao, Xiaoshan, Feng Jin, and Insu Jeon. 2011. "Calculation of Propagation Properties of Lamb Waves in a Functionally Graded Material (FGM) Plate by Power Series Technique." *NDT and E International* 44 (1). Elsevier: 84–92. doi:10.1016/j.ndteint.2010.09.010.

Cao, Xiaoshan, Feng Jin, Insu Jeon, and Tian Jian Lu. 2009. "Propagation of Love Waves in a Functionally Graded Piezoelectric Material (FGPM) Layered Composite System." *International Journal of Solids and Structures* 46 (22–23). Elsevier Ltd: 4123–32. doi:10.1016/j.ijsolstr.2009.08.005.

Chakraborty, a., and S. Gopalakrishnan. 2004. *Wave Propagation in Inhomogeneous Layered Media: Solution of Forward and Inverse Problems*. *Acta Mechanica*. Vol. 169. doi:10.1007/s00707-004-0080-7.

Chalivendra, V. B., a. Shukla, and V. Parameswaran. 2003. "Quasi-Static Stress Fields for a Crack Inclined to the Property Gradation in Functionally Graded Materials." *Acta Mechanica* 162 (1–4): 167–84. doi:10.1007/s00707-002-1019-5.

Chalivendra, Vijaya Bhaskar, and Arun Shukla. 2005. "Transient Elastodynamic Crack Growth in Functionally Graded Materials." *Journal of Applied Mechanics* 72 (2): 237. doi:10.1115/1.1831292.

Chang-Chun, Wu, He Peixiang, and Li Ziran. 2002. "Extension of J Integral to Dynamic Fracture of Functional Graded Material and Numerical Analysis." *Computers and Structures* 80 (5–6): 411–16. doi:10.1016/S0045-7949(02)00013-5.

Chen, L, G R Liu, Y Jiang, K Zeng, and J Zhang. 2011. "A Singular Edge-Based Smoothed Finite Element Method (ES-FEM) for Crack Analyses in Anisotropic Media." *Engineering Fracture Mechanics* 78 (1). Elsevier Ltd: 85–109. doi:10.1016/j.engfracmech.2010.09.018.

Chen, Y. M. 1974. "Numerical Computation of Dynamic Stress Intensity Factors by a Lagrangian Finite-Difference Method." *Mathematics and Computers*, 1–10. http://www.ncbi.nlm.nih.gov/pubmed/22104720.

Cheng, Zhanqi, Guanfeng Zhang, Yenan Wang, and Florin Bobaru. 2015. "A Peridynamic Model for Dynamic Fracture in Functionally Graded Materials." *Composite Structures* 133. Elsevier Ltd: 529–46. doi:10.1016/j.compstruct.2015.07.047.

Cherradi, N., A. Kawasaki, and M. Gasik. 1994. "Worldwide Trends in Functionally Gradient Materials Research and Development." *Composites Engineering* 8 (4): 883–94.

Chiong, Irene, Ean Tat Ooi, Chongmin Song, and Francis Tin-Loi. 2014a. "Computation of Dynamic Stress Intensity Factors in Cracked Functionally Graded Materials Using Scaled Boundary Polygons." *Engineering Fracture Mechanics* 131. Elsevier Ltd: 210–31. doi:10.1016/j.engfracmech.2014.07.030.

Chiong, Irene, Ean Tat Ooi, Chongmin Song, and Francis Tin-Loi. 2014b. "Scaled Boundary Polygons with Application to Fracture Analysis of Functionally Graded Materials." *International Journal for Numerical Methods in Engineering* 98: 562–89.

Choi, Hyung Jip. 2004. "Impact Response of a Surface Crack in a Coating/substrate System with a Functionally Graded Interlayer: Antiplane Deformation." *International Journal of Solids and Structures* 41 (20): 5631–45. doi:10.1016/j.ijsolstr.2004.04.020.

Choi, Hyung Jip. 2006. "Elastodynamic Analysis of a Crack at an Arbitrary Angle to the Graded Interfacial Zone in Bonded Half-Planes under Antiplane Shear Impact." *Mechanics Research Communications* 33: 636–650.

Chu, P., X.-F. Li, Z.-G. Wang, and K.Y. Lee. 2015. "Double Cantilever Beam Model for Functionally Graded Materials Based on Two-Dimensional Theory of Elasticity."

Engineering Fracture Mechanics 135: 232–44. doi:10.1016/j.engfracmech.2015.01.008.

Chung, Y, and Shyang-ho Chi. 2006. "Mechanical Behavior of Functionally Graded Material Plates under Transverse Load — Part I : Analysis." *International Journal of Solids and Structures* 43: 3657–74. doi:10.1016/j.ijsolstr.2005.04.011.

Dai, Hong-liang, Yan-ni Rao, and Ting Dai. 2016. "A Review of Recent Researches on FGM Cylindrical Structures under Coupled Physical Interactions , 2000 – 2015." *Composite Structures* 152. Elsevier Ltd: 199–225. doi:10.1016/j.compstruct.2016.05.042.

Delale, F, and F Erdogan. 1983. "The Crack Problem for a Nonhomogeneous Plane." *Journal of Applied Mechanics* 50 (3): 609–14.

Ding, X., X. Guo, B. Ilschner, and N. Merk. 1993. "DC- and Pulse-Plating of CuNi and CuZn Gradient Foils: Evaluation by SEM/TEM." In *2nd Int Symp. on FGMs*. San Francisco.

Dolbow, John, and M Gosz. 2002. "On the Computation of Mixed-Mode Stress Intensity Factors in Functionally Graded Materials." *International Journal of Solids and Structures* 39 (9): 2557–74. doi:10.1016/S0020-7683(02)00114-2.

Dominguez, J, and R Gallego. 1992. "Time Domain Boundary Element Method for Dynamic Stress Intensity Factor Computations." *International Journal for Numerical Methods in Engineering* 33: 635–47.

Dorduncu, Mehmet, M. Kemal Apalak, and H.P. Cherukuri. 2015. "Elastic Wave Propagation in Functionally Graded Circular Cylinders." *Composites Part B: Engineering* 73. Elsevier Ltd: 35–48. doi:10.1016/j.compositesb.2014.12.021.

Doyle, J F. 1988. "A Spectrally Formulated Finite Element for Longitudinal Wave Propagation." *International Journal of Analytical and Experimental Modal Analysis* 3: 1–5.

Erdogan, F. 1995. "Fracture Mechanics of Functionally Graded Materials." *Composites Engineering* 5 (7): 753–70. doi:10.1016/0961-9526(95)00029-M.

Eshraghi, Iman, Serkan Dag, and Nasser Soltani. 2016. "Bending and Free Vibrations of Functionally Graded Annular and Circular Micro-Plates under Thermal Loading." *COMPOSITE STRUCTURE* 137. Elsevier Ltd: 196–207. doi:10.1016/j.compstruct.2015.11.024.

Eskandari-Ghadi, Morteza, and Amirhossein Amiri-Hezaveh. 2014. "Wave Propagations in Exponentially Graded Transversely Isotropic Half-Space with Potential Function Method." *Mechanics of Materials* 68. Elsevier Ltd: 275–92. doi:10.1016/j.mechmat.2013.09.009.

Ferreira, A J M, C M C Roque, R M N Jorge, G E Fasshauer, R C Batra, C M C Roque, R M N Jorge, G E Fasshauer, and R C Batra. 2007. "Analysis of Functionally Graded Plates by a Robust Meshless Method." *Mechanics of Advanced Materials and Structures* 14 (September): 577–87. doi:10.1080/15376490701672732.

Fett, Theo. 1998. "Stress Intensity Factors and Weight Functions for Special Crack Problems." *Report FZKA* 6025: 1–36. http://www.ubka.uni-karlsruhe.de/volltexte/fzk/6025/6025.pdf.

Filiz, Seckin, and Metin Aydogdu. 2015. "Wave Propagation Analysis of Embedded (Coupled) Functionally Graded Nanotubes Conveying Fluid." *Composite Structures* 132. Elsevier Ltd: 1260–73. doi:10.1016/j.compstruct.2015.07.043.

Fomenko, S.I., M.V. Golub, Ch. Zhang, T.Q. Bui, and Y.-S. Wang. 2014. "In-Plane Elastic Wave Propagation and Band-Gaps in Layered Functionally Graded Phononic Crystals." *International Journal of Solids and Structures* 51 (13). Elsevier Ltd: 2491–2503. doi:10.1016/j.ijsolstr.2014.03.017.

Galvis, a F, and P Sollero. 2014. "Boundary Element Analysis of Crack Problems in Polycrystalline Materials." *Procedia Materials Science* 3: 1928–33.

doi:10.1016/j.mspro.2014.06.311.

Gao, X.W., Ch. Zhang, J. Sladek, and V. Sladek. 2008. "Fracture Analysis of Functionally Graded Materials by a BEM." *Composites Science and Technology* 68 (5): 1209–15. doi:10.1016/j.compscitech.2007.08.029.

Ghannadpour, S A M, and M M Alinia. 2006. "Large Deflection Behavior of Functionally Graded Plates under Pressure Loads." *Composite Structures* 75: 67–71. doi:10.1016/j.compstruct.2006.04.004.

Giannakopoulos, a.E., and S. Suresh. 1997. "Indentation of Solids with Gradients in Elastic Properties: Part II. Axisymmetric Indentors." *International Journal of Solids and Structures* 34 (19): 2393–2428. doi:10.1016/S0020-7683(96)00172-2.

Goli, E., and M.T. Kazemi. 2014. "XFEM Modeling of Fracture Mechanics in Transversely Isotropic FGMs via Interaction Integral Method." *Procedia Materials Science* 3. Elsevier B.V.: 1257–62. doi:10.1016/j.mspro.2014.06.204.

Golub, Mikhail V., Anders Boström, and Peter D. Folkow. 2013. "Wave Propagation of Functionally Graded Layers Treated by Recursion Relations and Effective Boundary Conditions." *International Journal of Solids and Structures* 50 (5). Elsevier Ltd: 766–72. doi:10.1016/j.ijsolstr.2012.11.003.

Guo, L, Lin-Zhi Wu, Tao Zeng, and Li Ma. 2004. "Fracture Analysis of a Functionally Graded Coating-Substrate Structure with a Crack Perpendicular to the Interface - Part II : Transient Problem." *International Journal of Fracture* 127 (2004): 39–59.

Gupta, Ankit, and Mohammad Talha. 2015. "Progress in Aerospace Sciences Recent Development in Modeling and Analysis of Functionally Graded Materials and Structures." *Progress in Aerospace Sciences* 79. Elsevier: 1–14. doi:10.1016/j.paerosci.2015.07.001.

Han, X., G.R. Liu, and K.. Lam. 2000. "A Quadratic Layer Element for Analyzing Stress Waves in FGMs and Its Application in Material Characterization." *Journal of Sound and Vibration* 236 (2): 307–21. doi:10.1006/jsvi.2000.2966.

Han, X, and G R Liu. 2002. "Effects of SH Waves in a Functionally Graded Plate." *Mechanics Research Communications* 29: 327–38.

Hassaine, Tahar, Abdelouahed Tounsi, El Abbes, and Adda Bedia. 2013. "Sharif University of Technology Analytical Solution for Bending Analysis of Functionally Graded Plates." *Scientia Iranica* 20 (3). Elsevier B.V.: 516–23. doi:10.1016/j.scient.2013.02.014.

Hedayatrasa, Saeid, Tinh Quoc Bui, Chuanzeng Zhang, and Chee Wah Lim. 2014. "Numerical Modeling of Wave Propagation in Functionally Graded Materials Using Time-Domain Spectral Chebyshev Elements." *Journal of Computational Physics* 258. Elsevier Inc.: 381–404. doi:10.1016/j.jcp.2013.10.037.

Hirano, T, J Teraki, and T Yamada. 1990a. "On the Design of Functionally Gradient Materials." In *Proceedings of the First International Symposium on Functionally Gradient Materials*, edited by M Yamanouchi, M Koizumi, T Hirai, and I Shiota, 5–10. Sendai, Japan.

Hirano, J. Teraki, and T. Yamada. 1990b. "On the Design of Functionally Gradient Materials." In *Proceedings of the First International Symposium on Functionally Gradient Materials*, 5–10.

Hong, Minwoo, and Usik Lee. 2015. "Dynamics of a Functionally Graded Material Axial Bar: Spectral Element Modeling and Analysis." *Composites Part B: Engineering* 69. Elsevier Ltd: 427–34. doi:10.1016/j.compositesb.2014.10.022.

Hosseini, S S, H Bayesteh, and S Mohammadi. 2013. "A Thermo-Mechanical XFEM Crack Propagation Analysis of Functionally Graded Materials." *Materials Science & Engineering*

A 561. Elsevier: 285–302. doi:10.1016/j.msea.2012.10.043.

Hosseini, Seyed Mahmoud. 2012a. "Analysis of Elastic Wave Propagation in a Functionally Graded Thick Hollow Cylinder Using a Hybrid Mesh-Free Method." *Engineering Analysis with Boundary Elements* 36 (11). Elsevier: 1536–45. doi:10.1016/j.enganabound.2012.05.001.

Hosseini, Seyed Mahmoud. 2012b. "Analysis of Elastic Wave Propagation in a Functionally Graded Thick Hollow Cylinder Using a Hybrid Mesh-Free Method." *Engineering Analysis with Boundary Elements* 36 (11). Elsevier: 1536–45. doi:10.1016/j.enganabound.2012.05.001.

Idesman, a. 2014. "Accurate Finite-Element Modeling of Wave Propagation in Composite and Functionally Graded Materials." *Composite Structure* 117. Elsevier Ltd: 298–308. doi:10.1016/j.compstruct.2014.06.032.

Itou, S. 2001. "Transient Dynamic Stress Intensity Factors around a Crack in a Nonhomogeneous Interfacial Layer between Two Dissimilar Elastic Half-Planes." *International Journal of Solids and Structures* 38: 3631–45.

Jain, N., C.E. Rousseau, and a. Shukla. 2004. "Crack-Tip Stress Fields in Functionally Graded Materials with Linearly Varying Properties." *Theoretical and Applied Fracture Mechanics* 42 (2): 155–70. doi:10.1016/j.tafmec.2004.08.005.

Jha, D K, Tarun Kant, and R K Singh. 2013. "A Critical Review of Recent Research on Functionally Graded Plates." *Composite Structures* 96. Elsevier Ltd: 833–49. doi:10.1016/j.compstruct.2012.09.001.

Jiangong, Yu, Wu Bin, and He Cunfu. 2007. "Characteristics of Guided Waves in Graded Spherical Curved Plates." *International Journal of Solids and Structures* 44 (11–12): 3627–37. doi:10.1016/j.ijsolstr.2006.10.006.

Jin, Fan, and Xu Guo. 2013. "Mechanics of Axisymmetric Adhesive Contact of Rough Surfaces Involving Power-Law Graded Materials." *International Journal of Solids and Structures* 50 (20–21). Elsevier Ltd: 3375–86. doi:10.1016/j.ijsolstr.2013.06.007.

Jin, Z. H., and R. C. Batra. 1996. "Some Basic Fracture Mechanics Concepts in Functionally Graded Materials." *Journal of the Mechanics and Physics of Solids* 44 (8): 1221–35. doi:10.1016/0022-5096(96)00041-5.

Karihaloo, B L, and Q Z Xiao. 2001. "Accurate Determination of the Coe • Cients of Elastic Crack Tip Asymptotic ® Eld by a Hybrid Crack Element with P -Adaptivity" 68: 1609–30.

Kim, Jeong-Ho, and G. H. Paulino. 2002a. "Isoparametric Graded Finite Elements for Nonhomogeneous Isotropic and Orthotropic Materials." *Journal of Applied Mechanics* 69 (4): 502. doi:10.1115/1.1467094.

Kim, Jeong-Ho, and Glaucio H Paulino. 2002b. "Finite Element Evaluation of Mixed Mode Stress Intensity Factors in Functionally Graded Materials." *International Journal for Numerical Methods in Engineering* 53 (8): 1903–35. doi:10.1002/nme.364.

Kulikov, G M, and S V Plotnikova. 2015. "A Sampling Surfaces Method and Its Implementation for 3D Thermal Stress Analysis of Functionally Graded Plates." *Composite Structure* 120. Elsevier Ltd: 315–25. doi:10.1016/j.compstruct.2014.10.012.

Kulikov, G M, S V Plotnikova, M G Kulikov, and P V Monastyrev. 2016. "Three-Dimensional Vibration Analysis of Layered and Functionally Graded Plates through Sampling Surfaces Formulation." *Composite Structures* 152. Elsevier Ltd: 349–61. doi:10.1016/j.compstruct.2016.05.043.

Lee, Chang-yull, and Ji-hwan Kim. 2015. "Evaluation of Homogenized Effective Properties for

FGM Panels in Aero-Thermal Environments." *Composite Structure* 120. Elsevier Ltd: 442–50. doi:10.1016/j.compstruct.2014.10.017.

Lee, Taeyoung, Melvin Leok, and N. Harris McClamroch. 2011. "Geometric Numerical Integration for Complex Dynamics of Tethered Spacecraft." *Proceedings of the 2011 American Control Conference*, no. February: 1885–91. doi:10.1002/nme.

Lee, Woo Y., David P. Stinton, Christopher C. Berndt, Fazil Erdogan, Yi-Der Lee, and Zaher Mutasim. 1996. "Concept of Functionally Graded Materials for Thermal Barrier Coating Applications.pdf." *Journal of the American Ceramic Society* 79: 3003–12.

Lee, Y D, and F Erdogan. 1994. "Residual/thermal Stresses in FGM and Laminated Thermal Barrier Coatings." *International Journal of Fracture* 69 (2): 145–65. doi:10.1007/bf00035027.

Li, C.Y., Z.Z. Zou, and Z.P. Duan. 1999. "Torsional Impact of Transversely Isotropic Solid with Functionally Graded Shear Moduli and a Penny-Shaped Crack." *Theoretical and Applied Fracture Mechanics* 32 (3): 157–63. doi:10.1016/S0167-8442(99)00036-1.

Li, C, G J Weng, New Brunswick, and Z Duan. 2001. "Dynamic Stress Intensity Factor of a Functionally Graded Material under Antiplane Shear Loading." *Acta Mechanica* 149 (1–4): 1–10.

Li, Chunyu, and George J. Weng. 2001. "Dynamic Stress Intensity Factor of a Cylindrical Interface Crack with a Functionally Graded Interlayer." *Mechanics of Materials* 33 (6): 325–33. doi:10.1016/S0167-6636(01)00058-8.

Li, Chunyu, George J. Weng, and Zhuping Duan. 2001. "Dynamic Behavior of a Cylindrical Crack in a Functionally Graded Interlayer under Torsional Loading." *International Journal of Solids and Structures* 38 (42–43): 7473–85. doi:10.1016/S0020-7683(01)00046-4.

Li, Li, Yujin Hu, and Ling Ling. 2015. "Flexural Wave Propagation in Small-Scaled Functionally Graded Beams via a Nonlocal Strain Gradient Theory." *Composite Structures* 133: 1079–92. doi:10.1016/j.compstruct.2015.08.014.

Li, Yong Dong, Kang Yong Lee, and Yao Dai. 2008. "Dynamic Stress Intensity Factors of Two Collinear Mode-III Cracks Perpendicular to and on the Two Sides of a Bi-FGM Weak-Discontinuous Interface." *European Journal of Mechanics, A/Solids* 27 (5): 808–23. doi:10.1016/j.euromechsol.2007.11.006.

Liang, Xu, Hai-lei Kou, Lizhong Wang, Andrew C Palmer, Zhenyu Wang, and Guohua Liu. 2015. "Three-Dimensional Transient Analysis of Functionally Graded Material Annular Sector Plate under Various Boundary Conditions." *Composite Structure* 132. Elsevier Ltd: 584–96. doi:10.1016/j.compstruct.2015.05.066.

Lin, Yi-Hsien, Yi-Shyong Ing, and Chien-Ching Ma. 2015. "Two-Dimensional Transient Analysis of Wave Propagation in Functionally Graded Piezoelectric Slabs Using the Transform Method." *International Journal of Solids and Structures* 52. Elsevier Ltd: 72–82. doi:10.1016/j.ijsolstr.2014.09.021.

Liu, G R, K Dai, and T T Nguyen. 2007. "A Smoothed Finite Element Method for Mechanics Problems." *Computational Mechanics*, 859–77. doi:10.1007/s00466-006-0075-4.

Liu, G R, T Nguyen-thoi, and K Y Lam. 2009. "An Edge-Based Smoothed Finite Element Method (ES-FEM) for Static , Free and Forced Vibration Analyses of Solids." *Journal of Sound and Vibration* 320: 1100–1130. doi:10.1016/j.jsv.2008.08.027.

Liu, G R, N Nourbakhshnia, and Y W Zhang. 2011. "A Novel Singular ES-FEM Method for Simulating Singular Stress Fields near the Crack Tips for Linear Fracture Problems." *Engineering Fracture Mechanics* 78 (6). Elsevier Ltd: 863–76.

doi:10.1016/j.engfracmech.2009.11.004.

Liu, Nan, Jiashi Yang, Zheng Hua Qian, and Sohichi Hirose. 2010. "Interface Waves in Functionally Graded Piezoelectric Materials." *International Journal of Engineering Science* 48 (2). Elsevier Ltd: 151–59. doi:10.1016/j.ijengsci.2009.07.008.

Liu, Peng, Tiantang Yu, Tinh Quoc Bui, and Chuanzeng Zhang. 2013. "Transient Dynamic Crack Analysis in Non-Homogeneous Functionally Graded Piezoelectric Materials by the X-FEM." *Computational Materials Science* 69: 542–58. doi:10.1016/j.commatsci.2012.11.009.

Ma, Li, Jia Li, Radhi Abdelmoula, and Lin Zhi Wu. 2007. "Dynamic Stress Intensity Factor for Cracked Functionally Graded Orthotropic Medium under Time-Harmonic Loading." *European Journal of Mechanics, A/Solids* 26 (2): 325–36. doi:10.1016/j.euromechsol.2006.06.003.

Ma, Li, Lin Zhi Wu, Li Cheng Guo, and Zhen Gong Zhou. 2005. "Dynamic Behavior of a Finite Crack in the Functionally Graded Materials." *Mechanics of Materials* 37 (11): 1153–65. doi:10.1016/j.mechmat.2005.05.004.

Main, M. Abid, and A. J. M. Spencer. 1998. "Exact Solutions for Functionally Graded and Laminated Elastic Materials." *Journal of the Mechanics and Physics of Solids* 46: 2283–95.

Makoto Sasaki, T.H. 1991. "Fubrication and Properties of Functionally Graded Materials." *J. Ceram. Soc. Jpn* 99 (10): 1002–13.

Malik, P., and R. Kadoli. 2016. "Nonlinear Bending and Free Vibration Response of SUS316-Al2O3 Functionally Graded Plasma Sparyed Beams: Theoretical and Experimental Study." *J. Vib. Control*.

Marur, Prabhakar R., and Hareesh V. Tippur. 2000. "Numerical Analysis of Crack-Tip Fields in Functionally Graded Materials with a Crack Normal to the Elastic Gradient." *International Journal of Solids and Structures* 37 (38): 5353–70. doi:10.1016/S0020-7683(99)00207-3.

Miyamoto, Y., W. Kaysser, B. Rabin, A. Kawasaki, and R. Ford, eds. 1999. "Functionally Graded Materials." In . Boston: Kluwer Academic Publishers.

Moes, Nicolas M O, John Dolbow, and T E D Belytschko. 1999. "A Finite Element Method for Crack Growth Without Remeshing." *International Journal for Numerical Methods in Engineering* 150 (February): 131–50.

Moghaddam, A Mortazavi, and M T Ahmadian. 2013. "Acoustic Wave Propagation through a Functionally Graded Material Plate with Arbitrary Material Properties." *Journal of Materials: Design and Applications* 227 (2): 100–110. doi:10.1177/1464420712472632.

Molavi Nojumi, Mohamad, and Xiaodong Wang. 2016. "Evaluation of Modified Finite Elements with Spatially Varying elastic Parameters for Functionally Graded Materials." *24th International Congress of Theoretical and Applied Mechanics (ICTAM 2016)*, Montreal, Canada.

Molavi Nojumi, Mohamad, and Xiaodong Wang. 2017. "A New Graded Singular Finite Element for Crack Problems in Functionally Graded Materials." *International Journal of Fracture* 205: 203–20. doi:10.1007/s10704-017-0191-5.

Molavi Nojumi, Mohamad, and Xiaodong Wang. 2018. "Dynamic Analysis of Crack Problems in Functionally Graded Materials Using a New Graded Singular Finite Element." *Theoretical and Applied Fracture Mechanics 93*: 183-194.

Monfared, M. M., and M. Ayatollahi. 2013. "Dynamic Stress Intensity Factors of Multiple Cracks in an Orthotropic Strip with FGM Coating." *Engineering Fracture Mechanics* 109. Elsevier Ltd: 45–57. doi:10.1016/j.engfracmech.2013.07.002.

Motamedi, D., and S. Mohammadi. 2010. "Dynamic Analysis of Fixed Cracks in Composites by

the Extended Finite Element Method." *Engineering Fracture Mechanics* 77 (17). Elsevier Ltd: 3373–93. doi:10.1016/j.engfracmech.2010.08.011.

Naebe, Minoo, and Kamyar Shirvanimoghaddam. 2016. "Functionally Graded Materials : A Review of Fabrication and Properties." *Applied Materials Today* 5. Elsevier Ltd: 223–45. doi:10.1016/j.apmt.2016.10.001.

Ooi, Ean Tat, Chongmin Song, Francis Tin-loi, and Zhenjun Yang. 2012. "Polygon Scaled Boundary Finite Elements for Crack Propagation Modelling," no. March: 319–42. doi:10.1002/nme.

Ooi, E T, M Shi, C Song, F Tin-loi, and Z J Yang. 2013. "Dynamic Crack Propagation Simulation with Scaled Boundary Polygon Elements and Automatic Remeshing Technique." *Engineering Fracture Mechanics* 106 (2012). Elsevier Ltd: 1–21. doi:10.1016/j.engfracmech.2013.02.002.

Ootao, Yoshihiro, and Yoshinobu Tanigawa. 2005. "Three-Dimensional Solution for Transient Thermal Stresses of Functionally Graded Rectangular Plate due to Nonuniform Heat Supply." *International Journal of Mechanical Sciences* 47: 1769–88. doi:10.1016/j.ijmecsci.2005.06.003.

Ootao, Yoshihiro, Yoshinobu Tanigawa, and Osamu Ishimaru. 2000. "Optimization of Material Composition of Functionally Graded Plate for Thermal Stress Relaxation Using a Genetic Algorithm." *Journal of Thermal Stresses* 23: 257–71. doi:10.1080/014957300280434.

Pan, Haizhu, Tianshu Song, and Zhihai Wang. 2015. "An Analytical Model for Collinear Cracks in Functionally Graded Materials with General Mechanical Properties." *Composite Structures* 132. Elsevier Ltd: 359–71. doi:10.1016/j.compstruct.2015.05.055.

Papargyri-Beskou, S., D. Polyzos, and D. E. Beskos. 2009. "Wave Dispersion in Gradient Elastic Solids and Structures: A Unified Treatment." *International Journal of Solids and Structures* 46 (21). Elsevier Ltd: 3751–59. doi:10.1016/j.ijsolstr.2009.05.002.

Papila, M, and R T Haftka. 2003. "Implementation of a Crack Propagation Constraint within a Structural Optimization Software." *Struct Multidisc Optim* 25: 327–38. doi:10.1007/s00158-003-0329-0.

Parameswaran, V., and a. Shukla. 2002. "Asymptotic Stress Fields for Stationary Cracks Along the Gradient in Functionally Graded Materials." *Journal of Applied Mechanics* 69 (3): 240. doi:10.1115/1.1459072.

Park, Kyoungsoo, and Glaucio H. Paulino. 2011. "Parallel Computing of Wave Propagation in Three Dimensional Functionally Graded Media." *Mechanics Research Communications* 38 (6). Elsevier Ltd.: 431–36. doi:10.1016/j.mechrescom.2011.04.007.

Paulino, Glaucio H., and Jeong-Ho Kim. 2007. "The Weak Patch Test for Nonhomogeneous Materials Modeled with Graded Finite Elements." *Journal of the Brazilian Society of Mechanical Sciences and Engineering* 29 (1): 63–81. doi:10.1590/S1678-58782007000100010.

Petrova, Vera, and Siegfried Schmauder. 2014. "FGM/homogeneous Bimaterials with Systems of Cracks under Thermo-Mechanical Loading: Analysis by Fracture Criteria." *Engineering Fracture Mechanics* 130. Elsevier Ltd: 12–20. doi:10.1016/j.engfracmech.2014.01.014.

Praveen, G N, and J N Reddy. 1998. "Nonlinear Transient Thermoelastic Analysis of Functionally Graded Ceramic-Metal Plates." *International Journal of Solids and Structures* 35 (33): 4457–76. doi:10.1016/S0020-7683(97)00253-9.

Ramirez, Fernando, Paul R Heyliger, and Ernian Pan. 2006. "Static Analysis of Functionally Graded Elastic Anisotropic Plates Using a Discrete Layer Approach." *Composites Part B:*

Engineering 37: 10–20. doi:10.1016/j.compositesb.2005.05.009.

Reddy, J N, and Zhen-qiang Cheng. 2001. "Three-Dimensional Thermomechanical Deformations of Functionally Graded Rectangular Plates." *European Journal of Mechanics, A/Solids* 20: 841–55.

Richter, V. 1995. "FGM'94, Proceedings of the 3rd International Symposium on Structural and Functional Gradient Materials." In , edited by B. Ilschner and N. Cherradi, 587–92. Lausanne.

Rosakis, Ares J, and K Ravi-Chandar. 1986. "On the Crack-Tip Stress State: An Experimental Evaluation of Three-Dimensional Effects." *International Journal of Solids and Structures* 22: 121–34. doi:10.1016/0020-7683(86)90002-8.

Salah, Issam Ben, Anouar Njeh, and Mohamed Hédi Ben Ghozlen. 2012. "A Theoretical Study of the Propagation of Rayleigh Waves in a Functionally Graded Piezoelectric Material (FGPM)." *Ultrasonics* 52 (2). Elsevier B.V.: 306–14. doi:10.1016/j.ultras.2011.08.016.

Santare, M. H., and J. Lambros. 2000. "Use of Graded Finite Elements to Model the Behavior of Nonhomogeneous Materials." *Journal of Applied Mechanics* 67 (4): 819. doi:10.1115/1.1328089.

Santare, Michael H., Priya Thamburaj, and George a. Gazonas. 2003. "The Use of Graded Finite Elements in the Study of Elastic Wave Propagation in Continuously Nonhomogeneous Materials." *International Journal of Solids and Structures* 40 (21): 5621–34. doi:10.1016/S0020-7683(03)00315-9.

Shojaee, S., and a. Daneshmand. 2015. "Crack Analysis in Media with Orthotropic Functionally Graded Materials Using Extended Isogeometric Analysis." *Engineering Fracture Mechanics* 147. Elsevier Ltd: 203–27. doi:10.1016/j.engfracmech.2015.08.025.

Shuvalov, a. L., E. Le Clezio, and G. Feuillard. 2008. "The State-Vector Formalism and the Peano-Series Solution for Modelling Guided Waves in Functionally Graded Anisotropic Piezoelectric Plates." *International Journal of Engineering Science* 46 (9): 929–47. doi:10.1016/j.ijengsci.2008.03.007.

Singh, I. V., B. K. Mishra, and S. Bhattacharya. 2011. "XFEM Simulation of Cracks, Holes and Inclusions in Functionally Graded Materials." *International Journal of Mechanics and Materials in Design* 7 (3): 199–218. doi:10.1007/s10999-011-9159-1.

Sladek, Jan, Vladimir Sladek, and Chuanzeng Zhang. 2005. "An Advanced Numerical Method for Computing Elastodynamic Fracture Parameters in Functionally Graded Materials." *Computational Materials Science* 32 (3–4): 532–43. doi:10.1016/j.commatsci.2004.09.011.

Sobczak, Jerzy J, and Ludmil Drenchev. 2013. "Metallic Functionally Graded Materials : A Speci Fi c Class of Advanced Composites." *Journal of Materials Science & Technology* 29 (4). Elsevier Ltd: 297–316. doi:10.1016/j.jmst.2013.02.006.

Song, Chongmin, Francis Tin-loi, and Wei Gao. 2010. "A Definition and Evaluation Procedure of Generalized Stress Intensity Factors at Cracks and Multi-Material Wedges." *Engineering Fracture Mechanics* 77 (12). Elsevier Ltd: 2316–36. doi:10.1016/j.engfracmech.2010.04.032.

Song, Chongmin, and John P Wolf. 1997. "The Scaled Boundary Finite-Element Method-Alias Consistent Infinitesimal Finite-Element Cell Method- for Elastodynamics." *Computer Methods in Applied Mechanics and Engineering* 147: 329–55.

Song, Chongmin, and John P Wolf. 1998. "The Scaled Boundary Finite-Element Method : Analytical Solution in Frequency Domain." *Computer Methods in Applied Mechanics and Engineering* 164.

Song, Seong Hyeok, and Glaucio H. Paulino. 2006. "Dynamic Stress Intensity Factors for Homogeneous and Smoothly Heterogeneous Materials Using the Interaction Integral Method." *International Journal of Solids and Structures* 43 (16): 4830–66. doi:10.1016/j.ijsolstr.2005.06.102.

Sun, Dan, and Song-Nan Luo. 2011a. "Wave Propagation and Transient Response of Functionally Graded Material Circular Plates under a Point Impact Load." *Composites Part B: Engineering* 42 (4). Elsevier Ltd: 657–65. doi:10.1016/j.compositesb.2011.02.020.

Sun, Dan, and Song Nan Luo. 2011b. "The Wave Propagation and Dynamic Response of Rectangular Functionally Graded Material Plates with Completed Clamped Supports under Impulse Load." *European Journal of Mechanics, A/Solids* 30 (3). Elsevier Masson SAS: 396–408. doi:10.1016/j.euromechsol.2011.01.001.

Suresh, S., and A. Mortensen. 1998. *Fundamentals of Functionally Graded Materials*. London, UK: IOM Communications Ltd.

Swaminathan, K, and D M Sangeetha. 2017. "Thermal Analysis of FGM Plates – A Critical Review of Various Modeling Techniques and Solution Methods." *Composite Structures* 160. Elsevier Ltd: 43–60. doi:10.1016/j.compstruct.2016.10.047.

Tan, Mingan. 1998. "On the Singular Stress Field at the Interface of Bimaterial Systems." University of Toronto.

Tat, Ean, Ooi Sundararajan, and Chongmin Song Francis Tin-loi. 2015. "Crack Propagation Modelling in Functionally Graded." *International Journal of Fracture*, 87–105. doi:10.1007/s10704-015-9987-3.

Tong, Pin, T. H. H. Pian, and S. J. Lasry. 1973. "A Hybrid-Element Approach to Crack Problems in Plane Elasticity." *International Journal for Numerical Methods in Engineering* 7 (3): 297–308. doi:10.1002/nme.1620070307.

Udupa, Gururaja, S. Shrikantha Rao, and K.V. Gangadharan. 2014. "Functionally Graded Composite Materials: An Overview." *Procedia Materials Science* 5: 1291–99. doi:10.1016/j.mspro.2014.07.442.

Wang, B L, J C Han, and S Y Du. 2000. "Multiple Crack Problem in Nonhomogeneous Composite Materials Subjected to Dynamic Anti-Plane Shearing." *International Journal of Fracture* 100 (4): 343–53.

Wang, B L, Yiu-wing Mai, and N Noda. 2006. "Fracture Mechanics Analysis Model for Functionally Graded Materials with Arbitrarily Distributed Properties." *International Journal of Fracture*, no. 1994: 161–77.

Whitney, J.M., and R.J. Nuismer. 1974. "Stress Fracture Criteria for Laminated Composites Containing Stress Concenterations." *J. Compos. Mater.* 8: 253–65.

Xu, Hongmin, Xuefeng Yao, Xiqiao Feng, and Yang Yeh Hisen. 2008. "Dynamic Stress Intensity Factors of a Semi-Infinite Crack in an Orthotropic Functionally Graded Material." *Mechanics of Materials* 40 (1–2): 37–47. doi:10.1016/j.mechmat.2007.06.003.

Yas, M. H., M. Shakeri, M. Heshmati, and S. Mohammadi. 2011. "Layer-Wise Finite Element Analysis of Functionally Graded Cylindrical Shell under Dynamic Load." *Journal of Mechanical Science and Technology* 25 (3): 597–604. doi:10.1007/s12206-011-0116-6.

Yu, J. G., F. E. Ratolojanahary, and J. E. Lefebvre. 2011. "Guided Waves in Functionally Graded Viscoelastic Plates." *Composite Structures* 93 (11): 2671–77. doi:10.1016/j.compstruct.2011.06.009.

Yu, J.G., X.D. Yang, J.E. Lefebvre, and Ch. Zhang. 2015. "Wave Propagation in Graded Rings with Rectangular Cross-Sections." *Wave Motion* 52: 160–70.

doi:10.1016/j.wavemoti.2014.09.009.

Yu, Jiangong, and Bin Wu. 2009. "The Inverse of Material Properties of Functionally Graded Pipes Using the Dispersion of Guided Waves and an Artificial Neural Network." *NDT and E International* 42 (5): 452–58. doi:10.1016/j.ndteint.2009.02.006.

Yu, Jiangong, Bin Wu, and Cunfu He. 2010. "Guided Thermoelastic Waves in Functionally Graded Plates with Two Relaxation Times." *International Journal of Engineering Science* 48 (12). Elsevier Ltd: 1709–20. doi:10.1016/j.ijengsci.2010.10.002.

Yu, Jiangong, and Ch Zhang. 2014. "Effects of Initial Stress on Guided Waves in Orthotropic Functionally Graded Plates." *Applied Mathematical Modelling* 38 (2). Elsevier Inc.: 464–78. doi:10.1016/j.apm.2013.06.029.

Zenkour, A M. 2005. "A Comprehensive Analysis of Functionally Graded Sandwich Plates : Part 1 — Deflection and Stresses." *International Journal of Solids and Structures* 42: 5224–42. doi:10.1016/j.ijsolstr.2005.02.015.

Zenkour, Ashraf M. 2006. "Generalized Shear Deformation Theory for Bending Analysis of Functionally Graded Plates." *Applied Mathematical Modelling* 30: 67–84. doi:10.1016/j.apm.2005.03.009.

Zhang, C., Jan Sladek, and Vladimir Sladek. 2003. "Numerical Analysis of Cracked Functionally Graded Materials." *Key Engineering Materials* 251–252: 463–72. doi:10.4028/www.scientific.net/KEM.251-252.463.

Zhang, Ch, a. Savaidis, G. Savaidis, and H. Zhu. 2003. "Transient Dynamic Analysis of a Cracked Functionally Graded Material by a BIEM." *Computational Materials Science* 26 (SUPPL.): 167–74. doi:10.1016/S0927-0256(02)00395-6.

Zhang, Ch, J. Sladek, and V. Sladek. 2003. "Effects of Material Gradients on Transient Dynamic Mode-III Stress Intensity Factors in a FGM." *International Journal of Solids and Structures* 40 (20): 5251–70. doi:10.1016/S0020-7683(03)00243-9.

Zhang, Ch., Sladek, J., and Sladek, V. 2005. "Antiplane Crack Analysis of a Functionally Graded Material by a BIEM." *Computational Materials Science* 32 (3–4): 611–19. doi:10.1016/j.commatsci.2004.09.002.

Zhao, L, W Q Chen, and C F Lü. 2012. "Symplectic Elasticity for Bi-Directional Functionally Graded Materials." *Mechanics of Materials* 54: 32–42. doi:10.1016/j.mechmat.2012.06.001.

Zhao, Wenbin, Zhixin Hu, Xuexia Zhang, Hailing Xie, and Lujuan Yu. 2014. "The Dynamic Stress Intensity Factor around the Anti-Plane Crack in an Infinite Strip Functionally Graded Material under Impact Loading." *Theoretical and Applied Fracture Mechanics* 74 (1). Elsevier Ltd: 1–6. doi:10.1016/j.tafmec.2014.05.002.

Zhou, Chuanping, Chao Hu, Fai Ma, and Diankui Liu. 2014. "Elastic Wave Scattering and Dynamic Stress Concentrations in Exponential Graded Materials with Two Elliptic Holes." *Wave Motion* 51 (3). Elsevier B.V.: 466–75. doi:10.1016/j.wavemoti.2013.11.005.

Zienkiewicz, O C, and Freng Emeritus. n.d. "The Finite Element Method Fifth Edition Volume 1 : The Basis" 1.

Zou, Z.Z., Sheng Xing Wu, and C.Y. Li. 2000. "On the Multiple Isoparametric Finite Element Method and Computation of Stress Intensity Factor for Cracks in FGMs." *Key Engineering Materials* 183–187: 511–16. doi:10.4028/www.scientific.net/KEM.183-187.511.